DETERMINATION OF THE IONOSPHERE PARAMETERS BY ANALYZING THE PROPAGATION AFTER-EFFECTS AFOSR GRANT NO. FA9550-07-1-0170 FINAL PERFORMANCE REPORT*

S. V. TSYNKOV†

Abstract. The key goal of the project was to analyze the distortions of spaceborne SAR images due to the Earth's ionosphere, and to suggest a mitigation strategy. Our approach to reducing the distortions is based on dual carrier probing. It provides additional information for deriving the unknown parameters of the ionosphere that are subsequently used for correcting the matched filter. In addition, we have analyzed the start-stop approximation, which is used commonly for processing the SAR data, and shown that it remains valid even in the case of a rapidly moving platform (radar mounted on a satellite).

*Grant performance period: March 1, 2007 through May 31, 2010.

†Principal investigator. Department of Mathematics, North Carolina State University, Box 8205, Raleigh, NC 27695, USA. Phone: 919-515-1877; Facsimile: 919-513-7336; E-mail: tsynkov@math.ncsu.edu, URL: http://www.math.ncsu.edu/∼stsynkov.

REPORT DOCUMENTATION PAGE

Form Approved
OMB No. 0704-0188

The public reporting burden for this collection of information is estimated to average 1 hour per response, including the time for reviewing instructions, searching existing data sources, gathering and maintaining the data needed, and completing and reviewing the collection of information. Send comments regarding this burden estimate or any other aspect of this collection of information, including suggestions for reducing the burden, to the Department of Defense, Executive Services and Communications Directorate (0704-0188). Respondents should be aware that notwithstanding any other provision of law, no person shall be subject to any penalty for failing to comply with a collection of information if it does not display a currently valid OMB control number.

PLEASE DO NOT RETURN YOUR FORM TO THE ABOVE ORGANIZATION.

1. REPORT DATE *(DD-MM-YYYY)*	2. REPORT TYPE	3. DATES COVERED *(From - To)*
June 27, 2010	Final	Mar 1, 2007 to May 31, 2010

4. TITLE AND SUBTITLE

DETERMINATION OF THE IONOSPHERE PARAMETERS BY ANALYZING THE PROPAGATION AFTER-EFFECTS

5a. CONTRACT NUMBER

5b. GRANT NUMBER

FA9550-07-1-0170

5c. PROGRAM ELEMENT NUMBER

6. AUTHOR(S)

Semyon Tsynkov,
CENTER FOR RESEARCH IN SCIENTIFIC COMPUTATION
NORTH CAROLINA STATE UNIVERSITY

5d. PROJECT NUMBER

5e. TASK NUMBER

5f. WORK UNIT NUMBER

7. PERFORMING ORGANIZATION NAME(S) AND ADDRESS(ES)

NORTH CAROLINA STATE UNIVERSITY
RESEARCH & ADMINISTRATION/SPARCS 2230
2230 STINSON DRIVE, 2 LEAZAR HALL, RALEIGH, NC 27695-7514

8. PERFORMING ORGANIZATION REPORT NUMBER

9. SPONSORING/MONITORING AGENCY NAME(S) AND ADDRESS(ES)

AF OFFICE OF SCIENTIFIC RESEARCH
875 NORTH RANDOLPH STREET ROOM 3112
ARLINGTON VA 22203

10. SPONSOR/MONITOR'S ACRONYM(S)

11. SPONSOR/MONITOR'S REPORT NUMBER(S)

12. DISTRIBUTION/AVAILABILITY STATEMENT

UNLIMITED

13. SUPPLEMENTARY NOTES

14. ABSTRACT

The objective of this basic research effort is to provide theoretical guidance for the design of EM/radar waveforms which suffer minimal distortion from propagation through the ionosphere. The PT and his team will initially derive a hierarchy of mathematical models for simulating the responses of the ionosphere to a variety of non-monochromatic radar waveforms. A time domain analysis of these propagating waves will be undertaken. The AF anticipates greater reliance on space-based radars as well as comm systems and this research will upgrade the fidelity of the predictions of such systems operations.

15. SUBJECT TERMS

16. SECURITY CLASSIFICATION OF:			17. LIMITATION OF ABSTRACT	18. NUMBER OF PAGES	19a. NAME OF RESPONSIBLE PERSON
a. REPORT	b. ABSTRACT	c. THIS PAGE			Semyon Tsynkov
					19b. TELEPHONE NUMBER *(Include area code)* 919-515-4323

CONTENTS

1. Introduction. Spaceborne imaging of the Earth's surface by synthetic aperture radars (SAR) may be adversely affected by the ionosphere that causes distortions of the signals emitted and received by the radar antenna. In Section 2 of the report, we analyzed those distortions for the inhomogeneous ionosphere described by the cold plasma model. Based on the analysis, we can conclude that the deterioration of SAR images is due to the mismatch between certain parameters of the actual received signal, which is slowed down by the temporal dispersion in the ionosphere, and the corresponding parameters of the matched filter, which is taken as if the propagation was unobstructed. Consequently, to improve the quality of the images the filter must be corrected. However, to get the appropriate correction one needs to know some key characteristics of the ionosphere precisely at the time and place the image is taken. To obtain those characteristics, we propose to probe the terrain, and hence the ionosphere, on two distinct carrier frequencies. We also investigate the performance of the matched filters that were corrected this way, and show that the final quality of the images indeed improves. The exposition of the material in Section 2 follows our recent paper [ST10], see also [Tsy09a].

The start-stop approximation is a standard tool for processing radar data in synthetic aperture imaging. It assumes that the antenna is motionless when a pulse is emitted and the scattered signal received, after which the antenna moves to its next sending/receiving position along the flight track. However, when the antenna is mounted on a satellite, as opposed to an airplane, its relatively high speed raises at least two questions. The first one is whether the image may be affected by the actual displacement of the antenna during the pulse round-trip time between the orbit and the Earth's surface. This displacement, in fact, can be rather large. Nonetheless, by analyzing the corresponding generalized ambiguity function of a SAR sensor (see Section 3 of the report) we show that in practice this issue can be disregarded. The second question is related to the Doppler frequency shift, which, again, is larger for spaceborne radars than for airborne radars. In the early SAR studies, this frequency shift provided a venue for understanding the azimuthal resolution of a radar. However, in a more rigorous analysis based on the generalized ambiguity function, the Doppler effect is typically left out of consideration. In Section 3 of the report, we also show that for the image to stay largely unaffected by Doppler, the frequency shift must be included in the definition of a matched filter. Otherwise, there will be a geometric shift (translation) of the entire imaged scene from its true position, and there may also be a slight deterioration of the image sharpness (contrast). The exposition of the material in Section 3 follows our paper [Tsy09b].

2. Dual carrier probing for spaceborne SAR imaging.

2.1. Background. Synthetic aperture radar (SAR) is a coherent imaging technology which is based predominantly on the phase information of the emitted and received waves (as opposed, say, to conventional photography, which is based on the amplitude). In particular, spaceborne SAR imaging of the Earth's surface involves sending specially shaped pulses of radio waves from the satellite to the ground, receiving the scattered response, and processing it by means of a matched filter [Che01, CB09]. In doing so, the received signal can, in some approximate sense, be interpreted as a Fourier transform of the ground reflectivity function, whereas filtering that yields the image is analogous to the inverse transform. The filter is called matched because its phase is supposed to match that of the received signal.

When radar signals travel back and forth from the satellite to the surface, they propagate through the Earth's ionosphere and hence undergo temporal dispersion. This causes delays in arrival times. If the filter does not take those delays into account, a mismatch of the phase occurs and accordingly, the quality of the image deteriorates [Tsy09a,ST10]. The extent of deterioration depends on the carrier frequency of the radar, or more precisely, on its ratio to the Langmuir frequency of the ionospheric plasma. The higher the carrier frequency the less prone the image to ionospheric distortions. Therefore, many modern spaceborne SAR sensors operate in the microwave band on the frequencies of around $10\,GHz$ or even higher. For example, the new European satellite TerraSAR-X operates in the X-band, on the frequencies between $7\,GHz$ and $11.2\,GHz$.

However, there is also substantial interest toward spaceborne SAR technology on lower carrier frequencies, in the VHF or UHF band, i.e., in the range of hundreds of megahertz. Radars of this type have a better surface penetrating capability. On the other hand, their images are much more sensitive to ionospheric distortions. Consequently, special means need to be developed to compensate for those distortions.

In [Tsy09a,ST10], we have analyzed the distortions for the case of SAR imaging by means of a scalar field that propagates through the inhomogeneous ionosphere described by the cold plasma model. We have also

proposed to probe the terrain, and hence the ionosphere, on two distinct carrier frequencies. This allows one to determine some key ionospheric parameters that control the propagation, and then correct the matched filter accordingly. We have also investigated the performance of the matched filters with the corrections introduced using dual carrier probing. Our main conclusion is that the new filters are capable of completely eliminating the distortions of SAR images due to the deterministic part of the charged particles content in the ionosphere, including the inhomogeneous case. Removing the distortions due to the random part of the charged particles content will be subject of the future work.

We emphasize that the corrections shall be obtained precisely for the time and place the image is taken. The reason is that the Earth's ionosphere is a very "lively" medium; its characteristics depend on many factors, such as time of the day, time of the year, geographic location, level of Solar activity, etc., and may change rapidly, e.g., considerably faster than the period of one revolution of the satellite around the Earth.

This part of the report is organized as follows. In Section 2.2, we describe the physical model and introduce the key assumptions. In Section 2.3, we build the generalized ambiguity function of a SAR, which provides a key tool for analyzing the radar resolution. In Section 2.4, we discuss the performance of a spaceborne SAR sensor in the case when no attempt is made to mitigate the distortions; this creates a foundation for the subsequent discussion of a corrected matched filter. In Section 2.5, we introduce the dual carrier probing as a venue for obtaining the parameters of the ionosphere needed for correcting the filter. In Section 2.6, we discuss the performance of the radar once the corrected filter has been implemented, and show that the resolution and sharpness of the images indeed improve. Finally, Section 2.7 presents a summary of what has been accomplished, and identifies directions for future work.

2.2. The model. For the following discussion we adopt the same model as in [Tsy09a, ST10]. We analyze the standard (as opposed to interferometric) SAR images [FL99]. We assume that the radar does not measure the polarization, and hence consider the propagation of scalar quantities only. All the targets are assumed deterministic and dispersionless; scattering of radar signals off the targets is linearized and interpreted using the first Born approximation. The start-stop approximation is employed to describe the synthetic antenna; its applicability to spaceborne SAR sensors (as opposed to airborne) is justified in [Tsy09b], see also Section 3 of this report.

The ionosphere is modeled as a layer of inhomogeneous dilute plasma, for which the mean concentration (number density) of electrons depends on the altitude but does not depend on the horizontal coordinates. The latter assumption holds provided that the characteristic distances along the Earth's surface are not very large. We disregard the effect of the magnetic field of the Earth on mean electron concentration and assume that the ionosphere is isotropic. This implies, in particular, that the Faraday rotation is not taken into account; of course, for scalar propagating fields (no polarization) it is not considered anyway.

On top of its mean value, the electron number density has a stochastic component due to the ionospheric turbulence, which is a quasi-homogeneous random field [MY71, RKT89a]. The effect of the Earth's magnetic field on the ionospheric turbulence is disregarded, and the turbulence is assumed isotropic.

The propagation of electromagnetic waves in the ionosphere is analyzed with the help of the cold plasma approximation [Gin64], which requires that the phase speed of the waves be much faster than the thermal speed of the electrons. The cold plasma approximation is equivalent to disregarding spatial dispersion and taking into account only temporal dispersion of radio waves in the plasma [MM91]. The ionospheric plasma is also assumed lossless, i.e., its Ohm conductivity is disregarded. This means that the effective collision frequencies between different species of particles in the plasma are much lower than the Langmuir frequency. Moreover, the propagation is assumed linear, because the power of signals emitted by spaceborne antennas is typically much lower than that needed for setting off the nonlinear effects, see [GG60, Gur78, Gur07], as well as [Gin64, Ch. VIII].

We use the classical Helmholtz theorem [MF53] to partition the overall electric field into the longitudinal and transverse components. Then, from the full Maxwell's equations and the equation of motion of electrons in the electric field one can derive the Klein-Gordon equation (see [Tsy09a, App. A]) that governs the propagation of high frequency transverse[1] electromagnetic waves in dilute plasma:

$$\frac{\partial^2 \boldsymbol{E}_\perp}{\partial t^2} - c^2 \Delta \boldsymbol{E}_\perp + \omega_{\rm pe}^2 \boldsymbol{E}_\perp = \boldsymbol{0}. \tag{2.1}$$

[1] The corresponding longitudinal oscillations are known as Langmuir waves, they have zero group velocity [MM91].

The quantity $\omega_{\rm pe}$ in equation (2.1) is the Langmuir frequency, or plasma electron frequency. It characterizes temporal responses of the plasma and is given by:

$$\omega_{\rm pe} = \sqrt{\frac{4\pi e^2 N_{\rm e}}{m_{\rm e}}}, \tag{2.2}$$

where e and $m_{\rm e}$ are the charge and mass of the electron, and $N_{\rm e}$ is the electron number density. The behavior of $\omega_{\rm pe}^2$ in the ionosphere follows that of $N_{\rm e}$; it has an altitude-dependent deterministic component and a stochastic component due to the turbulence. Typical values of the Langmuir frequency in the Earth's ionosphere range between $3MHz$ and $15MHz$.

Unlike in a vacuum, the propagation speed of electromagnetic waves in the ionosphere depends on the frequency. This phenomenon is known as temporal dispersion; it is due to the presence of the last, non-differentiated, term in equation (2.1). The dispersion relation for the Klein-Gordon equation reads:

$$\omega^2 = \omega_{\rm pe}^2 + c^2 k^2. \tag{2.3}$$

Dispersion (2.3) is anomalous, i.e., it is the short waves that are weakly dispersive, whereas the long waves are subject to stronger dispersion. Indeed, the phase and group velocity of the propagation are given by:

$$v_{\rm ph} = c\left(1 + \omega_{\rm pe}^2/c^2k^2\right)^{\frac{1}{2}} \tag{2.4}$$

and

$$v_{\rm gr} = c\left(1 + \omega_{\rm pe}^2/c^2k^2\right)^{-\frac{1}{2}}, \tag{2.5}$$

so that the shorter the wave, (the larger the k) the closer both velocities to the non-dispersive limit $v = c$.

In the Cartesian coordinates we can consider equation (2.1) for individual field components:

$$\frac{\partial^2 E}{\partial t^2} - c^2 \Delta E + \omega_{\rm pe}^2 E = 0. \tag{2.6}$$

Hereinafter, we will use the scalar governing equation (2.6) to describe the propagation of electromagnetic waves in the ionosphere. For a comprehensive account of the propagation of radio waves in plasma we refer the reader to the monographs [Gin64] and [Bud85].

To characterize the ionospheric turbulence, we write the electron number density as follows:

$$N_{\rm e} = \langle N_{\rm e} \rangle + \mu(\boldsymbol{x}), \tag{2.7}$$

where the angular brackets $\langle \cdot \rangle$ denote the expected value (mean) and μ represents the fluctuations: $\langle \mu \rangle = 0$. In the simplest case of constant $\langle N_{\rm e} \rangle$, $\mu(\boldsymbol{x})$ is a homogeneous and isotropic random field, and its correlation function depends only on the distance $r = |\boldsymbol{x}_1 - \boldsymbol{x}_2|$ and not on the individual locations $\boldsymbol{x}_1$ and $\boldsymbol{x}_2$:

$$V(\boldsymbol{x}_1, \boldsymbol{x}_2) \stackrel{\rm def}{=} \langle \mu(\boldsymbol{x}_1)\mu(\boldsymbol{x}_2) \rangle = V(|\boldsymbol{x}_1 - \boldsymbol{x}_2|) \equiv V(r). \tag{2.8}$$

In reality, however, $\langle N_{\rm e} \rangle$ is a function of the altitude h. At the same time, the ratio

$$M = \frac{\sqrt{\langle \mu^2 \rangle}}{\langle N_{\rm e} \rangle} \tag{2.9}$$

is assumed altitude independent. A typical numerical value of M is $5 \cdot 10^{-3}$, and in extreme situations it may reach 10^{-1} [Arm05]. Hence, $\sqrt{\langle \mu^2 \rangle}$ also depends on h, which makes $\mu(\boldsymbol{x})$ a quasi-homogeneous (rather than truly homogeneous) random field. While in this case we still keep the same notation (2.8) for the correlation function, in fact we have $V = V(h, r)$, where the dependence on h (altitude) is slow and the dependence on r (local variable) is fast. Hereafter, we will use the exponential correlation function

$$V(r) = C\pi^2 q_0^3 e^{-q_0 r}. \tag{2.10}$$

It accounts only for the short range phenomena in the ionosphere and has the spectrum [MY75, Sec. 12.1]

$$\widehat{V}(q) = \frac{C}{(1+q^2/q_0^2)^\kappa}, \quad \text{where} \quad \kappa = 2 \ \text{ and } \ C = \text{const}. \tag{2.11}$$

In formulae (2.10) and (2.11), we denote $q_0 = r_0^{-1}$, where r_0 is the correlation length or outer scale of turbulence. The latter may range between $1km$ and $10km$ according to different sources in the literature. An advantage of using the correlation function (2.10) is that one can easily make sure that it satisfies a necessary and sufficient condition of ergodicity given in [MY71, Sec. 4.7] (a 1938 theorem by E. E. Slutskii):

$$\lim_{S\to\infty} \frac{1}{S} \int_0^S V(s)ds = 0. \tag{2.12}$$

Ergodicity implies that statistical means can be substituted for spatial averages of μ whenever averaging is done over sufficiently long intervals. In that regard we note that if a random field is ergodic, then it must have $\langle\mu\rangle = \text{const}$, because the spatial average of μ does not depend on the location, whereas its statistical mean $\langle\mu\rangle$ may, generally speaking, be a function of the coordinates [MY71, Sec. 4.6]. In our particular case, however, we have $\langle\mu\rangle = 0$, which means that ergodicity can be employed even when the random field μ is quasi-homogeneous rather than truly homogeneous (because its variance depends on the altitude).

It should also be mentioned that for the true Kolmogorov-type turbulence we have $\kappa = 11/6$ rather than $\kappa = 2$ in formula (2.11), see [RKT89a, Ch. I]. From the standpoint of practice, the difference between the two cases is that $\kappa = 11/6$ allows one to take into account some long range phenomena in the ionosphere. As we have indicated in [Tsy09a], this is a separate interesting subject for the future study.

For the purpose of obtaining specific quantitative estimates, we will use the same typical values of the parameters as we have exploited in [Tsy09a,ST10]. A reference value of the mean electron concentration will be taken as $\langle N_\text{e}\rangle = 10^6 cm^{-3}$ (in fact, $\langle N_\text{e}\rangle = \langle N_\text{e}(h)\rangle$), which corresponds to the F-layer of the ionosphere and yields $\omega_\text{pe} \approx 9MHz$. The radar carrier frequency will be assumed equal to $1\,GHz$, which is the lower bound for the microwave band, and which yields the wavelength $\lambda = 30cm$. According to [Bro93], it is very difficult to achieve high resolution of spaceborne SAR images for carrier frequencies under $1\,GHz$ if no attempt is made to reduce the distortions due to the ionosphere. A typical one-way propagation distance between the satellite and the ground will be taken as $R_0 \approx 1000km$, and the orbit altitude H may be about $500km$ or higher. Other important parameters will be introduced as needed.

2.3. The generalized ambiguity function. The generalized ambiguity function offers a convenient way of assessing the radar performance. It is basically the image of a point target, i.e., that of a delta-type scatterer. In the ideal world, this image would be a delta-function as well. In reality, however, it is smeared out (by the nature of the radar signal processing, even when there is no ionosphere and no dispersion), and the extent of this smearing provides the limits of radar resolution.

The interrogating pulses emitted by the antenna of a SAR are taken as linear upchirps[2] of the form:

$$P(t) = A(t)e^{i\omega_0 t}, \quad \text{where} \quad A(t) = \chi_\tau(t)e^{i\alpha t^2}. \tag{2.13}$$

In formula (2.13), $\chi_\tau(t)$ is the indicator function of the interval of duration τ:

$$\chi_\tau(t) = \begin{cases} 1, & t \in [-\tau/2, \tau/2], \\ 0, & \text{otherwise}, \end{cases}$$

and $\alpha = B/(2\tau)$, where B is the bandwidth of the chirp. Accordingly, the instantaneous frequency of the chirp [Che01, CB09] is given by

$$\omega(t) = \omega_0 + \frac{Bt}{\tau}, \quad t \in [-\tau/2, \tau/2], \tag{2.14}$$

[2]High-range resolution waveforms, see [CB09].

where ω_0 is the center carrier frequency. The modulating function $A(t)$ in formula (2.13) is assumed slowly varying compared to the fast carrier oscillation $e^{i\omega_0 t}$. A typical duration of the pulse in actual SAR systems may be $\tau \sim 5 \cdot 10^{-5} sec$, a typical interval between two consecutive pulses $\sim 5 \cdot 10^{-4} sec$, and the bandwidth in formula (2.14) is $B \sim 10 MHz$ (it may be higher).

Hereafter, the radar is assumed to operate in the stripmap mode, see [CGM95], when the antenna points in a fixed direction relative to that of the satellite motion.[3] Hence, the footprint of the beam emitted by the antenna sweeps a strip on the Earth's surface parallel to the flight track, i.e., to the orbit.

To obtain the image, the antenna emits a series of pulses (2.13) when moving along the orbit. Those pulses travel to the Earth's surface, get scattered off the ground, and propagate back toward the satellite where they are received by the same antenna (in the case of a monostatic SAR [CGM95]). In doing so, clearly, both the emission and the reception of pulses are done by a moving antenna (which gives rise to the Doppler frequency shift) and moreover, the satellite travels a certain distance along the orbit during the pulse round-trip time between the antenna and the ground. However, in a simplified framework of the start-stop approximation those effects are disregarded. Instead, we assume that the pulse is emitted and the scattered response received while the antenna is at standstill at one and the same position, after which it moves to its next sending/receiving position along the orbit. This assumption has been used extensively in the SAR literature as it renders the corresponding analysis much easier. It, however, needs to be justified, especially when the antenna moves fast, such as when it is mounted on a satellite as opposed to an airplane. A full justification for the use of start-stop approximation for spaceborne SAR imaging can be found in [Tsy09b], see also Section 3 of this report.

2.3.1. Non-dispersive propagation. We first derive the generalized ambiguity function for the case of unobstructed propagation with the speed c. In this case, the field is governed by the standard d'Alembert equation, which is obtained from the Klein-Gordon equation (2.6) by dropping the last term, i.e., by setting $\omega_{\rm pe} = 0$. Suppose that the antenna is a motionless point source located at $\boldsymbol{x} \in \mathbb{R}^3$. Then, the propagating field due to the emitted chirp (2.13) is given by the standard retarded potential of the d'Alembert operator:

$$\varphi(t, \boldsymbol{z}) = \frac{1}{4\pi} \frac{P(t - |\boldsymbol{z} - \boldsymbol{x}|/c)}{|\boldsymbol{z} - \boldsymbol{x}|}. \tag{2.15}$$

Let us assume that the imaged terrain, which is also motionless, is characterized by the variable refraction index $n = n(\boldsymbol{z})$. Under the first Born approximation [BW99, Sec. 13.1.4], scattering is linearized so that the terrain is interpreted as a secondary waves' source due to the incident field $\varphi(t, \boldsymbol{z})$ of (2.15):

$$\frac{1 - n^2(\boldsymbol{z})}{c^2} \frac{\partial^2 \varphi}{\partial t^2} \stackrel{\rm def}{=} \nu(\boldsymbol{z}) \frac{\partial^2 \varphi}{\partial t^2}.$$

Consequently, the scattered field at the location $\boldsymbol{x}$ of the antenna and the moment of time t is given by the Kirchhoff integral:

$$\psi(t, \boldsymbol{x}) = \frac{1}{4\pi} \iiint\limits_{|\boldsymbol{x} - \boldsymbol{z}| \le ct} \frac{\nu(\boldsymbol{z})}{|\boldsymbol{x} - \boldsymbol{z}|} \frac{\partial^2 \varphi}{\partial t^2} \left(t - |\boldsymbol{x} - \boldsymbol{z}|/c, \boldsymbol{z}\right) d\boldsymbol{z}. \tag{2.16}$$

As the amplitude $A(t)$ in (2.13) is slowly varying, it can be left out when differentiating the incident field (2.15) for substitution into (2.16), which yields:

$$\frac{\partial^2 \varphi}{\partial t^2}(t, \boldsymbol{z}) \approx -\frac{\omega_0^2}{4\pi} \frac{P(t - |\boldsymbol{z} - \boldsymbol{x}|/c)}{|\boldsymbol{z} - \boldsymbol{x}|}. \tag{2.17}$$

Consequently,

$$\begin{aligned} \psi(t, \boldsymbol{x}) \approx & -\frac{\omega_0^2}{16\pi^2} \iiint\limits_{|\boldsymbol{x} - \boldsymbol{z}| \le ct} \frac{\nu(\boldsymbol{z})}{|\boldsymbol{x} - \boldsymbol{z}|^2} P\left(t - 2|\boldsymbol{x} - \boldsymbol{z}|/c\right) d\boldsymbol{z} \\ = & -\frac{\omega_0^2}{16\pi^2} \iiint\limits_{|\boldsymbol{x} - \boldsymbol{z}| \le ct} \frac{\nu(\boldsymbol{z})}{|\boldsymbol{x} - \boldsymbol{z}|^2} A\left(t - 2|\boldsymbol{x} - \boldsymbol{z}|/c\right) e^{i\omega_0 (t - 2|\boldsymbol{x} - \boldsymbol{z}|/c)} d\boldsymbol{z}. \end{aligned} \tag{2.18}$$

[3] When this direction is normal to the flight track, the imaging is referred to as broadside.

According to (2.18), the scattered field $\psi(t,\boldsymbol{x})$ can be interpreted a result of application of a Fourier integral operator (FIO) to the ground reflectivity function $\nu(\boldsymbol{z})$, see, e.g., [CN04, NC04, CB08, CB09].The FIO is approximately inverted by applying a matched filter to ψ and accumulating the information due to multiple interrogating pulses (2.13) emitted from and received by the antenna at different locations on the orbit. This procedure is similar to application of the adjoint operator, which would have coincided with the true inverse if the mapping (2.18) was a standard Fourier transform.

The matched filter is defined as follows. Assume that there is a point scatterer at the reference location $\boldsymbol{y}$, then the resulting field at $(t,\boldsymbol{x})$ is obtained by substituting $\nu(\boldsymbol{z})=\delta(\boldsymbol{z}-\boldsymbol{y})$ into formula (2.18):

$$\psi_1(t,\boldsymbol{x}) = -\frac{\omega_0^2}{16\pi^2}\frac{P(t-2|\boldsymbol{x}-\boldsymbol{y}|/c)}{|\boldsymbol{x}-\boldsymbol{y}|^2}. \tag{2.19}$$

The filter is essentially a complex conjugate of ψ_1 given by (2.19); for simplicity, the constant factor $-\omega_0^2/16\pi^2$, as well the entire denominator, which is a slowly varying function (compared to the fast oscillation $e^{i\omega_0 t}$), are disregarded. What remains is merely $\overline{P(t-2|\boldsymbol{x}-\boldsymbol{y}|/c)}$, where the overbar denotes complex conjugation. The idea of building the filter this way, i.e., the idea of matching, is to have the large phase cancel in the exponent, see formula (2.13). The application of this filter yields a single-look image:

$$\begin{aligned} I(\boldsymbol{y}) &= \int \overline{P(t-2|\boldsymbol{x}-\boldsymbol{y}|/c)}\psi(t,\boldsymbol{x})dt \\ &= -\frac{\omega_0^2}{16\pi^2}\iiint\limits_{|\boldsymbol{x}-\boldsymbol{z}|\le ct} \underbrace{\int \overline{P(t-2|\boldsymbol{x}-\boldsymbol{y}|/c)}P(t-2|\boldsymbol{x}-\boldsymbol{z}|/c)dt}_{W(\boldsymbol{y},\boldsymbol{z})}\frac{\nu(\boldsymbol{z})}{|\boldsymbol{x}-\boldsymbol{z}|^2}d\boldsymbol{z}, \end{aligned} \tag{2.20}$$

where we have changed the order of integration after substituting expression (2.18) for $\psi(t,\boldsymbol{x})$. The interior integral $W(\boldsymbol{y},\boldsymbol{z})$ in formula (2.20) is called the point spread function, see [Che01, CB09]. Up to a slowly varying denominator, the point spread function $W(\boldsymbol{y},\boldsymbol{z})$ yields a single-look image of the point scatterer located at $\boldsymbol{z}$, i.e., it is the field due to a unit magnitude delta-function at $\boldsymbol{z}$ processed with the matched filter $\overline{P(\,\cdot\,)}$.

As, however, has been mentioned, the full SAR image is built using multiple looks, when the antenna emits a sequence of chirps (2.13) from different locations on the orbit. It is precisely this approach based on incorporating the information from multiple looks that enables drastic improvements in the quality of the image compared to the single look strategy [Che01, CB09]. Let us therefore consider a sequence of emitting/receiving times and locations $(t_n,\boldsymbol{x}^n)$. For each n, we build the point spread function following (2.20):

$$W_n(\boldsymbol{y},\boldsymbol{z}) = \int \overline{P(t-t_n-2|\boldsymbol{x}^n-\boldsymbol{y}|/c)}P(t-t_n-2|\boldsymbol{x}^n-\boldsymbol{z}|/c)dt. \tag{2.21}$$

The generalized ambiguity function of a SAR system takes into account the information from multiple interrogating pulses by summing up the corresponding contributions (2.21):

$$W(\boldsymbol{y},\boldsymbol{z}) = \sum_n \vartheta(\boldsymbol{z},\boldsymbol{x}^n)W_n(\boldsymbol{y},\boldsymbol{z}). \tag{2.22}$$

The factor $\vartheta(\boldsymbol{z},\boldsymbol{x}^n)$ under the sum in (2.22) determines the range of summation. It comes from the directivity pattern of the antenna, because the actual SAR antenna is never a point monopole. The quantity $\vartheta(\boldsymbol{z},\boldsymbol{x}^n)$ can be approximated as follows:

$$\vartheta(\boldsymbol{z},\boldsymbol{x}^n) = \begin{cases} 1, & \text{if the target } \boldsymbol{z} \text{ is in the beam emitted from } \boldsymbol{x}^n, \\ 0, & \text{otherwise.} \end{cases}$$

In [Tsy09a, App. B] (see also [Che01, CB09]) we have shown that the antenna of longitudinal dimension L emits a beam of angular width $2\lambda/L$ provided that the carrier wavelength $\lambda = 2\pi c/\omega_0$ is much shorter

than L. Consequently, the longitudinal size of the antenna footprint on the ground in the case of broadside imaging is

$$R_0 \tan \frac{\lambda}{L} \approx R_0 \frac{\lambda}{L},$$

where R_0 is the distance from the location of the antenna $\boldsymbol{x}^n$ to the center of the footprint. Therefore,

$$\vartheta(\boldsymbol{z}, \boldsymbol{x}^n) = \begin{cases} 1, & \text{if } z_1 - R_0 \frac{\lambda}{L} \le x_1^n \le z_1 + R_0 \frac{\lambda}{L}, \\ 0, & \text{if } x_1^n < z_1 - R_0 \frac{\lambda}{L} \text{ or } x_1^n > z_1 + R_0 \frac{\lambda}{L}, \end{cases} \tag{2.23}$$

where the subscript "1" denotes the coordinate direction along the flight track (orbit).

The range of summation in (2.22) is therefore defined by taking into account only those $\boldsymbol{x}^n$, for which $\vartheta(\boldsymbol{z}, \boldsymbol{x}^n) = 1$, see (2.23). Let Δx_1 be the distance along the orbit between the successive emissions of pulses. We can also take $z_1 = 0$ with no loss of generality. Then, the inequality $-\frac{\lambda R_0}{L} \le x_1^n \le \frac{\lambda R_0}{L}$ translates into $-\frac{N}{2} \le n \le \frac{N}{2}$, where $N = \left[\frac{2\lambda R_0}{\Delta x_1 L}\right]$ and $[\,\cdot\,]$ is the integer part. Consequently, we recast (2.21), (2.22) as

$$\begin{aligned} W(\boldsymbol{y}, \boldsymbol{z}) = \sum_{-N/2}^{N/2} \int & \overline{A(t - t_n - 2|\boldsymbol{y} - \boldsymbol{x}^n|/c)} e^{2i\omega_0 |\boldsymbol{y} - \boldsymbol{x}^n|/c} \\ & \times A(t - t_n - 2|\boldsymbol{z} - \boldsymbol{x}^n|/c) e^{-2i\omega_0 |\boldsymbol{z} - \boldsymbol{x}^n|/c} dt. \end{aligned} \tag{2.24}$$

Next, we change the integration variable from t to $t - t_n$ in each term of the sum (2.24) and realize that neither $\overline{A(t - 2|\boldsymbol{y} - \boldsymbol{x}^n|/c)}$ nor $A(t - 2|\boldsymbol{z} - \boldsymbol{x}^n|/c)$ depends on n explicitly, except for the dependence via $\boldsymbol{x}^n$. The latter is weak, because for large R_0 both $|\boldsymbol{y} - \boldsymbol{x}^n|$ and $|\boldsymbol{z} - \boldsymbol{x}^n|$ are slowly varying functions of $\boldsymbol{x}^n$, and they appear as arguments of another slowly varying function, A. Hence, the factors $\bar{A}$ and A can be taken out of the sum (2.24), and $\boldsymbol{x}^n$ inside $\overline{A(\,\cdot\,)}$ and $A(\,\cdot\,)$ can be replaced by $\boldsymbol{x}^0$ for definiteness, which yields:

$$W(\boldsymbol{y}, \boldsymbol{z}) \approx \Big(\underbrace{\int \overline{A(t - 2|\boldsymbol{y} - \boldsymbol{x}^0|/c)} A(t - 2|\boldsymbol{z} - \boldsymbol{x}^0|/c) dt}_{W_R(\boldsymbol{y}, \boldsymbol{z})} \Big) \Big(\underbrace{\sum_{-N/2}^{N/2} e^{2i\omega_0 (|\boldsymbol{y} - \boldsymbol{x}^n|/c - |\boldsymbol{z} - \boldsymbol{x}^n|/c)}}_{W_A(\boldsymbol{y}, \boldsymbol{z})} \Big). \tag{2.25}$$

Hence, the generalized ambiguity function gets approximately split into the product of the range factor:

$$W_R(\boldsymbol{y}, \boldsymbol{z}) = \int \overline{A(t - 2|\boldsymbol{y} - \boldsymbol{x}^0|/c)} A(t - 2|\boldsymbol{z} - \boldsymbol{x}^0|/c) dt \tag{2.26}$$

and the azimuthal factor:

$$W_A(\boldsymbol{y}, \boldsymbol{z}) = \sum_{n=-N/2}^{N/2} e^{2i\omega_0 (|\boldsymbol{y} - \boldsymbol{x}^n|/c - |\boldsymbol{z} - \boldsymbol{x}^n|/c)}. \tag{2.27}$$

that control the range and azimuthal resolution of the radar,[4] respectively, see [Che01, CB09], in the case of unobstructed propagation between the orbit and the ground. Indeed, the generalized ambiguity function (2.25) is the image of a delta-type scatterer. Hence, if we could make it equal to a delta-function as well, $W(\boldsymbol{y}, \boldsymbol{z}) = \delta(\boldsymbol{y} - \boldsymbol{z})$, then the radar would have had perfect resolution. In reality this is never achieved, and instead $W(\boldsymbol{y}, \boldsymbol{z})$ has a peak of finite height and finite width when the reference point $\boldsymbol{y}$ approaches the target $\boldsymbol{z}$. The sharper (i.e., the narrower) this peak the better the resolution, because two sharper peaks can be told apart if they are closer.

[4] Resolution is a capability of the radar to distinguish between two different targets located a certain distance apart.

2.3.2. Dispersive propagation in the homogeneous medium. In the case of propagation through the ionosphere, both the shape and the speed of the pulse change because of the dispersion. The simplest case to analyze is that of a homogeneous ionosphere; a detailed analysis (based on the Fourier transform and linearization) is provided in Appendix A. The form of the propagating pulse emitted by the antenna at $\boldsymbol{x}$ is given by equation (A.16) [cf. formula (2.15)]:

$$\varphi(t,\boldsymbol{z}) = \frac{A'(t-|\boldsymbol{z}-\boldsymbol{x}|/v_{\rm gr}(\omega_0))}{4\pi|\boldsymbol{z}-\boldsymbol{x}|}e^{i\omega_0(t-|\boldsymbol{z}-\boldsymbol{x}|/v_{\rm ph}(\omega_0))}, \qquad \text{where} \quad A'(t)=\chi_{\tau'}(t)e^{i\alpha' t^2}, \tag{2.28}$$

and τ' and α' are the new chirp duration and rate given by equations (A.12) and (A.15), respectively:

$$\tau' = \tau + \delta\tau = \tau + 2\frac{|\boldsymbol{z}-\boldsymbol{x}|}{c}\frac{\omega_{\rm pe}^2}{\omega_0^2}\frac{B}{\omega_0}, \tag{2.29}$$

and

$$\alpha' = \alpha + \delta\alpha = \alpha - \frac{|\boldsymbol{z}-\boldsymbol{x}|}{c}\frac{\omega_{\rm pe}^2}{\omega_0^3}\frac{B^2}{\tau^2} = \alpha - \frac{\delta\tau}{2}\frac{B}{\tau^2} = \frac{B}{2\tau}\left(1-\frac{\delta\tau}{\tau}\right). \tag{2.30}$$

Let us emphasize that unlike in a vacuum, the shape of the pulse keeps changing as it propagates through the plasma; according to (2.29) and (2.30), the longer the distance $|\boldsymbol{z}-\boldsymbol{x}|$ that the pulse travels, the more it gets dilated (τ' becomes longer) and the more its rate decreases (α' becomes smaller).

We also emphasize that as formula (2.28) indicates, the chirp itself, i.e., its slowly varying envelope A' which presents a physical observable, travels with the group velocity $v_{\rm gr}(\omega_0)$ that corresponds to the center carrier frequency ω_0. For the high frequency case that we are interested in, $\omega_0 \gg \omega_{\rm pe}$, the group velocity (2.5) can be linearized:

$$v_{\rm gr} = v_{\rm gr}(\omega) \approx c\left(1-\frac{1}{2}\frac{\omega_{\rm pe}^2}{c^2k^2}\right) = c\left(1-\frac{1}{2}\frac{\omega_{\rm pe}^2}{\omega^2-\omega_{\rm pe}^2}\right) \approx c\left(1-\frac{1}{2}\frac{\omega_{\rm pe}^2}{\omega^2}\right). \tag{2.31}$$

At the same time, the center carrier oscillation per se, i.e., the wave $e^{i\omega_0 t}$, travels with the corresponding phase velocity $v_{\rm ph}(\omega_0)$ that can also be linearized:

$$v_{\rm ph} = v_{\rm ph}(\omega) \approx c\left(1+\frac{1}{2}\frac{\omega_{\rm pe}^2}{c^2k^2}\right) = c\left(1+\frac{1}{2}\frac{\omega_{\rm pe}^2}{\omega^2-\omega_{\rm pe}^2}\right) \approx c\left(1+\frac{1}{2}\frac{\omega_{\rm pe}^2}{\omega^2}\right). \tag{2.32}$$

Using the notions of the group and phase velocity (2.31) and (2.32), we can introduce the group and phase travel times, respectively, in the homogeneous ionosphere:

$$T_{\rm gr}(\boldsymbol{x},\boldsymbol{z},\omega) = \frac{|\boldsymbol{x}-\boldsymbol{z}|}{v_{\rm gr}(\omega)} \quad \text{and} \quad T_{\rm ph}(\boldsymbol{x},\boldsymbol{z},\omega) = \frac{|\boldsymbol{x}-\boldsymbol{z}|}{v_{\rm ph}(\omega)}, \tag{2.33}$$

and recast formula (2.28) as follows:

$$\varphi(t,\boldsymbol{z}) = \frac{A'(t-T_{\rm gr}(\boldsymbol{x},\boldsymbol{z},\omega_0))}{4\pi|\boldsymbol{z}-\boldsymbol{x}|}e^{i\omega_0(t-T_{\rm ph}(\boldsymbol{x},\boldsymbol{z},\omega_0))}. \tag{2.34}$$

It is important to point out that the group velocity $v_{\rm gr}$ of (2.31) is slower than the speed of light c, as it is supposed to be for any velocity associated with the propagation of physical observables. However, the phase velocity $v_{\rm ph}$ (2.32) is faster than the speed of light c, because the dispersion in the ionosphere is anomalous. Hence, if we introduce the neutral (non-dispersive) travel time $T = T(\boldsymbol{x},\boldsymbol{z}) = |\boldsymbol{x}-\boldsymbol{z}|/c$, then, according to (2.31) and (2.32), for the group and phase travel time we can write:

$$T_{\rm gr}(\boldsymbol{x},\boldsymbol{z},\omega) = T(\boldsymbol{x},\boldsymbol{z}) + \Delta T \quad \text{and} \quad T_{\rm ph}(\boldsymbol{x},\boldsymbol{z},\omega) = T(\boldsymbol{x},\boldsymbol{z}) - \Delta T, \qquad \text{where} \quad \Delta T = \Delta T(\boldsymbol{x},\boldsymbol{z},\omega) = \frac{|\boldsymbol{x}-\boldsymbol{z}|}{c}\frac{1}{2}\frac{\omega_{\rm pe}^2}{\omega^2}. \tag{2.35}$$

In other words, the group delay and the phase advance in formula (2.34) are equal to one another. Given (2.35), we can recast formula (2.29) for the pulse dilation as follows:

$$\delta\tau = 4\Delta T(\boldsymbol{x}, \boldsymbol{z}, \omega_0)\frac{B}{\omega_0}. \tag{2.36}$$

It shall also be noted that in our work [Tsy09a], we used a simpler semi-qualitative approach to analyze the propagation of chirps in the ionosphere. The result was the same as (2.34) with one important difference though: Instead of the phase advance that characterizes the propagation of the carrier frequency in formula (2.34), in [Tsy09a] we have incorporated a phase delay equal to the group delay. This could not affect the analysis of the range resolution as it is based on the propagation of envelopes, see formula (2.26). On the other hand, this could potentially affect our analysis of the azimuthal resolution in [Tsy09a], as the azimuthal factor of the generalized ambiguity function (2.27) includes the phase information. However, as shown in [ST10], our previous calculations of the azimuthal resolution are not affected either, because in the linearized high frequency framework that we employ, the group delay and the phase advance are equal in magnitude, see formulae (2.35).

2.3.3. Dispersive propagation in the inhomogeneous medium. In the actual ionosphere, the electron number density N_e is not constant, and this is going to affect the propagation times (2.33). For our subsequent analysis, we will assume that the mean electron number density $\langle N_\mathrm{e}\rangle$ depends on the altitude above the Earth's surface, but does not depend on the horizontal coordinates. A typical dependence of the mean electron number density on the altitude h is non-monotonic. The maximum is reached in the F-layer somewhere between $200km$ and $300km$ above the Earth's surface, and the characteristic scale h_0 of the variations of $\langle N_\mathrm{e}\rangle$ is on the order of tens of kilometers, see [Gin64, Ch. VI]. Clearly, $h_0 \gg \lambda$, where λ is the wavelength, which suggests that we can perhaps use the approximation of geometrical optics to analyze the propagation of SAR pulses in the inhomogeneous ionosphere.

We should remember, however, that the total electron number density N_e also has a stochastic component $\mu(\boldsymbol{x})$, see formula (2.7). It depends on all spatial coordinates, and can be interpreted as a quasi-homogeneous random field. To justify the use of geometrical optics for the study of pulse propagation through the turbulent ionosphere, the wavelength λ must be much shorter than the characteristic scale of turbulent inhomogeneities. If the latter is taken as r_0 (the outer scale of turbulence), the constraint $\lambda \ll r_0$ is obviously met. There is, however, a more subtle criterion for applicability of the geometrical optics. The characteristic scale of inhomogeneities must be much longer than the size of the first Fresnel zone $\sqrt{\lambda R_{\boldsymbol{z}}}$, where $R_{\boldsymbol{z}} = |\boldsymbol{z} - \boldsymbol{x}|$ is the propagation distance between the antenna and the target. The quantity $\sqrt{\lambda R_{\boldsymbol{z}}}$ comes to approximately $540m$ for $\lambda = 30cm$ and $R_{\boldsymbol{z}} = 1000km$, which is roughly $\frac{1}{2}r_0$ according to [Arm05] or $\frac{1}{20}r_0$ according to [BG88]. Technically speaking, this makes the geometrical optics a borderline approximation for the class of problems we are considering. It is known however, that there are fewer shorter scale inhomogeneities in the spectrum of ionospheric turbulence than longer scale inhomogeneities, which still leaves the main conclusions of geometrical optics valid even outside its formal applicability range, see [RKT89b, Ch. I].

The expressions for travel times in the inhomogeneous ionosphere that replace formulae (2.33) are derived in Appendix B for the deterministic case and in Appendix C for the stochastic case. The final expressions that we present correspond to the stochastic formulae (C.15) and (C.16); they reduce to the deterministic formulae (B.21) and (B.22) if $\mu = 0$:

$$T_\mathrm{gr}(\boldsymbol{x}, \boldsymbol{z}, \omega) = \frac{R_{\boldsymbol{z}}}{c}\left[1 + \frac{1}{2}\frac{4\pi e^2}{m_\mathrm{e}\omega^2}\left(\frac{\bar{N}_\mathrm{e}^{(H)}}{H} + \frac{1}{R_{\boldsymbol{z}}}\int_0^{R_{\boldsymbol{z}}}\mu(s)ds\right)\right], \tag{2.37a}$$

$$T_\mathrm{ph}(\boldsymbol{x}, \boldsymbol{z}, \omega) = \frac{R_{\boldsymbol{z}}}{c}\left[1 - \frac{1}{2}\frac{4\pi e^2}{m_\mathrm{e}\omega^2}\left(\frac{\bar{N}_\mathrm{e}^{(H)}}{H} + \frac{1}{R_{\boldsymbol{z}}}\int_0^{R_{\boldsymbol{z}}}\mu(s)ds\right)\right]. \tag{2.37b}$$

The quantity $\bar{N}_\mathrm{e}^{(H)}$ in formulae (2.37) is defined by (C.8), and H denotes the orbit altitude. Similarly to

(2.35), we can also write:

$$T_{\rm gr}(\boldsymbol{x},\boldsymbol{z},\omega)=T(\boldsymbol{x},\boldsymbol{z})+\Delta T \quad \text{and} \quad T_{\rm ph}(\boldsymbol{x},\boldsymbol{z},\omega)=T(\boldsymbol{x},\boldsymbol{z})-\Delta T,$$

$$\text{where} \quad T(\boldsymbol{x},\boldsymbol{z})=\frac{R_{\boldsymbol{z}}}{c} \quad \text{and} \quad \Delta T=\Delta T(\boldsymbol{x},\boldsymbol{z},\omega)=\frac{R_{\boldsymbol{z}}}{c}\frac{1}{2}\frac{4\pi e^2}{m_{\rm e}\omega^2}\underbrace{\left(\frac{\bar{N}_{\rm e}^{(H)}}{H}+\frac{1}{R_{\boldsymbol{z}}}\int\limits_0^{R_z}\mu(s)ds\right)}_{\mathcal{N}}. \tag{2.38}$$

Given the travel times (2.38), we can evaluate the dilation of the pulse on its way between the antenna $\boldsymbol{x}$ and the target $\boldsymbol{z}$ using formula (2.36):

$$\delta\tau=4\Delta T(\boldsymbol{x},\boldsymbol{z},\omega_0)\frac{B}{\omega_0}=\frac{2R_{\boldsymbol{z}}}{c}\frac{4\pi e^2}{m_{\rm e}\omega_0^2}\frac{B}{\omega_0}\mathcal{N}. \tag{2.39}$$

On the way between the antenna and the target and back, the dilation (2.39) doubles because the travel distance doubles. The pulse rate (2.30) changes accordingly.

Finally, we can modify the generalized ambiguity function derived in Section 2.3.1, see formula (2.25), by substituting the actual travel times (2.37) instead of the unobstructed travel time $|\boldsymbol{z}-\boldsymbol{x}^0|/c$ into those factors that correspond to the received signal. According to the form (2.34) of the propagating pulse, the group travel time $T_{\rm gr}(\boldsymbol{x}^0,\boldsymbol{z},\omega_0)$ of (2.37a) shall be substituted into $W_R(\boldsymbol{y},\boldsymbol{z})$ and the phase travel time $T_{\rm ph}(\boldsymbol{x}^n,\boldsymbol{z},\omega_0)$ of (2.37b) shall be substituted into $W_A(\boldsymbol{y},\boldsymbol{z})$. Then, instead of formulae (2.26) and (2.27) we have:

$$W_R'(\boldsymbol{y},\boldsymbol{z})=\int\overline{A(t-2|\boldsymbol{y}-\boldsymbol{x}^0|/c)}A_{2\delta\tau}'(t-2T_{\rm gr}(\boldsymbol{x}^0,\boldsymbol{z},\omega_0))dt \tag{2.40}$$

and

$$W_A'(\boldsymbol{y},\boldsymbol{z})=\sum_{n=-N/2}^{N/2}e^{2i\omega_0(|\boldsymbol{y}-\boldsymbol{x}^n|/c-T_{\rm ph}(\boldsymbol{x}^n,\boldsymbol{z},\omega_0))}. \tag{2.41}$$

The subscript $2\delta\tau$ in formula (2.40) indicates that the round trip pulse dilation is twice the $\delta\tau$ of (2.39).

We emphasize that in formulae (2.40) and (2.41) the factors that correspond to the actual field received by the antenna take into account the dispersion of radio waves in the ionosphere. However, the factors that represent the matched filter remain the same as in the non-dispersive case. This creates a mismatch, and as has been shown in [Tsy09a], it is precisely this mismatch that is responsible for the deterioration of the image. In the next section, we briefly reproduce the corresponding arguments from [Tsy09a]. It will also help us better understand the mechanism of correcting the matched filter.

2.4. Performance of the radar with non-corrected filter.

2.4.1. Range resolution. Integration (2.40) has been performed in [Tsy09a, App. C]. Up to a factor of magnitude one, integral (2.40) takes the form:

$$W_R'(\boldsymbol{y},\boldsymbol{z})\propto\int_{\max\{-\tau/2+2R_{\boldsymbol{y}}/c,\,-\tau'/2+2T_{\rm gr}(\boldsymbol{x}^0,\boldsymbol{z},\omega_0)\}}^{\min\{\tau/2+2R_{\boldsymbol{y}}/c,\,\tau'/2+2T_{\rm gr}(\boldsymbol{x}^0,\boldsymbol{z},\omega_0)\}}e^{i(\alpha'-\alpha)t^2}e^{4i(\alpha R_{\boldsymbol{y}}/c-\alpha' T_{\rm gr}(\boldsymbol{x}^0,\boldsymbol{z},\omega_0))t}dt, \tag{2.42}$$

where $R_{\boldsymbol{y}}=|\boldsymbol{y}-\boldsymbol{x}^0|$. In the simplest case, we disregard the quadratic term in the exponent under the integral (2.42). Then, taking the limits as $\mp\tau/2+2R_{\boldsymbol{y}}/c$ and changing the integration variable: $t=u+2R_{\boldsymbol{y}}/c$, we have:

$$W_R'(\boldsymbol{y},\boldsymbol{z})\propto\tau\,\mathrm{sinc}\left(2[\alpha' R_{\boldsymbol{y}}/c-\alpha' T_{\rm gr}(\boldsymbol{x}^0,\boldsymbol{z},\omega_0)]\tau\right). \tag{2.43}$$

When analyzing radar resolution, the $\mathrm{sinc}\,x\stackrel{\rm def}{=}\frac{\sin x}{x}$ function is what one typically gets instead of the "genuine" δ-function, see [Che01,CB09]. The sharper the central peak of the sinc (i.e., its main lobe between

the first zeros on either side of the maximum), the "closer" it is to the δ-function and hence the better the resolution. The width (or sometimes, semi-width) of the main lobe of the sinc is actually taken as a measure of radar resolution, because it is considered the distance at which two such peaks can be clearly told apart.

In the non-dispersive case $T(\boldsymbol{x}^0, \boldsymbol{z}, \omega_0) = R_{\boldsymbol{z}}/c$ and $\alpha' = \alpha$. Hence, $W'_R(\boldsymbol{y}, \boldsymbol{z})$ reduces to $W_R(\boldsymbol{y}, \boldsymbol{z})$ and consequently, the sinc attains its maximum when $R_{\boldsymbol{y}} = R_{\boldsymbol{z}}$, i.e., when the distance from the antenna to the reference location $\boldsymbol{y}$ coincides with that for the target location $\boldsymbol{z}$. The resolution is then controlled by how widely the sinc is "spread around" its central maximum. The semi-width of the main lobe of the sinc corresponds to the value of its argument equal to π and therefore, for the full width we find $\Delta R = 2\pi c/B$. It is the quantity ΔR that is interpreted as the range resolution, i.e., the minimum distance, at which the SAR system can distinguish between two point targets located on the same line of sight normal to the orbit.

The situation with the dispersive range factor $W'_R(\boldsymbol{y}, \boldsymbol{z})$ of (2.43) is somewhat different. The maximum of the sinc is attained when its full argument is zero, i.e., when $R_{\boldsymbol{y}} = cT(\boldsymbol{x}^0, \boldsymbol{z}, \omega_0)$, which yields:

$$R_{\boldsymbol{y}} - R_{\boldsymbol{z}} = cT(\boldsymbol{x}^0, \boldsymbol{z}, \omega_0) - R_{\boldsymbol{z}} = R_{\boldsymbol{z}} \frac{1}{\omega_0^2} \frac{4\pi e^2}{2m_{\mathrm{e}}} \mathcal{N}. \tag{2.44}$$

This is obviously not equivalent to $R_{\boldsymbol{y}} - R_{\boldsymbol{z}} = 0$, which implies that on the image the target is shifted in range from its absolute position by the value of the right hand side of (2.44). The range resolution per se, however, is still given by the width of the main lobe of the sinc as a function of the argument $R_{\boldsymbol{y}} - R_{\boldsymbol{z}}$:

$$\Delta R = \frac{\pi c}{\alpha' \tau} = \frac{2\pi c}{B} \left(1 + \frac{2\delta\tau}{\tau} \right). \tag{2.45}$$

The factor of 2 in front of $\delta\tau$ in equation (2.45) appears because the pulse dilation is evaluated for the round-trip between the antenna and the target. The relative deterioration of the range resolution compared to the non-dispersive case is therefore $\sim 2\delta\tau/\tau$, see (2.45). As shown in [Tsy09a], for the typical values of all the relevant parameters in the deterministic ionosphere this quantity is very small, about 0.02%.

If the quadratic term is retained in the exponent under the integral (2.42) after the change of variables, then the integration yields a complex-valued function $W'_R(\boldsymbol{y}, \boldsymbol{z})$ rather than the actual sinc. As shown in [Tsy09a], the maxima and minima of its absolute value $|W'_R(\boldsymbol{y}, \boldsymbol{z})|$ are located precisely where the maxima and zeros of the sinc are. In this sense, the range resolution remains unchanged. However, instead of the actual zeros the new $|W'_R(\boldsymbol{y}, \boldsymbol{z})|$ now has minima with some nonzero values. In particular, for the first minimum we have

$$|W'_R(\boldsymbol{y}, \boldsymbol{z})| \Big|_{4\alpha'(R_{\boldsymbol{y}}/c - T(\boldsymbol{x}^0, \boldsymbol{z}, \omega_0)) = \frac{2\pi}{\tau}} = \tau \frac{\delta\alpha\tau^2}{\pi^2} \left(1 + \mathcal{O}(\delta\alpha\tau^2) \right), \tag{2.46}$$

The right-hand side of equality (2.46) is about $0.02 \cdot \tau$ for the typical parameters involved. Therefore, the dispersion of radio waves in the ionosphere causes a deterioration of the image sharpness. As the central maximum of $|W'_R(\boldsymbol{y}, \boldsymbol{z})|$ basically remains equal to τ, the extent of deterioration appears 2%, but this value can, of course, vary both ways depending on the parameters of the radar and the conditions of the ionosphere.

Let us also recall that the quantity $\mathcal{N}$ that determines the dilation of the pulse and its new rate, see formulae (2.39) and (2.30), as well as the shift of the target position, see formula (2.44), does not only contain a deterministic component, but also a stochastic one. The latter is the average value of μ along the ray trajectory, see (2.37). Hence, based on the idea of ergodicity, and recalling that $\langle \mu \rangle = 0$, we can expect that the effect of the aforementioned stochastic component on the radar performance in range will not be large.

To quantify this argument further, we denote the random contribution to $T_{\mathrm{gr}}(\boldsymbol{x}^0, \boldsymbol{z}, \omega)$ by

$$\varphi_0 = \int_0^{R_{\boldsymbol{z}}} \mu(s) ds, \quad R_{\boldsymbol{z}} = |\boldsymbol{x}^0 - \boldsymbol{z}|, \quad \langle \varphi_0 \rangle = 0, \tag{2.47}$$

where the integration is conducted along the unperturbed trajectory, and also introduce the mean dilation according to (2.39):

$$\langle \delta\tau \rangle = \frac{2R_{\boldsymbol{z}}}{c} \frac{4\pi e^2}{m_{\mathrm{e}}\omega_0^2} \frac{B}{\omega_0} \langle \mathcal{N} \rangle = \frac{2R_{\boldsymbol{z}}}{c} \frac{4\pi e^2}{m_{\mathrm{e}}\omega_0^2} \frac{B}{\omega_0} \frac{\bar{N}_{\mathrm{e}}^{(H)}}{H}.$$

Standard deviations of both φ_0 and $\delta\tau$ were computed in [Tsy09a] using the spectrum of turbulent fluctuations (2.11). It was also shown that $\sqrt{\langle\varphi_0^2\rangle} \ll \bar{N}_{\rm e}^{(H)}$ and $\sqrt{\langle\delta\tau^2\rangle} \ll \langle\delta\tau\rangle$, or more precisely, for the case of a homogeneous ionosphere,

$$\frac{\sqrt{\langle\varphi_0^2\rangle}}{\bar{N}_{\rm e}^{(H)}} = \frac{\sqrt{\langle\delta\tau^2\rangle}}{\langle\delta\tau\rangle} \approx \sqrt{\frac{r_0}{R_{\boldsymbol{z}}}}M \ll 1,$$

where r_0 is the correlation length, and M is given by (2.9). In the case of a stratified ionosphere, the variance of fluctuations becomes a function of the altitude h: $\langle\mu^2\rangle = \langle\mu^2(h)\rangle$, and one can show [Tsy09a] that

$$\sqrt{\frac{\langle\varphi_0^2\rangle}{\bar{N}_{\rm e}^{2,(H)}\cdot H}} \approx \sqrt{\frac{r_0}{R_{\boldsymbol{z}}}}M, \quad \text{where} \quad \bar{N}_{\rm e}^{2,(H)} = \int\limits_0^H \langle N_{\rm e}(h)\rangle^2 dh. \tag{2.48}$$

According to [Arm05], the value of $\bar{N}_{\rm e}^{2,(H)}$ for high altitudes H is between $9.3\cdot 10^{18} cm^{-5}$ and $9.9\cdot 10^{20} cm^{-5}$, with the average about $1.5\cdot 10^{19} cm^{-5}$. Then, say, for $H = 500km$ we have $(\bar{N}_{\rm e}^{2,(H)}\cdot H)^{1/2} \approx 2.7\cdot 10^{13} cm^{-2}$, which is close to $\bar{N}_{\rm e}^{(H)} \sim \langle N_{\rm e}\rangle \cdot H \approx 5\cdot 10^{13} cm^{-2}$ if one takes $\langle N_{\rm e}\rangle = 10^6 cm^{-3}$. We therefore conclude that the contribution of turbulent fluctuations to travel delays, as well as to the change of the pulse shape during its propagation in the ionosphere, is much smaller than that of the baseline dispersion. Therefore, the role of randomness in the deterioration of SAR performance in range appears minute, and can be disregarded for the typical values of the parameters involved.

2.4.2. Azimuthal resolution. The azimuthal factor (2.41) of the generalized ambiguity function has also been computed in [Tsy09a]. Similarly to (2.47), let us denote

$$\varphi_n = \int\limits_0^{R_z} \mu(s)ds, \quad R_{\boldsymbol{z}} = |\boldsymbol{x}^n - \boldsymbol{z}|. \tag{2.49}$$

We also linearize the travel distances:

$$\begin{aligned} R_{\boldsymbol{z}} &= |\boldsymbol{z} - \boldsymbol{x}^n| = \sqrt{R_0^2 + (z_1 - x_1^n)^2} = R_0\sqrt{1 + \frac{(x_1^n)^2}{R_0^2}} \approx R_0\left(1 + \frac{1}{2}\frac{(x_1^n)^2}{R_0^2}\right), \\ R_{\boldsymbol{y}} &= |\boldsymbol{y} - \boldsymbol{x}^n| = \sqrt{R_0^2 + (y_1 - x_1^n)^2} = R_0\sqrt{1 + \frac{(y_1 - x_1^n)^2}{R_0^2}} \approx R_0\left(1 + \frac{1}{2}\frac{(y_1 - x_1^n)^2}{R_0^2}\right), \end{aligned} \tag{2.50}$$

because $|x_1^n| \ll R_0$ and $|y_1 - x_1^n| \ll R_0$, where R_0 is the distance along the normal (recall, the subscript "1" denotes the coordinate along the orbit, and $z_1 = 0$, as in Section 2.3.1). Then, up to a factor of magnitude one, formula (2.41) along with (2.37b) yields:

$$W'_A(\boldsymbol{y},\boldsymbol{z}) \propto \sum_{n=-N/2}^{N/2} e^{\frac{2i\omega_0}{c}\left(-\frac{y_1 x_1^n}{R_0} + \frac{1}{2}\frac{(x_1^n)^2}{2R_0}\frac{4\pi e^2}{m_{\rm e}\omega_0^2}\frac{\bar{N}_{\rm e}^{(H)}}{H} + \frac{1}{2}\frac{4\pi e^2}{m_{\rm e}\omega_0^2}\varphi_n\right)}. \tag{2.51}$$

According to the central limit theorem, for long integration distances $R_{\boldsymbol{z}}$ each quantity φ_n of (2.49) becomes a Gaussian random variable with zero mean, see [RKT89b, Ch. I]. Hence, the mean of each term of (2.51) is

$$\begin{aligned} &\left\langle e^{\frac{2i\omega_0}{c}\left(-\frac{y_1 x_1^n}{R_0} + \frac{1}{2}\frac{(x_1^n)^2}{2R_0}\frac{4\pi e^2}{m_{\rm e}\omega_0^2}\frac{\bar{N}_{\rm e}^{(H)}}{H} + \frac{1}{2}\frac{4\pi e^2}{m_{\rm e}\omega_0^2}\varphi_n\right)}\right\rangle \\ &= e^{\frac{2i\omega_0}{c}\left(-\frac{y_1 x_1^n}{R_0} + \frac{1}{2}\frac{(x_1^n)^2}{2R_0}\frac{4\pi e^2}{m_{\rm e}\omega_0^2}\frac{\bar{N}_{\rm e}^{(H)}}{H}\right)} \frac{1}{\sqrt{2\pi\langle\varphi_n^2\rangle}} \int\limits_{-\infty}^{\infty} e^{\frac{i\omega_0}{c}\frac{4\pi e^2}{m_{\rm e}\omega_0^2}\xi} e^{-\frac{\xi^2}{2\langle\varphi_n^2\rangle}} d\xi \\ &= e^{\frac{2i\omega_0}{c}\left(-\frac{y_1 x_1^n}{R_0} + \frac{1}{2}\frac{(x_1^n)^2}{2R_0}\frac{4\pi e^2}{m_{\rm e}\omega_0^2}\frac{\bar{N}_{\rm e}^{(H)}}{H}\right)} e^{-\frac{1}{2}\frac{\omega_0^2}{c^2}\left(\frac{4\pi e^2}{m_{\rm e}\omega_0^2}\right)^2\langle\varphi_n^2\rangle}, \end{aligned} \tag{2.52}$$

and the variance is given by (see [Tsy09a]):

$$\sigma_n^2 = e^{-\frac{\omega_0^2}{c^2}\left(\frac{4\pi e^2}{m_e\omega_0^2}\right)^2\langle\varphi_n^2\rangle}\left(e^{\frac{\omega_0^2}{c^2}\left(\frac{4\pi e^2}{m_e\omega_0^2}\right)^2\langle\varphi_n^2\rangle}-1\right)\approx\frac{\omega_0^2}{c^2}\left(\frac{4\pi e^2}{m_e\omega_0^2}\right)^2\langle\varphi_n^2\rangle. \tag{2.53}$$

The (dimensionless) quantity on the right-hand side of (2.53), which is obtained by Taylor's formula, is the variance of the phase; it is small for the typical values of the parameters involved. Thus, the decrease of the amplitude on the right-hand side of (2.52) is also small; in the literature it is known as extinction [RKT89b, Ch. I].

To obtain the mean and variance of the sum (2.51), we will assume that all individual variances (2.53) are the same, $\sigma_n^2=\sigma^2$, $n=-N/2,\dots,N/2$. To that effect we note that while the integration distance $R_{\boldsymbol{z}}$ in formula (2.49) depends on n, its variation compared to R_0 is small, see (2.50).

For the mean value of (2.51) we can therefore write using (2.52):

$$\langle W_A'(\boldsymbol{y},\boldsymbol{z})\rangle\ \propto\ e^{-\sigma^2/2}\sum_{n=-N/2}^{N/2}e^{\frac{2i\omega_0}{c}\left(-\frac{y_1x_1^n}{R_0}+\frac{1}{2}\frac{(x_1^n)^2}{2R_0}\frac{4\pi e^2}{m_e\omega_0^2}\frac{\bar N_e^{(H)}}{H}\right)}, \tag{2.54}$$

where the deterministic sum on the right-hand side of (2.54) controls the azimuthal resolution in the case of non-fluctuating ionosphere. There are two terms in the exponent on the right-hand side of (2.54). The first one, linear with respect to x_1^n, is the only thing that one would have obtained if the propagation was unobstructed. The second term, which is quadratic with respect to x_1^n, is due to the phase mismatch between the actual received signal subject to ionospheric delays and the non-corrected matched filter.

With no quadratic term we have

$$\sum_{n=-N/2}^{N/2}e^{-\frac{2i\omega_0}{c}\frac{y_1x_1^n}{R_0}}\approx(N+1)\mathrm{sinc}\frac{\omega_0y_1\Delta x_1(N+1)}{R_0c}, \tag{2.55}$$

where Δx_1 is the distance that the satellite travels along the orbit between the successive emission of pulses, $x_1^n=n\cdot\Delta x_1$, and we have assumed that $\frac{\omega_0y_1\Delta x_1}{R_0c}\ll1$, which holds for the typical values of all parameters. The semi-width of the main lobe of the sinc corresponds to the value of its argument equal to π:

$$\frac{2\pi y_1\Delta x_1}{R_0\lambda}\frac{2\lambda R_0}{\Delta x_1L}=\pi,$$

where we have replaced $N+1$ by $N=\left[\frac{2\lambda R_0}{\Delta x_1L}\right]\approx\frac{2\lambda R_0}{\Delta x_1L}$, because $N\gg1$ ($\Delta x_1\approx4m$ for the satellite travel speed of $8km/sec$). Consequently, the azimuthal resolution in the undistorted case is $2y_1=L/2$.

With the quadratic term taken into account, the function $\langle W_A'(\boldsymbol{y},\boldsymbol{z})\rangle$ of (2.54) becomes complex-valued. The central maximum of its modulus is attained when the argument is equal to zero, and the first minimum appears precisely where the first zero of the sinc (2.55) is. In this sense, the azimuthal resolution per se remains unaffected. However, similarly to the case of range resolution, the sharpness of the image deteriorates, and this deterioration for the azimuthal resolution appears stronger. Specifically, one can show [Tsy09a] that

$$|\langle W_A'(\boldsymbol{y},\boldsymbol{z})\rangle|\Big|_{\frac{\omega_0y_1\Delta x_1(N+1)}{R_0c}=\pi}\approx e^{-\sigma^2/2}\,(N+1)\frac{\omega_0(\Delta x_1)^2}{2R_0c}\frac{4\pi e^2}{m_e\omega_0^2}\frac{\bar N_e^{(H)}}{H}\frac{(N+1)^2}{2\pi^2}, \tag{2.56}$$

which is approximately $0.09\cdot(N+1)$ for the typical values of the parameters involved. Hence, there may be about 9% degradation of image sharpness in the azimuthal direction due to the dispersion of radio waves in the ionosphere.

The effect of randomness on the azimuthal resolution is also stronger than that on the range resolution. Recall, range resolution is basically determined by a single look, and because of the ergodicity the contribution of turbulent fluctuations into the radar reading on this single look effectively vanishes (i.e., averages out). On the contrary, azimuthal resolution is determined based on multiple looks, $n=-N/2,\dots,N/2$, and whereas the contribution of randomness into each individual reading is still small, it can get amplified when those individual readings are summed up. In [Tsy09a, ST10], we call this effect "un-averaging."

To estimate the variance of the sum (2.51) one needs to see to what extent the individual random variables that compose this sum are dependent or independent. Each of these random variables has a logarithmically normal probability distribution, and similarly to the standard Gaussian variables, if they are uncorrelated, they are independent [Tsy09a, App. F]. Therefore, the covariance (correlation function) of the received field along the synthetic antenna can provide a measure of dependence or independence for the random variables that compose the sum (2.51). In [RKT89b, Ch. I] it is shown that if the fluctuations of the phase are small, then the correlation function for the field approximately coincides with the correlation function for the electron number density (2.8). Consequently, the correlation length r_0, see formula formula (2.11), will also provide a characteristic scale of how rapidly the received field decorrelates along the synthetic antenna. Roughly speaking, for the locations that are further apart than r_0 the received pulses will be uncorrelated and hence independent, whereas for the locations that are closer than r_0 they will not be independent.

Based on these considerations, the following expression was obtained in [Tsy09a] for the variance of (2.51):

$$\sigma_\Sigma^2 = \frac{D}{r_0} N_c^2 \sigma^2 = \frac{r_0}{D}(N+1)^2\sigma^2, \tag{2.57}$$

where $D = R_0 \frac{2\lambda}{L}$ is the length of the synthetic array. It has also been shown in [Tsy09a] that the corresponding relative change of the azimuthal resolution is $\frac{\sigma}{2}\sqrt{\frac{r_0}{D}}$. This quantity is about 0.3% for the typical values of the parameters, and it is also proportional to $\omega_0^{-1/2}$, i.e., increases as the carrier frequency decreases.

A 0.3% degradation of the azimuthal resolution is not negligible but is still rather small. However, when estimating σ via $\langle\varphi^2\rangle$, see formulae (2.48) and (2.53), we have taken the average values for M and $N_{\rm e}^{2,(H)}$. Taking the corresponding values from the upper part of their respective ranges may result in a much larger value of $\langle\varphi^2\rangle$ and as such, in a noticeable deterioration of azimuthal resolution.

2.5. Dual carrier probing. To remove the mismatch that causes distortions of the image, one needs to correct the filter, i.e., replace the unobstructed travel times $|\boldsymbol{y}-\boldsymbol{x}^n|/c$ by $T_{\rm gr}(\boldsymbol{x}^n,\boldsymbol{y},\omega_0)$ in (2.40) and by $T_{\rm ph}(\boldsymbol{x}^n,\boldsymbol{y},\omega_0)$ in (2.41), and also adjust the chirp duration and chirp rate in the filter factor under the integral (2.40). However, unlike in the received field, which is a physical observable, the correction in the filter must be done theoretically. Therefore, one needs to know the quantity $\mathcal{N}$, see formula (2.38), that characterizes the ionosphere. The availability of $\mathcal{N}$ will allow one to calculate the dilation (2.39) and the new chirp rate (2.30) for any reference location $\boldsymbol{y}$.

The quantity $\mathcal{N}$ depends on the deterministic part of the electron number density, see formula (C.8), and also has a random component obtained by integrating $\mu(\boldsymbol{x})$ along the ray trajectory. In the literature, many estimates are available for the electron number density in the ionosphere, see, e.g., [Gin64] or [Bud85]. Those estimates, however, can only provide a typical range of values, especially as the parameters of the ionosphere are known to vary in space and in time. This does not allow one to correct the filter with a sufficient degree of reliability. What is rather needed is an accurate value of $\mathcal{N}$ exactly at the time and place the image is taken.

Hereafter, we exploit the idea of dual carrier probing for deriving $\mathcal{N}$. Let us assume that there is an object or feature in the scene that can be clearly identified on the image. This object does not have to be artificial. It does not have to dominate the scene, say, by having the highest reflectivity. Its location does not have to be known ahead of time. It merely has to be something that can be fairly easily picked out and matched on different images that represent the same terrain. For example, it can be some landmark, such as a hilltop, a building, a road intersection, etc.

Let ω_0 and ω_1 be two distinct carrier frequencies, $\omega_0 \neq \omega_1$, and let $R_{\boldsymbol{y}}^{(0)}$ and $R_{\boldsymbol{y}}^{(1)}$ be the corresponding ranges of the aforementioned object measured by the radar, whereas its true range is $R_{\boldsymbol{z}}$ (unknown yet). Then, we can consider the corresponding two equations (2.44) as a system:

$$\begin{aligned} R_{\boldsymbol{y}}^{(0)} &= cT_{\rm gr}(\boldsymbol{x}^0,\boldsymbol{z},\omega_0),\\ R_{\boldsymbol{y}}^{(1)} &= cT_{\rm gr}(\boldsymbol{x}^0,\boldsymbol{z},\omega_1), \end{aligned} \tag{2.58}$$

where the group travel time $T_{\rm gr}$ is given by formula (2.37a). With the data $R_{\boldsymbol{y}}^{(0)}$ and $R_{\boldsymbol{y}}^{(1)}$ available, system (2.58) can be solved with respect to the two unknown quantities: the true range $R_{\boldsymbol{z}}$ and the integral quantity $\mathcal{N}$ that characterizes the plasma.

More precisely, the true range $R_{\boldsymbol{z}}$ enters into the expression for $T_{\rm gr}$ as a factor in front of the formula, and also as the integration limit for the random component of the electron number density, see (2.37a). As, however, we have seen in Section 2.4, the contribution of randomness into the single-look image is very small for large $R_{\boldsymbol{z}}$ because of the ergodicity. Randomness rather manifests itself when the information from multiple looks is combined for the analysis of azimuthal resolution. Therefore, since system (2.58) contains only single-look information, we can disregard the stochastic contribution into $T_{\rm gr}$ and instead of (2.37a) substitute the expression

$$\tilde{T}_{\rm gr}(\boldsymbol{x}^0,\boldsymbol{z},\omega)=\frac{R_{\boldsymbol{z}}}{c}\left[1+\frac{1}{\omega^2}\frac{4\pi e^2}{2m_{\rm e}}\frac{\bar{N}_{\rm e}^{(H)}}{H}\right] \tag{2.59}$$

on the right hand side of equations (2.58). We emphasize that the simplification offered by formula (2.59) compared to formula (2.37a) is due to the ergodicity of μ that can be employed in the context of single-look imaging. This simplification is important as it allows one to determine the plasma quantity $\bar{N}_{\rm e}^{(H)}$ defined by formula (C.8), as well as the true range $R_{\boldsymbol{z}}$.

Let us introduce the following notation for brevity:

$$\bar{\omega}_{\rm pe}^2=\frac{4\pi e^2}{m_{\rm e}}\frac{\bar{N}_{\rm e}^{(H)}}{H}. \tag{2.60}$$

Using this notation, system (2.58) with the expression for $\tilde{T}_{\rm gr}$ given by (2.59) is recast as

$$\begin{aligned} R_{\boldsymbol{y}}^{(0)}&=R_{\boldsymbol{z}}\left(1+\frac{\bar{\omega}_{\rm pe}^2}{2\omega_0^2}\right),\\ R_{\boldsymbol{y}}^{(1)}&=R_{\boldsymbol{z}}\left(1+\frac{\bar{\omega}_{\rm pe}^2}{2\omega_1^2}\right). \end{aligned} \tag{2.61}$$

The range $R_{\boldsymbol{z}}$ can be eliminated from system (2.61) by dividing the equations by one another. Then, after simple transformations, we have:

$$\bar{\omega}_{\rm pe}^2=\frac{2\omega_0^2\omega_1^2(R_{\boldsymbol{y}}^{(0)}-R_{\boldsymbol{y}}^{(1)})}{\omega_1^2R_{\boldsymbol{y}}^{(1)}-\omega_0^2R_{\boldsymbol{y}}^{(0)}}. \tag{2.62}$$

We note that the denominator in formula (2.62) does not turn into zero, because if it was equal to zero, then system (2.61) would immediately yield $\omega_0=\omega_1$. The actual electron content $\bar{N}_{\rm e}^{(H)}$ can be determined using (2.60) once $\bar{\omega}_{\rm pe}^2$ has been evaluated according to (2.62). Moreover, if there is a need to know the true range $R_{\boldsymbol{z}}$ of the chosen reference object, it can be easily found from any of the equations (2.61).

2.6. Correcting the matched filter. Once the quantity $\bar{N}_{\rm e}^{(H)}$ has been found, one can use formulae (2.37) and accurately evaluate the deterministic contributions to the travel times $T_{\rm ph}(\boldsymbol{x}^n,\boldsymbol{y},\omega_0)$ and $T_{\rm gr}(\boldsymbol{x}^n,\boldsymbol{y},\omega_0)$ for any location $\boldsymbol{y}$. Then, one can also compute the pulse dilation for the reference point $\boldsymbol{y}$ using formula (2.39), and the new pulse rate according to (2.30). Those quantities are needed to modify the definition of the matched filter in formulae (2.40) and (2.41), i.e., to correct the matched filter.

2.6.1. Range resolution. The matched filter is corrected by using the actual travel times instead of the travel times in vacuum, and by taking into account the dilation and the rate change of the pulse upon its arrival. With this correction in place, the range factor of the generalized ambiguity function becomes [cf. formula (2.42)]:

$$\begin{aligned} W_R'(\boldsymbol{y},\boldsymbol{z})&=\int_{\max\{-\tau'(\boldsymbol{y})/2+2\tilde{T}_{\rm gr}(\boldsymbol{y}),\,-\tau'(\boldsymbol{z})/2+2T_{\rm gr}(\boldsymbol{z})\}}^{\min\{\tau'(\boldsymbol{y})/2+2\tilde{T}_{\rm gr}(\boldsymbol{y}),\,\tau'(\boldsymbol{z})/2+2T_{\rm gr}(\boldsymbol{z})\}} e^{-i\alpha'(\boldsymbol{y})(t-2\tilde{T}_{\rm gr}(\boldsymbol{y}))^2}e^{i\alpha'(\boldsymbol{z})(t-2T_{\rm gr}(\boldsymbol{z}))^2}dt\\ &\propto\int_{\max\{-\tau'(\boldsymbol{y})/2+2\tilde{T}_{\rm gr}(\boldsymbol{y}),\,-\tau'(\boldsymbol{z})/2+2T_{\rm gr}(\boldsymbol{z})\}}^{\min\{\tau'(\boldsymbol{y})/2+2\tilde{T}_{\rm gr}(\boldsymbol{y}),\,\tau'(\boldsymbol{z})/2+2T_{\rm gr}(\boldsymbol{z})\}} e^{i(\alpha'(\boldsymbol{z})-\alpha'(\boldsymbol{y}))t^2}e^{4i(\alpha'(\boldsymbol{y})\tilde{T}_{\rm gr}(\boldsymbol{y})-\alpha'(\boldsymbol{z})T_{\rm gr}(\boldsymbol{z}))}dt, \end{aligned} \tag{2.63}$$

where we have introduced the abbreviated notations $T_{\rm gr}(\boldsymbol{z}) = T_{\rm gr}(\boldsymbol{x}^0, \boldsymbol{z}, \omega_0)$ and $\tilde{T}_{\rm gr}(\boldsymbol{y}) = \tilde{T}_{\rm gr}(\boldsymbol{x}^0, \boldsymbol{y}, \omega_0)$. We emphasize that for the filter part of the generalized ambiguity function we can substitute only the deterministic component of the group travel time (2.59), because this is what we derive from the single-look information, see Section 2.5. The primed quantities τ' and α' in formula (2.63) are to be evaluated for the pulse round-trip between the antenna and the target [cf. formulae (2.29) and (2.30)]:

$$\tau' = \tau + 2\delta\tau \quad \text{and} \quad \alpha' = \alpha - \delta\tau\frac{B}{\tau^2} = \frac{B}{2\tau}\left(1 - \frac{2\delta\tau}{\tau}\right), \tag{2.64}$$

where $\delta\tau$ is given by formula (2.39). For the integral (2.63), we consider the integration limits $\mp\tau'(\boldsymbol{y})/2 + 2\tilde{T}(\boldsymbol{y})$, and, changing the integration variable: $u = t - 2\tilde{T}(\boldsymbol{y})$, obtain:

$$\begin{aligned} W'_R(\boldsymbol{y}, \boldsymbol{z}) &\propto \int_{-\tau'(\boldsymbol{y})/2}^{\tau'(\boldsymbol{y})/2} e^{-i\alpha'(\boldsymbol{y})u^2} e^{i\alpha'(\boldsymbol{z})(u+2\tilde{T}_{\rm gr}(\boldsymbol{y})-2T_{\rm gr}(\boldsymbol{z}))^2} du \\ &\propto \int_{-\tau'(\boldsymbol{y})/2}^{\tau'(\boldsymbol{y})/2} e^{i(\alpha'(\boldsymbol{z})-\alpha'(\boldsymbol{y}))u^2} e^{4i\alpha'(\boldsymbol{z})(\tilde{T}_{\rm gr}(\boldsymbol{y})-T_{\rm gr}(\boldsymbol{z}))u} du, \end{aligned} \tag{2.65}$$

where the constant factors of magnitude one in front of the integrals are dropped.

Following the analysis of Section 2.4.1, we first disregard the quadratic term $\sim u^2$ in the exponent under the integral (2.65), because this term is small. Then, integral (2.65) evaluates to

$$W'_R(\boldsymbol{y}, \boldsymbol{z}) \propto \tau'(\boldsymbol{y}) \mathrm{sinc}[2\alpha'(\boldsymbol{z})(\tilde{T}_{\rm gr}(\boldsymbol{y}) - T_{\rm gr}(\boldsymbol{z}))\tau'(\boldsymbol{y})]. \tag{2.66}$$

The range resolution of the radar is defined as the full width of the sinc function (2.66) interpreted as a function of $R_{\boldsymbol{y}} - R_z$, and hence can be obtained by setting the argument of the sinc equal to 2π:

$$2\alpha'(\boldsymbol{z})(\tilde{T}_{\rm gr}(\boldsymbol{y}) - T_{\rm gr}(\boldsymbol{z}))\tau'(\boldsymbol{y}) = 2\pi.$$

With the help of (2.64), the previous equality transforms into

$$\frac{B}{\tau}\left(1 - \frac{2\delta\tau}{\tau}\right)(\tilde{T}_{\rm gr}(\boldsymbol{y}) - T_{\rm gr}(\boldsymbol{z}))\tau\left(1 + \frac{2\delta\tau}{\tau}\right) = 2\pi. \tag{2.67}$$

We first notice that the correction due to the dilation of the pulse in formula (2.67) becomes quadratic with respect to $\frac{2\delta\tau}{\tau}$. For the typical values of the parameters involved, we have $\frac{\delta\tau}{\tau} \sim 10^{-4}$, see [Tsy09a, ST10]. Consequently, we can disregard this correction completely and instead of (2.67) write:

$$B(\tilde{T}_{\rm gr}(\boldsymbol{y}) - T_{\rm gr}(\boldsymbol{z})) = 2\pi. \tag{2.68}$$

Then, we can use formulae (2.37a), (2.47), (2.59), and (2.60), and express the difference between the group travel times in (2.68) as follows:

$$\tilde{T}_{\rm gr}(\boldsymbol{y}) - T_{\rm gr}(\boldsymbol{z}) = \frac{R_{\boldsymbol{y}} - R_z}{c}\left(1 + \frac{1}{2}\frac{\bar{\omega}_{\rm pe}^2}{\omega_0^2}\right) - \frac{1}{2}\frac{4\pi e^2}{m_{\rm e}\omega_0^2}\frac{1}{c}\varphi_0(\boldsymbol{z}). \tag{2.69}$$

As $\langle\varphi_0(\boldsymbol{z})\rangle = 0$, we can say that for every particular realization of the random field μ we have $|\varphi_0(\boldsymbol{z}))| \sim \sqrt{\langle\varphi_0^2\rangle}$. Hence, the second term on the right-hand side of equality (2.69) appears much smaller than the first term, because the exact same argument applies here as given in Section 2.4.1, see the discussion around equation (2.48). Thus, disregarding this second term and substituting the result into (2.68), we arrive at the following expression for the range resolution:

$$\Delta R = R_{\boldsymbol{y}} - R_z \approx \frac{2\pi c}{B}\left(1 - \frac{1}{2}\frac{\bar{\omega}_{\rm pe}^2}{\omega_0^2}\right). \tag{2.70}$$

This is an improvement over (2.45) and even a slight improvement over the non-dispersive resolution $\Delta R = 2\pi c/B$, because the center frequency group velocity that essentially enters into the numerator of formula

(2.70) is slower than the speed of light c. However, as indicated in Section 2.4.1, the range resolution of a SAR sensor does not suffer much from the ionospheric dispersion in any event. Therefore, what is even more important is that when the filter is corrected, the target is no longer shifted in range from its true position as in formula (2.44). That is because the maximum of the sinc in formula (2.66) is attained precisely at $R_{\boldsymbol{y}} = R_{\boldsymbol{z}}$.

What is also very important is that the degradation of image sharpness becomes negligible once the filter has been corrected. To analyze this effect, we bring back the quadratic term in the exponent under the integral (2.65). First, we recast this integral in the form

$$W'_R(\boldsymbol{y},\boldsymbol{z}) \propto \int_{-\tau'(\boldsymbol{y})/2}^{\tau'(\boldsymbol{y})/2} e^{i\gamma u^2} e^{i\zeta u} du, \tag{2.71}$$

where

$$\gamma = \alpha'(\boldsymbol{z}) - \alpha'(\boldsymbol{y}) = \frac{B}{\tau^2}(\delta\tau(\boldsymbol{y}) - \delta\tau(\boldsymbol{z})) = \frac{B}{\tau^2}\frac{2(R_{\boldsymbol{y}} - R_z)}{c}\frac{4\pi e^2}{m_{\mathrm{e}}\omega_0^2}\frac{B}{\omega_0}\mathcal{N}, \tag{2.72}$$

$$\zeta = 4\alpha'(\boldsymbol{z})(\tilde{T}_{\mathrm{gr}}(\boldsymbol{y}) - T_{\mathrm{gr}}(\boldsymbol{z})), \tag{2.73}$$

and the quantity $\mathcal{N}$ is defined in formula (2.38). The quadratic term in the exponent under the integral (2.71) is small: $|\gamma u^2| \ll 1$ for $u \in [-\tau'(\boldsymbol{y})/2, \tau'(\boldsymbol{y})/2]$, and consequently we have:

$$\begin{aligned} W'_R(\boldsymbol{y},\boldsymbol{z}) &\approx \int_{-\tau'(\boldsymbol{y})/2}^{\tau'(\boldsymbol{y})/2} (1 + i\gamma u^2) e^{i\zeta u} du \\ &= \tau' \mathrm{sinc}[2\alpha'(\boldsymbol{z})(\tilde{T}_{\mathrm{gr}}(\boldsymbol{y}) - T_{\mathrm{gr}}(\boldsymbol{z}))\tau'] + i\gamma \frac{4\zeta\tau' \cos\frac{\zeta\tau'}{2} + (-8 + \zeta^2\tau'^2)\sin\frac{\zeta\tau'}{2}}{2\zeta^3}, \end{aligned} \tag{2.74}$$

where $\tau' = \tau'(\boldsymbol{y})$. The first term on the right-hand side of (2.74) obviously coincides with (2.66), and the second term represents a correction. According to (2.72) and (2.73), (2.69), both γ and ζ vanish as $R_{\boldsymbol{y}}$ approaches $R_{\boldsymbol{z}}$. However, the fraction on the right-hand side of (2.74) remains bounded as $\zeta \to 0$ (and $\gamma \to 0$). It is, in fact, easy to see that

$$W'_R(\boldsymbol{y},\boldsymbol{z}) \approx \tau' \mathrm{sinc}[2\alpha'(\boldsymbol{z})(\tilde{T}_{\mathrm{gr}}(\boldsymbol{y}) - T_{\mathrm{gr}}(\boldsymbol{z}))\tau'] + \frac{3}{16} i\gamma\tau'^3. \tag{2.75}$$

As the first term on the right-hand side of (2.75) is proportional to τ', the relative magnitude of the correction is $\sim \gamma\tau'^2$ (this is a dimensionless quantity). There is no correction at the central peak of the sinc, because $\gamma = 0$ when $R_{\boldsymbol{y}} = R_{\boldsymbol{z}}$. To quantify the extent to what the image sharpness is affected, we estimate the correction at the first zero of the sinc. Using formulae (2.72) and (2.64), we obtain:

$$\gamma\tau'^2 = B\frac{2(R_{\boldsymbol{y}} - R_z)}{c}\frac{4\pi e^2}{m_{\mathrm{e}}\omega_0^2}\frac{B}{\omega_0}\mathcal{N}\left(1 + \frac{2\delta\tau}{\tau}\right)^2,$$

where the value of $R_{\boldsymbol{y}} - R_{\boldsymbol{z}}$ shall be taken according to formula (2.70). For the typical values of the parameters involved, we have

$$\frac{4\pi e^2}{m_{\mathrm{e}}\omega_0^2}\mathcal{N} \approx \frac{\bar{\omega}_{\mathrm{pe}}^2}{\omega_0^2} \sim 10^{-4} \quad \text{and} \quad \frac{B}{\omega_0} \sim 10^{-2},$$

so that altogether we can write:

$$\frac{3}{16}\gamma\tau'^2 \approx \frac{3\pi}{4}\frac{\bar{\omega}_{\mathrm{pe}}^2}{\omega_0^2}\frac{B}{\omega_0}\left(1 - \frac{1}{2}\frac{\bar{\omega}_{\mathrm{pe}}^2}{\omega_0^2}\right)\left(1 + \frac{4\delta\tau}{\tau}\right) \sim \frac{3\pi}{4}\cdot 10^{-6}.$$

We therefore conclude that the degradation of image contrast in range decreases to approximately 0.0002% as opposed to 2% in the non-corrected case, see formula (2.46).

2.6.2. Azimuthal resolution. Once the matched filter has been corrected, expression (2.41) for the azimuthal component of the generalized ambiguity function becomes

$$W'_A(\boldsymbol{y},\boldsymbol{z}) = \sum_{n=-N/2}^{N/2} e^{2i\omega_0(\tilde{T}_{\rm ph}(\boldsymbol{x}^n,\boldsymbol{y},\omega_0)-T_{\rm ph}(\boldsymbol{x}^n,\boldsymbol{z},\omega_0))}, \tag{2.76}$$

where in the filter part we have substituted the deterministic portion of the phase travel time:

$$\tilde{T}_{\rm ph}(\boldsymbol{x}^0,\boldsymbol{z},\omega) = \frac{R_{\boldsymbol{z}}}{c}\left[1-\frac{1}{\omega^2}\frac{4\pi e^2}{2m_{\rm e}}\frac{\bar{N}_{\rm e}^{(H)}}{H}\right]$$

because this is what we derive from the sing-look image by means of dual carrier probing, see Section 2.5. Then, using formulae (2.37b), (2.49), and (2.50), we can transform expression (2.76) into [cf. formula (2.51]:

$$W'_A(\boldsymbol{y},\boldsymbol{z}) \propto \sum_{n=-N/2}^{N/2} e^{\frac{2i\omega_0}{c}\left[-\frac{y_1x_1^n}{R_0}\left(1-\frac{1}{2}\frac{4\pi e^2}{m_{\rm e}\omega_0^2}\frac{\bar{N}_{\rm e}^{(H)}}{H}\right)+\frac{1}{2}\frac{4\pi e^2}{m_{\rm e}\omega_0^2}\varphi_n\right]}, \tag{2.77}$$

where the constant factor of unit magnitude in front of the sum was dropped. Next, following the same derivation as in Section 2.4.2 (see also [Tsy09a]), we compute the mean and variance of each term in the sum (2.77):

$$\begin{aligned}&\left\langle e^{\frac{2i\omega_0}{c}\left[-\frac{y_1x_1^n}{R_0}\left(1-\frac{1}{2}\frac{4\pi e^2}{m_{\rm e}\omega_0^2}\frac{\bar{N}_{\rm e}^{(H)}}{H}\right)+\frac{1}{2}\frac{4\pi e^2}{m_{\rm e}\omega_0^2}\varphi_n\right]}\right\rangle \\ &= e^{\frac{2i\omega_0}{c}\left[-\frac{y_1x_1^n}{R_0}\left(1-\frac{1}{2}\frac{4\pi e^2}{m_{\rm e}\omega_0^2}\frac{\bar{N}_{\rm e}^{(H)}}{H}\right)\right]}e^{-\frac{1}{2}\frac{\omega_0^2}{c^2}\left(\frac{4\pi e^2}{m_{\rm e}\omega_0^2}\right)^2\langle\varphi_n^2\rangle},\end{aligned} \tag{2.78}$$

$$\sigma_n^2 \approx \frac{\omega_0^2}{c^2}\left(\frac{4\pi e^2}{m_{\rm e}\omega_0^2}\right)^2\langle\varphi_n^2\rangle. \tag{2.79}$$

Also as in Section 2.4.2, the individual variances (2.79) can be assumed approximately equal to one another, $\sigma_n^2 \approx \sigma^2$, $n = -N/2,\ldots,N/2$, because the integration distance for φ_n depends on n weakly. Hence, we can use (2.78) and derive the mean value of the sum (2.77):

$$\langle W'_A(\boldsymbol{y},\boldsymbol{z})\rangle \ \propto\ e^{-\sigma^2/2}\sum_{n=-N/2}^{N/2} e^{\frac{2i\omega_0}{c}\left[-\frac{y_1x_1^n}{R_0}\left(1-\frac{1}{2}\frac{4\pi e^2}{m_{\rm e}\omega_0^2}\frac{\bar{N}_{\rm e}^{(H)}}{H}\right)\right]}. \tag{2.80}$$

The sum (2.80) can be actually computed using the same approach as employed in Section 2.4.2 and in [Tsy09a]. The result is another sinc function, and it leads to the following estimate of the azimuthal resolution in the case of a non-fluctuating ionosphere:

$$2y_1 \approx \frac{L}{2}\left(1+\frac{1}{2}\frac{4\pi e^2}{m_{\rm e}\omega_0^2}\frac{\bar{N}_{\rm e}^{(H)}}{H}\right) = \frac{L}{2}\left(1+\frac{1}{2}\frac{\bar{\omega}_{\rm pe}^2}{\omega_0^2}\right).$$

This value is only marginally worse than that obtained in the non-dispersive case: $2y_1 = L/2$. Even more important, correction of the filter restores the sharpness of the image for the non-fluctuating ionosphere, so that there is no deterioration like in the non-corrected case, see formula (2.56). The reason is that unlike in formula (2.51), there is no quadratic term with respect to x_1^n in the exponent in the sum (2.77).

As, however, the proposed correction is based on the single look data that essentially do not account for randomness (due to the ergodicity), it does not offer any remedy for the stochastic part of image distortions in the azimuthal direction. In other words, we can expect that even with the corrected filter in place, the azimuthal factor $W'_A(\boldsymbol{y},\boldsymbol{z})$ of the generalized ambiguity function will still have the variance of order (2.57), which will result in the same extent of deterioration in the azimuthal resolution as estimated in [Tsy09a].

2.7. Discussion. SAR images obtained from satellites are prone to deterioration due to the temporal dispersion of radio waves in the Earth's ionosphere. The deterioration is stronger for lower carrier frequencies and weaker for higher carrier frequencies. We have analyzed this phenomenon in the case of a scalar field (polarization of radar pulses is not taken into account) propagating in an inhomogeneous cold plasma. Our analysis shows that image deterioration is due to the mismatch between the actual signals scattered off the Earths' surface and received by the radar antenna and the matched filter (an image processing tool) designed as if the propagation between the antenna and the ground was unobstructed.

To correct the filter, one needs to know a key characteristic of the ionosphere precisely at the time and place the image is taken. This key characteristic is the integral content of electrons per unit area in the layer of ionospheric plasma between the satellite and the ground. We have proposed to derive this quantity by probing the terrain, and hence the ionosphere, on two distinct carrier frequencies. We have also shown that the resulting correction of the filter completely eliminates all the distortions of the image that are due to the deterministic part of the electron content in the ionosphere.

The correction, however, is not efficient for removing the distortions due to the random part of the charged particle content, i.e., turbulent fluctuations of the electron number density. The reason is that the correction is based on the data from a single-look image, for which the effect of randomness is "downplayed" by ergodicity. Mitigating the stochastic part of image distortions will be a subject for the future study.

In addition, we should note that our approach to correcting the filter relies on an important consideration that the mean parameters of the ionosphere do not vary in the horizontal direction. This assumption will hold only if the size of the imaged scene is relatively small. For larger scenes, the procedure of dual carrier probing needs to be carried out repeatedly, and the filter needs to be adjusted accordingly, as the satellite travels along the orbit and the antenna's footprint sweeps the imaged stripmap.

The issues to be studied in the future may include:

- An investigation of whether the stochastic component of image distortions can be tackled by any of the "black box" image sharpening and deblurring techniques developed previously in the general framework, see, e.g., [GW08], with no direct relation to spaceborne SAR. The considerations based on the central limit theorem that are outlined in Section 2.4.2 may be useful in this perspective.
- Introduction of a vector propagation model, analysis of SAR imaging with polarization, accounting for anisotropy of the medium due to the magnetic field of the Earth, and for the Faraday rotation.
- Analysis of the effect of turbulent fluctuations in the ionosphere on the image using true Kolmogorov-type spectra, as opposed to the modified spectrum (2.11) that accounts only for the short range phenomena. Accounting for anisotropic turbulence due to the magnetic field of the Earth.
- Approaches for reducing the noise that is always present, regardless of whether the imaging is done through the ionosphere or not, for example, instrument noise or rough terrain noise. As a minimum requirement, this noise may not be amplified by any of the techniques used for mitigating the ionospheric distortions.
- Analysis of the dispersion on the target, and distinguishing between the target dispersion and the ionospheric dispersion. Possible applications to material identification SAR (MISAR).
- Optimization of interrogating waveforms for the ionosphere, beyond the standard linear upchirps.

3. On the use of start-stop approximation for spaceborne SAR imaging.

3.1. Background. A synthetic aperture radar (SAR) builds an image of a target (could be an area of the Earth's surface) by successively illuminating it with a series of electromagnetic pulses transmitted from different locations, and subsequently processing the scattered waves with the help of a matched filter. Typically, the antenna of such a radar is mounted on an aircraft (airborne radar) or a satellite (spaceborne radar), and the interrogating pulses are emitted and received as the craft travels along its flight track or orbit, respectively. A standard approach employed when processing the SAR data is based on the start-stop approximation, when the antenna is assumed at standstill while it sends a pulse and receives the scattered response, after which it moves on to the position where the next pulse is emitted, see, e.g., [CM91, CGM95, FL99] and also [Che01]. This approximation is intuitively well justified for an airborne radar. Indeed, a typical aircraft speed is between $200m/sec$ and $300m/sec$. Then, even when the look angle is large (close to $\pi/2$) so that the radar scans the surface far to the side rather than directly underneath the flight track, the round-trip travel time for the pulse will still be under $10^{-3}sec$. This yields the displacement of the antenna

between $20cm$ and $30cm$, see Section 3.3, which is on the order of one to a few wavelengths for the microwave frequency band that the radar typically operates in, and is also far shorter than the typical antenna size. Besides, the magnitude of the linear Doppler frequency shift in this case is rather small, under 10^{-6}, see Section 3.4.

On the other hand, using the start-stop approximation for a spaceborne radar may raise questions. With the round-trip travel times $\sim 1/200sec$ and the speed of $8km/sec$, the displacement of the antenna over the period of time between the emission and arrival of a pulse may reach about $40m$, which is several times longer than the antenna size and much larger than the wavelength. It is not clear ahead of time whether neglecting this displacement may affect the quality of the image. Moreover, the Doppler frequency shift, which is $\sim v/c$, where v is the speed of the satellite and c is the speed of light, see Section 3.4, will also be about one and a half orders of magnitude larger than in the case of an airborne radar. In the earlier SAR studies, the Doppler shift was used to explain the mechanism of along-the-track resolution, see, e.g., [FL99]. However, when building a generalized ambiguity function the Doppler effect is often neglected, and it is not apparent whether it may cause a deterioration of the image.

In this part of the report, we analyze the generalized ambiguity function of a SAR system while taking the two foregoing phenomena into account. To enable the analysis, we need to re-derive the non-dispersive generalized ambiguity function of Section 2.3.1 for the case when the sending and receiving locations can be different, see Section 3.2. Our analysis subsequently shows that the displacement of the antenna, even though quite noticeable, has a very small detrimental effect $\mathcal{O}(v/c)$ on the resolution of the image and can therefore be disregarded for all practical purposes, see Section 3.3. As for the Doppler effect, disregarding it in the generalized ambiguity function may cause an overall translation of the entire scene on the image, as well as a slight deterioration of the sharpness (contrast), see Section 3.4. To avoid this, one must include the frequency shift into the definition of a matched filter.

3.2. The generalized ambiguity function. For the analysis in this section, we will employ the following assumptions. The electromagnetic field propagating between the antenna and the target will be assumed scalar and will be governed by the standard d'Alembert equation with the speed c (the speed of light). In other words, we will disregard the polarization. The image will be assumed two-dimensional, i.e., the radar will measure coordinates of the targets along the Earth's surface, but will not measure their elevation. All targets will be assumed dispersionless, and scattering off the targets will be linearized and analyzed using the first Born approximation, see [BW99, Section 13.1.4].

The radar will be assumed to operate in the standard mode known as stripmap, see [CGM95]. In this case, the antenna points in the direction which is fixed relative to that of the satellite motion. Hence, the footprint of the beam emitted by the antenna sweeps a strip on the Earth's surface parallel to flight track, i.e., to the orbit. In doing so, the antenna does not necessarily have to point precisely sideways, i.e., normally to the direction of motion. Instead, it can point either forward or backward at a fixed angle, which corresponds to the so-called squinted stripmap mode.

Finally, we will need to use the Lorentz transform [Gar07, Chapter 3, Section 3] that preserves the form of the d'Alembert equation in the case of moving transmitters and/or receivers, see Section 3.4. To be able to do so, we will have to assume that the motion of the antenna is straightforward and uniform. Technically speaking, this is not true for a satellite orbiting the Earth. However, for a relatively short stretch of the orbit, along which the measurements are taken of a given small target (i.e., for which a given target stays in the beam, see Section 3.3), this is a sufficiently accurate approximation.

Hereafter, we adopt some notations of [Che01]. The interrogating pulses emitted by the antenna of a SAR are taken as linear upchirps of the form:

$$P(t) = A(t)e^{i\omega_0 t}, \quad \text{where} \quad A(t) = \chi_\tau(t)e^{i\alpha t^2}. \tag{3.1}$$

In formula (2.13), $\chi_\tau(t)$ is the indicator function of the interval of duration τ:

$$\chi_\tau(t) = \begin{cases} 1, & t \in [-\tau/2, \tau/2], \\ 0, & \text{otherwise}, \end{cases}$$

and $\alpha = B/(2\tau)$, where B is the bandwidth of the chirp. Accordingly, the instantaneous frequency of the

chirp is given by

$$\omega(t) = \omega_0 + \frac{Bt}{\tau}, \quad t \in [-\tau/2, \tau/2], \tag{3.2}$$

where ω_0 is the center carrier frequency. The modulating function $A(t)$ in formula (3.1) is assumed slowly varying compared to the fast carrier oscillation $e^{i\omega_0 t}$.

Suppose first that the antenna is a motionless point source located at $\boldsymbol{x} \in \mathbb{R}^3$. Then, the propagating field due to the emitted chirp (3.1) is given by the standard retarded potential:

$$\varphi(t, \boldsymbol{z}) = \frac{1}{4\pi} \frac{P(t - |\boldsymbol{z} - \boldsymbol{x}|/c)}{|\boldsymbol{z} - \boldsymbol{x}|}. \tag{3.3}$$

Let us assume that the imaged terrain, which is also motionless, is characterized by the variable refraction index $n = n(\boldsymbol{z})$. Under the first Born approximation [BW99, Section 13.1.4], scattering is linearized so that the terrain is interpreted as a secondary waves' source due to the incident field $\varphi(t, \boldsymbol{z})$ of (3.3):

$$\frac{1 - n^2(\boldsymbol{z})}{c^2} \frac{\partial^2 \varphi}{\partial t^2} \stackrel{\text{def}}{=} \nu(\boldsymbol{z}) \frac{\partial^2 \varphi}{\partial t^2}.$$

Consequently, the scattered field at the location $\tilde{\boldsymbol{x}}$ and time t is given by the Kirchhoff integral:

$$\psi(t, \tilde{\boldsymbol{x}}) = \frac{1}{4\pi} \iiint\limits_{|\tilde{\boldsymbol{x}} - \boldsymbol{z}| \le ct} \frac{\nu(\boldsymbol{z})}{|\tilde{\boldsymbol{x}} - \boldsymbol{z}|} \frac{\partial^2 \varphi}{\partial t^2} \left(t - |\tilde{\boldsymbol{x}} - \boldsymbol{z}|/c, \boldsymbol{z}\right) d\boldsymbol{z}. \tag{3.4}$$

As the amplitude $A(t)$ in (3.1) is slowly varying, it can be left out when differentiating the incident field (3.3) for substitution into (3.4), which yields:

$$\frac{\partial^2 \varphi}{\partial t^2}(t, \boldsymbol{z}) \approx -\frac{\omega_0^2}{4\pi} \frac{P(t - |\boldsymbol{z} - \boldsymbol{x}|/c)}{|\boldsymbol{z} - \boldsymbol{x}|}. \tag{3.5}$$

Consequently,

$$\begin{aligned} \psi(t, \tilde{\boldsymbol{x}}) \approx & -\frac{\omega_0^2}{16\pi^2} \iiint\limits_{|\tilde{\boldsymbol{x}} - \boldsymbol{z}| \le ct} \frac{\nu(\boldsymbol{z})}{|\tilde{\boldsymbol{x}} - \boldsymbol{z}||\boldsymbol{z} - \boldsymbol{x}|} P\left(t - |\tilde{\boldsymbol{x}} - \boldsymbol{z}|/c - |\boldsymbol{z} - \boldsymbol{x}|/c\right) d\boldsymbol{z} \\ = & -\frac{\omega_0^2}{16\pi^2} \iiint\limits_{|\tilde{\boldsymbol{x}} - \boldsymbol{z}| \le ct} \frac{\nu(\boldsymbol{z})}{|\tilde{\boldsymbol{x}} - \boldsymbol{z}||\boldsymbol{z} - \boldsymbol{x}|} A\left(t - |\tilde{\boldsymbol{x}} - \boldsymbol{z}|/c - |\boldsymbol{z} - \boldsymbol{x}|/c\right) e^{i\omega_0 (t - |\tilde{\boldsymbol{x}} - \boldsymbol{z}|/c - |\boldsymbol{z} - \boldsymbol{x}|/c)} d\boldsymbol{z}. \end{aligned} \tag{3.6}$$

Formula (3.6) indicates that the scattered field $\psi(t, \tilde{\boldsymbol{x}})$ is obtained by applying a Fourier integral operator to the target reflectivity function $\nu(\boldsymbol{z})$, see, e.g., [CN04, CB08]. The key goal of radar imaging is to build an (approximate) inverse to this operator and thus reconstruct $\nu(\boldsymbol{z})$ from the observed scattered field.

The approximate inversion is done in two stages; first, by applying a matched filter to the field ψ, and then by accumulating the information due to multiple interrogating pulses (3.1) emitted from and received at different locations on the orbit. As one will see from our subsequent analysis (a more detailed derivation can be found in [Che01, CN04, CB08]), this procedure resembles the application of an adjoint operator, which would have coincided with the true inverse if the mapping (3.6) was a standard Fourier transform (a unitary operator).

The matched filter is defined as follows. Assume that there is a point scatterer at a reference location $\boldsymbol{y}$, then the resulting field at $(t, \tilde{\boldsymbol{x}})$ is obtained by substituting $\nu(\boldsymbol{z}) = \delta(\boldsymbol{z} - \boldsymbol{y})$ into formula (3.6):

$$\psi_1(t, \tilde{\boldsymbol{x}}) = -\frac{\omega_0^2}{16\pi^2} \frac{P(t - |\tilde{\boldsymbol{x}} - \boldsymbol{y}|/c - |\boldsymbol{y} - \boldsymbol{x}|/c)}{|\tilde{\boldsymbol{x}} - \boldsymbol{y}||\boldsymbol{y} - \boldsymbol{x}|}. \tag{3.7}$$

The filter is essentially a complex conjugate of ψ_1 given by (3.7); for simplicity, the constant factor $-\omega_0^2/16\pi^2$, as well the entire denominator, which is a slowly varying function (compared to the fast oscillation $e^{i\omega_0 t}$),

are disregarded. What remains is merely $\overline{P(t-|\tilde{\boldsymbol{x}}-\boldsymbol{y}|/c-|\boldsymbol{y}-\boldsymbol{x}|/c)}$, where the overbar denotes complex conjugation. The application of this filter yields the image:

$$I(\boldsymbol{y}) = \int \overline{P(t-|\tilde{\boldsymbol{x}}-\boldsymbol{y}|/c-|\boldsymbol{y}-\boldsymbol{x}|/c)}\psi(t,\tilde{\boldsymbol{x}})dt \tag{3.8}$$

$$= -\frac{\omega_0^2}{16\pi^2}\iiint\limits_{|\tilde{\boldsymbol{x}}-\boldsymbol{z}|\le ct}\underbrace{\int \overline{P(t-|\tilde{\boldsymbol{x}}-\boldsymbol{y}|/c-|\boldsymbol{y}-\boldsymbol{x}|/c)}P(t-|\tilde{\boldsymbol{x}}-\boldsymbol{z}|/c-|\boldsymbol{z}-\boldsymbol{x}|/c)dt}_{W(\boldsymbol{y},\boldsymbol{z})}\frac{\nu(\boldsymbol{z})}{|\tilde{\boldsymbol{x}}-\boldsymbol{z}||\boldsymbol{z}-\boldsymbol{x}|}d\boldsymbol{z},$$

where we have changed the order of integration after substituting expression (3.6) for $\psi(t,\tilde{\boldsymbol{x}})$. The interior integral that we denote $W(\boldsymbol{y},\boldsymbol{z})$ in formula (3.8) is called the point spread function,[5] see [Che01]. Up to a slowly varying denominator, the point spread function $W(\boldsymbol{y},\boldsymbol{z})$ yields the image of a point scatterer located at $\boldsymbol{z}$, i.e., it is the field due to a unit magnitude delta-function at $\boldsymbol{z}$ processed with the matched filter $\overline{P(\,\cdot\,)}$.

The antenna of a real SAR sensor emits and receives a series of chirps (3.1) as the satellite travels along the orbit. Let us therefore consider a sequence of emitting times and locations $(t_n,\boldsymbol{x}^n)$ and the corresponding sequence of receiving locations $\tilde{\boldsymbol{x}}^n$. For each n, we build the point spread function following (3.8):

$$W_n(\boldsymbol{y},\boldsymbol{z}) = \int \overline{P(t-t_n-|\tilde{\boldsymbol{x}}^n-\boldsymbol{y}|/c-|\boldsymbol{y}-\boldsymbol{x}^n|/c)}P(t-t_n-|\tilde{\boldsymbol{x}}^n-\boldsymbol{z}|/c-|\boldsymbol{z}-\boldsymbol{x}^n|/c)dt. \tag{3.9}$$

The generalized ambiguity function of a SAR system takes into account the information from multiple interrogating pulses by summing up the corresponding contributions (3.9):

$$W(\boldsymbol{y},\boldsymbol{z}) = \sum_n \vartheta(\boldsymbol{z},\boldsymbol{x}^n)W_n(\boldsymbol{y},\boldsymbol{z}). \tag{3.10}$$

The factor $\vartheta(\boldsymbol{z},\boldsymbol{x}^n)$ under the sum in (3.10) determines the range of summation. It comes from the directivity pattern of the antenna, because in real-life settings the antenna is never a point monopole with isotropic radiation. In fact, the actual antenna emits a rather narrow beam, see [Che01], and the quantity $\vartheta(\boldsymbol{z},\boldsymbol{x}^n)$ can be approximated as follows:

$$\vartheta(\boldsymbol{z},\boldsymbol{x}^n) = \begin{cases} 1, & \text{if the target } \boldsymbol{z} \text{ is in the beam emitted from } \boldsymbol{x}^n, \\ 0, & \text{otherwise.} \end{cases}$$

We will later see (Section 3.3) how to determine whether a given target is in the antenna beam or not. We will also see that it is precisely the summation (3.10) that can help interpret the processing of the received field $\psi(t,\tilde{\boldsymbol{x}})$ in the sense of the (discrete) inverse Fourier transform (Sections 3.3 and 3.4).

The generalized ambiguity function (3.10) is a key construct that allows one to analyze the performance of a SAR system. Indeed, it yields the image of an ultimately simplified target, which is a point scatterer, whereas other, more complex, targets can be assembled of point scatterers. Of central importance in terms of performance is the resolution of a radar, i.e., its ability to distinguish between two different targets located at a certain distance apart. If we could make the generalized ambiguity function (3.10) equal to the delta-function, $W(\boldsymbol{y},\boldsymbol{z}) = \delta(\boldsymbol{y}-\boldsymbol{z})$, then the radar would have had an ideal resolution. In reality, however, this is never achieved, but the sharper (i.e., narrower) the peak that $W(\boldsymbol{y},\boldsymbol{z})$ has when the reference location $\boldsymbol{y}$ approaches the actual target location $\boldsymbol{z}$, the better.

Note that in most studies of monostatic synthetic aperture radar resolution,[6] the receiving locations $\tilde{\boldsymbol{x}}^n$ are taken the same as the emitting locations $\boldsymbol{x}^n$, see, e.g., Section 2.3.1. This corresponds to the start-stop approximation, when the antenna emits the interrogating pulse and receives the scattered response while at the same position, and then continues to move along the orbit to the next position. In this section though, we have intentionally allowed for the receiving and emitting locations to differ in the expressions for the point spread function (3.9) and the generalized ambiguity function (3.10). This will let us take into account the actual antenna displacement during the pulse round-trip time between the orbit and the ground, and

[5] Recall that both $I(\boldsymbol{y})$ and $W(\boldsymbol{y},\boldsymbol{z})$ also depend on the emitting and receiving locations $\boldsymbol{x}$ and $\tilde{\boldsymbol{x}}$, respectively.

[6] Bistatic systems, unlike monostatic, have separate transmitting and receiving antennas, see, e.g., [CGM95, page 18].

thus analyze the effect of the start-stop approximation on the quality of the image, see Section 3.3. Note also that formulae (3.9) and (3.10) assume that both the antenna and the target are motionless when the pulse is emitted and received. To account for the motion and hence for the Doppler effect, the expressions for the point spread function and the generalized ambiguity function will be modified with the help of the Lorentz transform, see Section 3.4.

3.3. Antenna displacement. For the analysis of SAR resolution, the generalized ambiguity function (3.10) can be conveniently decomposed into the product of two factors, transverse and longitudinal, that will be responsible for the range and azimuthal (i.e., cross-range) resolution, respectively, see [Che01]. To do so, we first use formulae (3.1) and (3.9) and recast expression (3.10) as follows:

$$W(\boldsymbol{y},\boldsymbol{z}) = \sum_n \vartheta(\boldsymbol{z},\boldsymbol{x}^n) \int \overline{A(t-t_n-|\tilde{\boldsymbol{x}}^n-\boldsymbol{y}|/c-|\boldsymbol{y}-\boldsymbol{x}^n|/c)} e^{i\omega_0(|\tilde{\boldsymbol{x}}^n-\boldsymbol{y}|/c+|\boldsymbol{y}-\boldsymbol{x}^n|/c)} \times A(t-t_n-|\tilde{\boldsymbol{x}}^n-\boldsymbol{z}|/c-|\boldsymbol{z}-\boldsymbol{x}^n|/c) e^{-i\omega_0(|\tilde{\boldsymbol{x}}^n-\boldsymbol{z}|/c+|\boldsymbol{z}-\boldsymbol{x}^n|/c)} dt. \tag{3.11}$$

Next, we take the new integration variable as $t-t_n$ in each term of the sum (3.11) and denote it by t again. Then, we realize that neither $\overline{A(t-|\tilde{\boldsymbol{x}}^n-\boldsymbol{y}|/c-|\boldsymbol{y}-\boldsymbol{x}^n|/c)}$ nor $A(t-|\tilde{\boldsymbol{x}}^n-\boldsymbol{z}|/c-|\boldsymbol{z}-\boldsymbol{x}^n|/c)$ depends on n explicitly, except for the dependence via $\boldsymbol{x}^n$ and $\tilde{\boldsymbol{x}}^n$. The latter is weak, because we are assuming that the distance from the orbit to the ground is much larger than the distance between the successive emitting (or receiving) positions of the antenna on the orbit. Hence, $|\boldsymbol{y}-\boldsymbol{x}^n|/c$, etc., are slowly varying functions of n, and on top of it we have another slowly varying function $A(\,\cdot\,)$. Therefore, the amplitudes $A(\,\cdot\,)$ and $\overline{A(\,\cdot\,)}$ can be taken outside the sum (3.11), and we obtain:

$$W(\boldsymbol{y},\boldsymbol{z}) \approx \underbrace{\Big(\sum_n \vartheta(\boldsymbol{z},\boldsymbol{x}^n) e^{i\omega_0(|\tilde{\boldsymbol{x}}^n-\boldsymbol{y}|/c+|\boldsymbol{y}-\boldsymbol{x}^n|/c-|\tilde{\boldsymbol{x}}^n-\boldsymbol{z}|/c-|\boldsymbol{z}-\boldsymbol{x}^n|)}\Big)}_{W_A(\boldsymbol{y},\boldsymbol{z})} \times \underbrace{\Big(\int \overline{A(t-|\tilde{\boldsymbol{x}}^0-\boldsymbol{y}|/c-|\boldsymbol{y}-\boldsymbol{x}^0|/c)} A(t-|\tilde{\boldsymbol{x}}^0-\boldsymbol{z}|/c-|\boldsymbol{z}-\boldsymbol{x}^0|/c) dt\Big)}_{W_R(\boldsymbol{y},\boldsymbol{z})},$$

where we have replaced the superscript "n" by "0" in the factor $W_R(\boldsymbol{y},\boldsymbol{z})$ for definiteness. Consequently, the generalized ambiguity function can be (approximately) represented as a product of the azimuthal factor:

$$W_A(\boldsymbol{y},\boldsymbol{z}) = \sum_n \vartheta(\boldsymbol{z},\boldsymbol{x}^n) e^{i\omega_0(|\tilde{\boldsymbol{x}}^n-\boldsymbol{y}|/c+|\boldsymbol{y}-\boldsymbol{x}^n|/c-|\tilde{\boldsymbol{x}}^n-\boldsymbol{z}|/c-|\boldsymbol{z}-\boldsymbol{x}^n|/c)} \tag{3.12}$$

and the range factor:

$$W_R(\boldsymbol{y},\boldsymbol{z}) = \int \overline{A(t-|\tilde{\boldsymbol{x}}^0-\boldsymbol{y}|/c-|\boldsymbol{y}-\boldsymbol{x}^0|/c)} A(t-|\tilde{\boldsymbol{x}}^0-\boldsymbol{z}|/c-|\boldsymbol{z}-\boldsymbol{x}^0|/c) dt. \tag{3.13}$$

We will see that the factor $W_A(\boldsymbol{y},\boldsymbol{z})$ of (3.12) is responsible for the resolution in the longitudinal, or azimuthal, direction (i.e., along the orbit), whereas the factor $W_R(\boldsymbol{y},\boldsymbol{z})$ of (3.13) is responsible for the resolution in the transverse, or range, direction (perpendicular to the orbit).

3.3.1. Azimuthal resolution. Hereafter, we will denote individual Cartesian coordinates by subscripts: $\boldsymbol{x}=(x_1,x_2,x_3)$, $\boldsymbol{y}=(y_1,y_2,y_3)$, $\boldsymbol{z}=(z_1,z_2,z_3)$. With no loss of generality we can assume that the orbit is parallel to the Cartesian direction "1" (recall, we are considering only short stretches of the orbit and hence can neglect its curvature). To analyze the azimuthal resolution we will assume that both the target $\boldsymbol{z}$ and the reference point $\boldsymbol{y}$ are located on the Earth's surface at the same distance R_0 from the orbit, see Figure 3.1. Let κ denote the angle between the velocity $\boldsymbol{v}$ of the satellite (positive x_1 direction) and the direction of the antenna beam (i.e., its central line). If $\kappa<\pi/2$, then the antenna is pointing forward; if $\kappa>\pi/2$, then the antenna is pointing backward; and the value $\kappa=\pi/2$ corresponds to broadside imaging.

Let us denote the center of the antenna beam footprint on the Earth's surface by $\boldsymbol{q}=(q_1,q_2,q_3)$. Clearly, we have: $q_1=x_1+R_0\cot\kappa$, see Figure 3.1. Hereafter, we will assume with no loss of generality that both

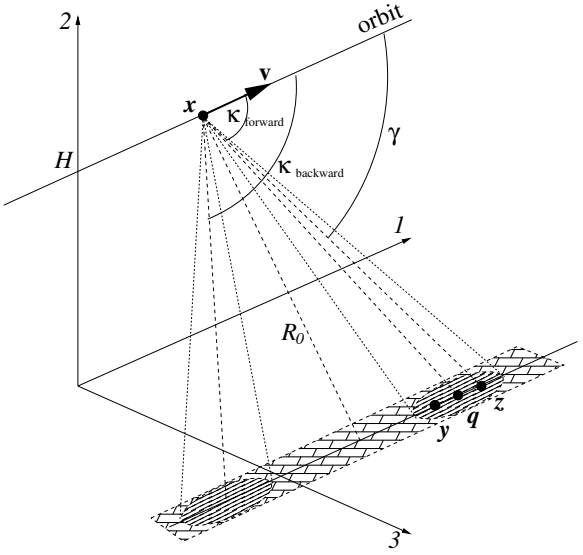

FIG. 3.1. *SAR imaging schematic for the squinted stripmap mode with the antenna pointing either forward or backward:* $\kappa_{\text{forward}} < \pi/2$ *and* $\kappa_{\text{backward}} > \pi/2$.

the target $\boldsymbol{z}$ and the reference point $\boldsymbol{y}$ are close to the center of the footprint $\boldsymbol{q}$ so that $|q_1 - z_1| \ll R_0$ and $|q_1 - y_1| \ll R_0$. Then, we can use the law of cosines and the first order Taylor expansion of the square root to obtain approximate expressions for the distances that appear in the exponent in formula (3.12), see Figure 3.1. For example, we have:

$$\begin{aligned} |\boldsymbol{z} - \boldsymbol{x}^n| &= \sqrt{\frac{R_0^2}{\sin^2\kappa} + (z_1 - q_1^n)^2 - 2\frac{R_0}{\sin\kappa}(z_1 - q_1^n)\cos(\pi - \kappa)} \\ &= \frac{R_0}{\sin\kappa}\sqrt{1 + \frac{(z_1 - q_1^n)^2\sin^2\kappa}{R_0^2} + 2\frac{(z_1 - q_1^n)\sin\kappa\cos\kappa}{R_0}} \\ &\approx \frac{R_0}{\sin\kappa} + \frac{(z_1 - q_1^n)^2\sin\kappa}{2R_0} + (z_1 - q_1^n)\cos\kappa, \end{aligned} \tag{3.14}$$

and similarly for the remaining three quantities: $|\boldsymbol{y} - \boldsymbol{x}^n|$, $|\tilde{\boldsymbol{x}}^n - \boldsymbol{y}|$, and $|\tilde{\boldsymbol{x}}^n - \boldsymbol{z}|$.

Expression (3.14) and analogous expressions for other distances need to be substituted into formula (3.12). Before doing that, let us determine the range of summation in (3.12). Let L be the size of the antenna in the direction parallel to the orbit, and let $\lambda = 2\pi c/\omega_0$ denote the carrier wavelength. Typically we have $\lambda \ll L$, in which case the antenna emits a narrow beam with the angular width of approximately $2\lambda/L$, see [Che01] and [Tsy09a, Appendix B]. Then, it is easy to see (from Figure 3.1) that the target $\boldsymbol{z}$ is in the beam as long as

$$|z_1 - q_1^n| \le \frac{R_0}{\sin\kappa}\left(\tan\frac{\lambda}{L}\right)\frac{1}{\sin\kappa} \approx \frac{R_0}{\sin^2\kappa}\frac{\lambda}{L}.$$

Consequently, we can write:

$$\vartheta(\boldsymbol{z}, \boldsymbol{x}^n) = \begin{cases} 1, & \text{if } z_1 - \frac{\lambda R_0}{L\sin^2\kappa} \le q_1^n \le z_1 + \frac{\lambda R_0}{L\sin^2\kappa}, \\ 0, & \text{if } q_1^n < z_1 - \frac{\lambda R_0}{L\sin^2\kappa} \text{ or } q_1^n > z_1 + \frac{\lambda R_0}{L\sin^2\kappa}. \end{cases} \tag{3.15}$$

Let Δx_1 be the distance along the orbit between the successive emissions of pulses so that $x_1^n = n\Delta x_1$. Let us also recall that $q_1^n = x_1^n + R_0\cot\kappa$, see Figure 3.1, and introduce

$$N = \left[\frac{2\lambda R_0}{\Delta x_1 L\sin^2\kappa}\right] \quad \text{and} \quad N_0 = \left[\frac{z_1 - R_0\cot\kappa}{\Delta x_1}\right],$$

where $[\,\cdot\,]$ stands for the integer part. Then, according to (3.15) we can re-write the sum (3.12) as follows:

$$W_A(\boldsymbol{y},\boldsymbol{z}) = \sum_{n=N_0-N/2}^{N_0+N/2} e^{i\omega_0(|\tilde{\boldsymbol{x}}^n-\boldsymbol{y}|/c+|\boldsymbol{y}-\boldsymbol{x}^n|/c-|\tilde{\boldsymbol{x}}^n-\boldsymbol{z}|/c-|\boldsymbol{z}-\boldsymbol{x}^n|/c)}. \tag{3.16}$$

Next, we substitute expression (3.14) and the like into the exponents in formula (3.16). In doing so, we take the terms that do not depend on n outside the sum:

$$\begin{aligned} W_A(\boldsymbol{y},\boldsymbol{z}) &= e^{\frac{i\omega_0\cos\kappa}{c}(2y_1-2z_1)} \sum_{n=N_0-N/2}^{N_0+N/2} e^{\frac{i\omega_0\sin\kappa}{2R_0c}((y_1-\tilde{q}_1^n)^2+(y_1-q_1^n)^2-(z_1-\tilde{q}_1^n)^2-(z_1-q_1^n)^2)} \\ &= e^{\frac{i\omega_0\cos\kappa}{c}(2y_1-2z_1)} e^{\frac{i\omega_0\sin\kappa}{2R_0c}(2y_1^2-2z_1^2)} \sum_{n=N_0-N/2}^{N_0+N/2} e^{\frac{i\omega_0\sin\kappa}{R_0c}(z_1\tilde{q}_1^n+z_1q_1^n-y_1\tilde{q}_1^n-y_1q_1^n)} \\ &= e^{\frac{i\omega_0\cos\kappa}{c}(2y_1-2z_1)} e^{\frac{i\omega_0\sin\kappa}{2R_0c}(2y_1^2-2z_1^2)} \sum_{n=N_0-N/2}^{N_0+N/2} e^{\frac{i\omega_0\sin\kappa}{R_0c}(2(z_1-y_1)q_1^n+(z_1-y_1)(\tilde{q}_1^n-q_1^n))}. \end{aligned} \tag{3.17}$$

We have now arrived at the point when we need to identify a relationship between the quantities q_1^n and $\tilde{q}_1^n$ or equivalently, between $x_1 = q_1 - R_0\cot\kappa$ and $\tilde{x}_1 = \tilde{q}_1 - R_0\cot\kappa$. For each n, x_1^n denotes the first coordinate of the location at which the n-th pulse is emitted, whereas $\tilde{x}_1^n$ is the first coordinate of the location at which the scattered signal is received. Clearly, $\tilde{q}_1^n - q_1^n = \tilde{x}_1^n - x_1^n = vT$, where $v = |\boldsymbol{v}|$ is the speed of the satellite and $T = T(\boldsymbol{z})$ is the round-trip travel time between the antenna and the target. To find T, let us denote by γ the angle between the velocity $\boldsymbol{v}$ and the direction $\boldsymbol{z}-\boldsymbol{x}$ from the antenna $\boldsymbol{x}$ to the target $\boldsymbol{z}$; it is easy to see from Figure 3.1 that $\cot\gamma = (z_1 - x_1)/R_0$. Using the law of cosines, we can then write:

$$\begin{aligned} T(\boldsymbol{z}) &= \frac{|\boldsymbol{z}-\boldsymbol{x}|}{c} + \frac{1}{c}\sqrt{|\boldsymbol{z}-\boldsymbol{x}|^2 + (vT)^2 - 2|\boldsymbol{z}-\boldsymbol{x}|(vT)\cos\gamma} \\ &= \frac{|\boldsymbol{z}-\boldsymbol{x}|}{c} + \frac{1}{c}\sqrt{|\boldsymbol{z}-\boldsymbol{x}|^2 + (vT)^2 - 2(z_1-x_1)(vT)}. \end{aligned} \tag{3.18}$$

This is a quadratic equation with respect to T. Solving it, we obtain:

$$T(\boldsymbol{z}) = 2\frac{|\boldsymbol{z}-\boldsymbol{x}|/c - (z_1-x_1)/c(v/c)}{1-v^2/c^2}. \tag{3.19}$$

Then, combining (3.19) with (3.14) and disregarding the v^2/c^2 term in the denominator, we can write:

$$\tilde{q}_1^n - q_1^n = vT = 2\frac{v}{c}\cdot\frac{R_0}{\sin\kappa} + \frac{v}{c}\cdot\frac{(z_1-q_1^n)^2\sin\kappa}{R_0} + 2\frac{v}{c}(z_1-q_1^n)\cos\kappa - 2\frac{v^2}{c^2}(z_1-x_1^n). \tag{3.20}$$

In the previous expression, we can also drop the second term on the right-hand side as it is much smaller than the third term. Consequently, we can continue equality (3.17) as follows:

$$\begin{aligned} W_A(\boldsymbol{y},\boldsymbol{z}) &= e^{\frac{i\omega_0\cos\kappa}{c}(2y_1-2z_1)} e^{\frac{i\omega_0\sin\kappa}{2R_0c}(2y_1^2-2z_1^2)} \sum_{n=N_0-N/2}^{N_0+N/2} e^{\frac{i\omega_0\sin\kappa}{R_0c}(z_1-y_1)(2q_1^n+vT)} \\ &= e^{\frac{i\omega_0\cos\kappa}{c}(2y_1-2z_1)} e^{\frac{i\omega_0\sin\kappa}{2R_0c}(2y_1^2-2z_1^2+2(z_1-y_1)\frac{v}{c}(\frac{R_0}{\sin\kappa}+z_1\cos\kappa))} \sum_{n=N_0-N/2}^{N_0+N/2} e^{\frac{i\omega_0\sin\kappa}{R_0c}2(z_1-y_1)(1-\frac{v}{c}\cos\kappa)q_1^n}, \end{aligned}$$

where we have taken the factors that do not depend on n outside the sum, and besides, we have neglected

the last term of (3.20) in the exponent as it was only a $\sim v^2/c^2$ correction to the zeroth order term. Then,

$$\begin{aligned} W_A(\boldsymbol{y},\boldsymbol{z}) &= e^{\frac{i\omega_0\cos\kappa}{c}(2y_1-2z_1)} e^{\frac{i\omega_0\sin\kappa}{R_0 c}(y_1^2-z_1^2+(z_1-y_1)(\frac{v}{c}(\frac{R_0}{\sin\kappa}+z_1\cos\kappa)+2(1-\frac{v}{c}\cos\kappa)R_0\cot\kappa))} \\ &\times \sum_{n=N_0-N/2}^{N_0+N/2} e^{\frac{i\omega_0\sin\kappa}{R_0 c}2(z_1-y_1)(1-\frac{v}{c}\cos\kappa)x_1^n} \\ &= e^{\frac{i\omega_0\cos\kappa}{c}(2y_1-2z_1)} e^{\frac{i\omega_0\sin\kappa}{R_0 c}(y_1^2-z_1^2+(z_1-y_1)(\frac{v}{c}(\frac{R_0}{\sin\kappa}+z_1\cos\kappa)+2(1-\frac{v}{c}\cos\kappa)(R_0\cot\kappa+N_0\Delta x_1)))} \\ &\times \sum_{n=-N/2}^{N/2} e^{\frac{i\omega_0\sin\kappa}{R_0 c}2(z_1-y_1)(1-\frac{v}{c}\cos\kappa)n\Delta x_1}. \end{aligned} \tag{3.21}$$

Two observations can immediately be made. First, the factor in front of the sum in formula (3.21) has magnitude one and can be left out of consideration when analyzing the SAR resolution. Second, the effect of the antenna displacement during the round-trip travel time between the orbit and the ground is accounted for by the factor $(1-\frac{v}{c}\cos\kappa)$ in the exponent under the sum in formula (3.21). To actually estimate the azimuthal resolution, one needs to compute the sum:

$$W_A(\boldsymbol{y},\boldsymbol{z}) \propto \sum_{n=-N/2}^{N/2} e^{\frac{i\omega_0\sin\kappa}{R_0 c}2(z_1-y_1)(1-\frac{v}{c}\cos\kappa)n\Delta x_1}. \tag{3.22}$$

This sum can be interpreted as the discrete (inverse) Fourier transform which, for example, is encountered frequently in the analysis of finite-difference approximations (see, e.g., [RT07]), as well as in a variety of other contexts. Sum (3.22) is a geometric sequence and can therefore be evaluated easily. Again, up to a factor of magnitude one we have:

$$W_A(\boldsymbol{y},\boldsymbol{z}) \propto \frac{\sin\left[\frac{\omega_0\sin\kappa}{R_0 c}(z_1-y_1)(1-\frac{v}{c}\cos\kappa)(N+1)\Delta x_1\right]}{\sin\left[\frac{\omega_0\sin\kappa}{R_0 c}(z_1-y_1)(1-\frac{v}{c}\cos\kappa)\Delta x_1\right]}. \tag{3.23}$$

Let us further assume that

$$|z_1-y_1| \ll \frac{R_0 c}{\omega_0\sin\kappa\Delta x_1} = \frac{R_0\lambda}{2\pi\sin\kappa\Delta x_1},$$

which simply means that for the purpose of conducting the analysis we would like the reference point to be sufficiently close to the target. In this case the argument of the sine function in the denominator of (3.23) is small and we can write:

$$W_A(\boldsymbol{y},\boldsymbol{z}) \propto (N+1)\mathrm{sinc}\left[\frac{\omega_0\sin\kappa}{R_0 c}(z_1-y_1)\left(1-\frac{v}{c}\cos\kappa\right)(N+1)\Delta x_1\right]. \tag{3.24}$$

The sinc function (3.24) is what one typically gets instead of the ideal $\delta(z_1-y_1)$ when analyzing radar performance. The sharper the maximum of the sinc, i.e., the closer it is to the delta-function, the better the resolution of the SAR, i.e., the minimum distance between the two point targets that the radar can still tell apart. Therefore, it is natural to estimate the resolution as the width of the main lobe of the sinc:[7]

$$(z_1-y_1)\left(1-\frac{v}{c}\cos\kappa\right) = \frac{2\pi R_0 c}{\omega_0\sin\kappa(N+1)\Delta x_1} = \frac{R_0\lambda}{\sin\kappa(N+1)\Delta x_1} \approx \frac{L\sin\kappa}{2},$$

so that we can write ($v/c \ll 1$):

$$z_1-y_1 \approx \frac{L\sin\kappa}{2}\left(1+\frac{v}{c}\cos\kappa\right). \tag{3.25}$$

[7] Sometimes, it is taken as half this width.

If not for the additional factor $\left(1+\frac{v}{c}\cos\kappa\right)$, formula (3.25) would yield a standard expression for the azimuthal SAR resolution in the framework of the start-stop approximation (in the squinted stripmap mode). The additional factor disappears when $\kappa=\pi/2$. In other words, in the case of broadside imaging, the start-stop approximation does not affect the azimuthal resolution of a SAR sensor at all. Otherwise, when $\cos\kappa\neq 0$, the foregoing analysis indicates that the actual resolution may be slightly worse than that obtained with the help of the start-stop approximation. The deterioration, however, is minute, on the order of v/c, which is about $2.7\cdot 10^{-5}$ for low orbit satellites, and which can be safely disregarded for all practical purposes.

3.3.2. Range resolution. To analyze the range resolution, we substitute the envelope A of the chirp, see (3.1), into formula (3.13):

$$W_R(\boldsymbol{y},\boldsymbol{z})=\int_{-\tau/2+\tau_{\min}}^{\tau/2+\tau_{\max}}\overline{e^{i\alpha(t-|\tilde{\boldsymbol{x}}^0-\boldsymbol{y}|/c-|\boldsymbol{y}-\boldsymbol{x}^0|/c)^2}}e^{i\alpha(t-|\tilde{\boldsymbol{x}}^0-\boldsymbol{z}|/c-|\boldsymbol{z}-\boldsymbol{x}^0|/c)^2}dt, \tag{3.26}$$

where

$$\tau_{\max}=\max\{(|\tilde{\boldsymbol{x}}^0-\boldsymbol{y}|/c+|\boldsymbol{y}-\boldsymbol{x}^0|/c),(|\tilde{\boldsymbol{x}}^0-\boldsymbol{z}|/c+|\boldsymbol{z}-\boldsymbol{x}^0|/c)\} \tag{3.27a}$$

and

$$\tau_{\min}=\min\{(|\tilde{\boldsymbol{x}}^0-\boldsymbol{y}|/c+|\boldsymbol{y}-\boldsymbol{x}^0|/c),(|\tilde{\boldsymbol{x}}^0-\boldsymbol{z}|/c+|\boldsymbol{z}-\boldsymbol{x}^0|/c)\}. \tag{3.27b}$$

Formula (3.26) holds provided that $\Delta\tau\stackrel{\text{def}}{=}\tau_{\max}-\tau_{\min}<\tau$, otherwise the integral is equal to zero. If it is not zero, then from (3.26) we find:

$$\begin{aligned}W_R(\boldsymbol{y},\boldsymbol{z})&=e^{i\alpha((|\tilde{\boldsymbol{x}}^0-\boldsymbol{z}|/c+|\boldsymbol{z}-\boldsymbol{x}^0|/c)^2-(|\tilde{\boldsymbol{x}}^0-\boldsymbol{y}|/c+|\boldsymbol{y}-\boldsymbol{x}^0|/c)^2)}\\&\quad\times\int_{-\tau/2+\tau_{\max}}^{\tau/2+\tau_{\min}}e^{2i\alpha t((|\tilde{\boldsymbol{x}}^0-\boldsymbol{y}|/c+|\boldsymbol{y}-\boldsymbol{x}^0|/c)-(|\tilde{\boldsymbol{x}}^0-\boldsymbol{z}|/c+|\boldsymbol{z}-\boldsymbol{x}^0|/c))}dt.\end{aligned} \tag{3.28}$$

The factor in front of the integral in (3.28) can be disregarded because in has magnitude one. The integral itself needs to be evaluated for the case when the reference location $\boldsymbol{y}$ is close to the target $\boldsymbol{z}$; then, the length of the interval of integration, $\tau+\tau_{\min}-\tau_{\max}=\tau-\Delta\tau$, will also be close to τ. The integration yields:

$$\begin{aligned}W_R(\boldsymbol{y},\boldsymbol{z})&\propto\frac{c}{2i\alpha((|\tilde{\boldsymbol{x}}^0-\boldsymbol{y}|+|\boldsymbol{y}-\boldsymbol{x}^0|)-(|\tilde{\boldsymbol{x}}^0-\boldsymbol{z}|+|\boldsymbol{z}-\boldsymbol{x}^0|))}\\&\quad\times e^{2i\alpha t((|\tilde{\boldsymbol{x}}^0-\boldsymbol{y}|/c+|\boldsymbol{y}-\boldsymbol{x}^0|/c)-(|\tilde{\boldsymbol{x}}^0-\boldsymbol{z}|/c+|\boldsymbol{z}-\boldsymbol{x}^0|/c))}\Big|_{-\tau/2+\tau_{\max}}^{\tau/2+\tau_{\min}}\end{aligned}$$

or equivalently (up to another factor of magnitude one):

$$\begin{aligned}W_R(\boldsymbol{y},\boldsymbol{z})&\propto\frac{c}{2i\alpha((|\tilde{\boldsymbol{x}}^0-\boldsymbol{y}|+|\boldsymbol{y}-\boldsymbol{x}^0|)-(|\tilde{\boldsymbol{x}}^0-\boldsymbol{z}|+|\boldsymbol{z}-\boldsymbol{x}^0|))}\\&\quad\times e^{2i\alpha t((|\tilde{\boldsymbol{x}}^0-\boldsymbol{y}|/c+|\boldsymbol{y}-\boldsymbol{x}^0|/c)-(|\tilde{\boldsymbol{x}}^0-\boldsymbol{z}|/c+|\boldsymbol{z}-\boldsymbol{x}^0|/c))}\Big|_{-\tau/2+\Delta\tau/2}^{\tau/2-\Delta\tau/2}\\&=\frac{2c\tau}{B((|\tilde{\boldsymbol{x}}^0-\boldsymbol{y}|+|\boldsymbol{y}-\boldsymbol{x}^0|)-(|\tilde{\boldsymbol{x}}^0-\boldsymbol{z}|+|\boldsymbol{z}-\boldsymbol{x}^0|))}\\&\quad\times\sin\left(\frac{B((|\tilde{\boldsymbol{x}}^0-\boldsymbol{y}|+|\boldsymbol{y}-\boldsymbol{x}^0|)-(|\tilde{\boldsymbol{x}}^0-\boldsymbol{z}|+|\boldsymbol{z}-\boldsymbol{x}^0|))}{2c}\pm\frac{B\Delta\tau^2}{2\tau}\right),\end{aligned} \tag{3.29}$$

where B is the bandwidth of the chirp, see (3.2), and the sign plus or minus under the sine function in (3.29) depends on what actual value delivers the maximum and minimum in formulae (3.27a) and (3.27b). In any event, as we are primarily interested in the case $\Delta\tau/\tau\ll 1$, we can disregard the second term under the sine and obtain:

$$W_R(\boldsymbol{y},\boldsymbol{z})\propto\tau\cdot\operatorname{sinc}\left(\frac{B((|\tilde{\boldsymbol{x}}^0-\boldsymbol{y}|+|\boldsymbol{y}-\boldsymbol{x}^0|)-(|\tilde{\boldsymbol{x}}^0-\boldsymbol{z}|+|\boldsymbol{z}-\boldsymbol{x}^0|))}{2c}\right). \tag{3.30}$$

If the receiving location $\tilde{\boldsymbol{x}}^0$ coincides with the emitting location $\boldsymbol{x}^0$, which corresponds to the start-stop approximation, then formula (3.30) yields a standard expression for the range resolution, i.e., for the resolution of the distance between the antenna and the target. It is given by the full width of the main lobe of the sinc, which is twice its half-width, and the latter is obtained by setting the argument of the sinc equal to π:

$$|\boldsymbol{x}^0 - \boldsymbol{y}| - |\boldsymbol{x}^0 - \boldsymbol{z}| = \frac{2\pi c}{B}. \tag{3.31}$$

If the emitting and receiving locations are different, then instead of (3.31) we have:

$$(|\tilde{\boldsymbol{x}}^0 - \boldsymbol{y}| + |\boldsymbol{y} - \boldsymbol{x}^0|) - (|\tilde{\boldsymbol{x}}^0 - \boldsymbol{z}| + |\boldsymbol{z} - \boldsymbol{x}^0|)) = \frac{4\pi c}{B}. \tag{3.32}$$

Formula (3.31) can be interpreted as if the target $\boldsymbol{z}$ and the reference location $\boldsymbol{y}$ lie on two concentric spheres centered at $\boldsymbol{x}^0$, and these two spheres can be told apart if their radii differ by more than $2\pi c/B$. Likewise, formula (3.32) shall be interpreted as if the target $\boldsymbol{z}$ and the reference location $\boldsymbol{y}$ lie on two ellipsoids of revolution with common foci $\boldsymbol{x}^0$ and $\tilde{\boldsymbol{x}}^0$, and these two ellipsoids can be told apart if the corresponding sums of distances to the foci (each sum is equal to twice the major semi-axis) differ by more than $4\pi c/B$.

Hence, the eccentricity of the ellipsoids in (3.32) will provide a measure of the difference between the resolution obtained using the start-stop approximation and the resolution obtained with no use of this approximation. It turns out that this eccentricity is extremely close to one, i.e., that the ellipsoids are almost indistinguishable from spheres. Indeed, if the major semi-axis is estimated as $a = R_0 \approx 1000km$, then the minor semi-axis is $b = \sqrt{R_0^2 - (vT/2)^2} \approx R_0(1-(vT)^2/8R_0^2) \approx R_0(1-2\cdot 10^{-10})$, because $vT \approx 40m$. With the chirp bandwidth $B \gtrsim 10^7 Hz$, the resolution given by either (3.31) or (3.32) appears to be on the order of meters, whereas the correction due to the eccentricity will be fractions of a millimeter. Clearly, it can be disregarded, which altogether means that in practice the displacement of the antenna during the round-trip travel time between the orbit and the Earth does not affect the resolution of a spaceborne SAR sensor.

3.4. The Doppler effect. In Section 3.3, we do take into account that the antenna changes its position as the signal it emits travels to the target and back. We still assume though that the antenna is motionless during the time the signal is emitted and the scattered response received. In reality, however, the antenna is moving continuously. Therefore, the expressions for the emitted and scattered field that we employed for constructing the generalized ambiguity function in Section 3.2 may themselves need to be corrected. In particular, expression (3.3) yields the field emitted by a motionless antenna; it will need to be modified to account for the actual motion. Likewise, expression (3.7) yields the scattered field in the original motionless coordinate system; it will need to be modified because the field is received by a moving antenna.

In this section, we will use the Lorentz transform to address the fact that the antenna is moving. We will see, in particular, that once the motion of the wave's emitter and/or receiver is properly accounted for, the observable frequency of the signal changes. This phenomenon is known as the Doppler frequency shift, see, e.g., [LL75] for electromagnetic waves and [LL87] for acoustics. In the literature on SAR, this frequency shift is sometimes used to explain the mechanism of azimuthal resolution, because the sequence of signals that illuminate the target from different emitting positions along the orbit can be interpreted as a linear chirp, see, e.g., [FL99]. A relation between the Doppler approach and that often used in tomography has also been established [MOJ83, AM89]. However, in the rigorous analysis based on the generalized ambiguity function, the Doppler effect is often disregarded. We, on the other hand, will show that the Doppler frequency shift should be included into the definition of a matched filter so that to minimize the distortions of the image.

Let us assume that the antenna is engaged in a straightforward uniform motion along the coordinate "1" of a Cartesian coordinate system, and that the speed of motion is v, see Figure 3.1. Of course, strictly speaking this is not true for a satellite orbiting the Earth, but it is a sufficiently good approximation for short stretches of the orbit. We will denote the position of the antenna by $\boldsymbol{x} = \boldsymbol{x}(t) = (vt, H, 0)$, where H is the orbit altitude, see Figure 3.1, and we will also assume that the pointwise antenna emits a signal $P(t)$. To find the corresponding field $\varphi(t, \boldsymbol{z})$ as a function of the time t and the observer's (target) location $\boldsymbol{z}$, we first change the coordinates so that in the new frame the antenna becomes motionless. Using the standard

notation for the relativistic square root: $\beta = \sqrt{1 - v^2/c^2}$, where c is the propagation speed, we write:

$$\theta = \frac{t}{\beta} - \frac{v/c}{\beta}\frac{z_1}{c}, \tag{3.33a}$$

$$\zeta_1 = -\frac{v/c}{\beta}ct + \frac{z_1}{\beta}. \tag{3.33b}$$

The remaining two spatial coordinates, z_2 and z_3, do not change, so that the overall transformation is $(t, z_1, z_2, z_3) \mapsto (\theta, \zeta_1, z_2, z_3)$. It is known as the Lorentz transform, and its distinctive feature is that it preserves the form of the d'Alembert operator [Gar07, Chapter 3, Section 3]. In particular, the equation

$$\begin{aligned}\frac{1}{c^2}\frac{\partial^2\varphi}{\partial t^2} - \frac{\partial^2\varphi}{\partial z_1^2} - \frac{\partial^2\varphi}{\partial z_2^2} - \frac{\partial^2\varphi}{\partial z_3^2} \\ = P(t)\delta(\boldsymbol{z} - \boldsymbol{x}(t)) \equiv P(t)\delta(z_1 - vt)\delta(z_2 - H)\delta(z_3),\end{aligned} \tag{3.34a}$$

becomes

$$\begin{aligned}\frac{1}{c^2}\frac{\partial^2\varphi}{\partial \theta^2} - \frac{\partial^2\varphi}{\partial \zeta_1^2} - \frac{\partial^2\varphi}{\partial z_2^2} - \frac{\partial^2\varphi}{\partial z_3^2} \\ = P\Big(\frac{\theta}{\beta} + \frac{v/c}{\beta}\frac{\zeta_1}{c}\Big)\delta(\beta\zeta_1)\delta(z_2 - H)\delta(z_3) \stackrel{\text{def}}{=} f(\theta, \zeta_1, z_2, z_3).\end{aligned} \tag{3.34b}$$

Note that if the standard Galileo transform was used instead of (3.33), then the differential operator in (3.34b) would not have been the same as in (3.34a), even though the antenna would still have been motionless in the new frame. Solution of equation (3.34b) subject to zero initial conditions can be easily found with the help of the Kirchhoff integral in the new coordinates:

$$\varphi(\theta, \zeta_1, z_2, z_3) = \frac{1}{4\pi}\iiint\limits_{\rho' \le c\theta} \frac{f(\theta - \rho'/c, \zeta_1', z_2', z_3')}{\rho'} d\zeta_1' dz_2' dz_3' = \frac{1}{4\pi\beta}\frac{P((\theta - \rho/c)/\beta)}{\rho}, \tag{3.35}$$

where $\rho' = \sqrt{(\zeta_1 - \zeta_1')^2 + (z_2 - z_2')^2 + (z_3 - z_3')^2}$ and $\rho = \sqrt{\zeta_1^2 + (z_2 - H)^2 + z_3^2}$. Note that up to the relativistic factors β, solution (3.35) is a standard retarded potential [compare with formula (3.3)] from the point source located at $(0, H, 0)$ in the new coordinates, which is expected. Note also that as an alternative, solution (3.35) could have been obtained in a "brute force" way, by computing the convolution with the fundamental solution of (3.34a) in the original coordinates, see Appendix D.

To understand the Doppler effect, solution (3.35) needs to be cast back to the original coordinates. Let us denote $r = \sqrt{z_1^2 + (z_2 - H)^2 + z_3^2}$. Then, according to (3.33b) we can write:

$$\begin{aligned}\zeta_1^2 = \frac{1}{\beta^2}(z_1 - vt)^2 = \frac{1}{\beta^2}(z_1^2 - 2z_1vt + (vt)^2) = z_1^2 + \frac{1 - \beta^2}{\beta^2}z_1^2 + \frac{1}{\beta^2}(-2z_1vt + (vt)^2) \\ = z_1^2 - 2z_1vt + \frac{1 - \beta^2}{\beta^2}(z_1 - vt)^2 + (vt)^2 = z_1^2 - 2rvt\cos\gamma + \frac{1 - \beta^2}{\beta^2}(z_1 - vt)^2 + (vt)^2,\end{aligned}$$

where as before (in Section 3.3), γ denotes the angle between the velocity $\boldsymbol{v}$ (positive first coordinate) and the direction from the antenna to the target, see Figure 3.1. Consequently,

$$\rho^2 = r^2 - 2rvt\cos\gamma + (vt)^2 + \frac{1 - \beta^2}{\beta^2}(z_1 - vt)^2. \tag{3.36}$$

The last term in equality (3.36) is $\sim v^2/c^2$, where v/c itself is small, $v/c \ll 1$. The second to last term is also quadratic with respect to v/c for the times of interest $t \sim r/c$. Hence, for the values of γ away from $\pi/2$ (so that $\cos\gamma \neq 0$) these two terms can be dropped, which yields the following approximate expression:

$$\rho \approx \sqrt{r^2 - 2rvt\cos\gamma} = r\sqrt{1 - \frac{2vt}{r}\cos\gamma} \approx r - vt\cos\gamma. \tag{3.37}$$

Then, substituting the value of ρ given by (3.37) into the solution (3.35), using the definition of the Lorentz transform (3.33), and approximating: $1/\beta = (1 - v^2/c^2)^{-1/2} \approx 1 + v^2/2c^2 \approx 1$, we arrive at

$$\varphi(t,\boldsymbol{z}) \approx \frac{1}{4\pi\beta}\frac{P\Big(\Big(\frac{1}{\beta}\left(t - \frac{vz_1}{c^2}\right) - \frac{r}{c} + \frac{v}{c}t\cos\gamma\Big)}{\rho} \approx \frac{1}{4\pi}\frac{P\left(\left(t - \frac{r}{c}\right)\left(1 + \frac{v}{c}\cos\gamma\right)\right)}{\rho}. \tag{3.38}$$

If the function $P(t)$ is a fast oscillation with the frequency ω_0, then it is also possible to replace ρ by r in the denominator of (3.38) because it only amounts to a slow and small ($\sim v/c$) variation of the amplitude:

$$\varphi(t,\boldsymbol{z}) \approx \frac{1}{4\pi}\frac{P\left(\left(t - \frac{r}{c}\right)\left(1 + \frac{v}{c}\cos\gamma\right)\right)}{r}. \tag{3.39}$$

Formula (3.39) is almost the standard retarded potential, except for the correction factor $1 + \frac{v}{c}\cos\gamma$ inside $P(\,\cdot\,)$. The presence of this factor means that if the field emitted by a moving antenna is received at a motionless target, then the frequency measured at the target changes, instead of the original ω_0 it becomes $\omega_0\left(1 + \frac{v}{c}\cos\gamma\right)$. This implies the increase of the frequency if the antenna is moving toward the target, $0 \le \gamma < \pi/2$, and the decrease of the frequency if the antenna is moving away from the target, $\pi/2 < \gamma \le \pi$. The correction to the frequency is linear with respect to v/c (since we have dropped the quadratic terms $\sim v^2/c^2$ in our analysis) and accordingly, the foregoing phenomenon is called the linear Doppler effect or linear Doppler frequency shift. Note also that in the same linear framework we can recast formula (3.39) as

$$\varphi(t,\boldsymbol{z}) \approx \frac{1}{4\pi r}P\left(\frac{t - \frac{r}{c}}{1 - \frac{v}{c}\cos\gamma}\right). \tag{3.40}$$

Expression (3.40) can be obtained independently, after equation (3.34a) has been solved directly by computing the convolution with the fundamental solution, see Appendix D.

For the sake of completeness, let us also comment briefly on the quadratic Doppler effect. The last two terms that we have disregarded on the right hand side of (3.36) become important, i.e., comparable to the second term, if $\cos\gamma \sim v/c$ or equivalently, $\pi/2 - v/c \lesssim \gamma \lesssim \pi/2 + v/c$, where $v/c \ll 1$. This means that the quadratic effect can manifest itself only for the broadside imaging, when the direction of the beam is normal to the orbit. On top of that, it may only be noticeable in a very narrow central part of the beam, because in practice $v/c \sim 10^{-5}$, whereas the angular semi-width of the beam λ/L could be about $1/30$ for the wavelength $\lambda = 30cm$ (corresponds to the carrier frequency $\omega_0 = 1GHz$) and the antenna size $L = 10m$. Hereafter, the quadratic Doppler effect $\sim v^2/c^2 \sim 10^{-10}$ will be neglected.

To account for the linear Doppler effect when building the generalized ambiguity function, we replace formula (3.3) with formula (3.39). Then, we differentiate $\varphi(t,\boldsymbol{z})$ and thus derive the sources of the scattered field in the framework of the first Born approximation [cf. formula (3.5)]:

$$\frac{\partial^2\varphi}{\partial t^2}(t,\boldsymbol{z}) \approx -\frac{\omega_0^2\left(1 + \frac{v}{c}\cos\gamma\right)^2}{4\pi}\frac{P\left(\left(t - \frac{r}{c}\right)\left(1 + \frac{v}{c}\cos\gamma\right)\right)}{r}. \tag{3.41}$$

For the point target located at $\boldsymbol{z}$, the scattered wave at $(t,\boldsymbol{x})$ is a retarded potential centered at $\boldsymbol{z}$ and modulated by the function (3.41) as a function of time [cf. formula (3.7)]:

$$\psi(t,\boldsymbol{x}) = -\frac{\omega_0^2\left(1 + \frac{v}{c}\cos\gamma\right)^2}{16\pi^2}\frac{P\left(\left(t - \frac{|\boldsymbol{x}-\boldsymbol{z}|}{c} - \frac{r}{c}\right)\left(1 + \frac{v}{c}\cos\gamma\right)\right)}{r\cdot|\boldsymbol{x}-\boldsymbol{z}|}. \tag{3.42}$$

When the scattered pulse (3.42) travels back from the target to the antenna, it generates another contribution to the Doppler frequency shift. The corresponding analysis can be conducted as before, by going to the frame of reference in which the receiver (antenna) is motionless. To do so, we employ essentially the same Lorentz transform except that as we want the solution in the form of a retarded potential centered around the origin, we need to have the origin of the new system initially located at the target $\boldsymbol{z}$, rather than at $\boldsymbol{x}(0) = (0,H,0)$.

As the scattered field is received at the antenna $\boldsymbol{x}$, we will use the variables $\boldsymbol{x} = (x_1, x_2, x_3)$ to write the transform, whereas the location of the target $\boldsymbol{z} = (z_1, z_2, z_3)$ will be considered fixed [cf. formulae (3.33)]:

$$\hat{\theta} = \frac{t}{\beta} - \frac{v/c}{\beta}\frac{x_1 - z_1}{c}, \tag{3.43a}$$

$$\xi_1 = -\frac{v/c}{\beta}ct + \frac{x_1 - z_1}{\beta}. \tag{3.43b}$$

Similarly to (3.33), the remaining two spatial coordinates do not get changed so that altogether we have the transformation $(t, x_1, x_2, x_3) \mapsto (\hat{\theta}, \xi_1, x_2, x_3)$. Relation (3.43b) implies, in particular, that in the new coordinates the antenna is not moving, because $x_1 = vt$ corresponds to $\xi_1 = -z_1/\beta = \text{const}$.

Let us introduce $\hat{\rho} = \sqrt{\xi_1^2 + (x_2 - z_2)^2 + (x_3 - z_3)^2}$ and $\hat{r} = \sqrt{(x_1 - z_1)^2 + (x_2 - z_2)^2 + (x_3 - z_3)^2} = |\boldsymbol{x} - \boldsymbol{z}|$. Then, $x_1 - z_1 = -\hat{r}\cos\gamma$, see Figure 3.1, and repeating the same derivation as led us to formula (3.37), we arrive at the following linearized relation between the distances:

$$\hat{\rho} \approx \hat{r} + vt\cos\gamma. \tag{3.44}$$

Consequently, letting $\beta \approx 1$ and using (3.43b), we can write:

$$\begin{aligned}\hat{\rho}\cos\gamma &\approx \hat{r}\cos\gamma + vt\cos^2\gamma = -(x_1 - z_1) + vt\cos^2\gamma \\ &\approx -\xi_1 - vt + vt\cos^2\gamma = -\xi - vt\sin^2\gamma\end{aligned}$$

so that

$$\xi_1 = -\hat{\rho}\cos\gamma - vt\sin^2\gamma. \tag{3.45}$$

Next, using formula (3.43a) and again neglecting quadratic terms with respect to v/c, we obtain from (3.44):

$$\hat{r} \approx \hat{\rho} - vt\cos\gamma = \hat{\rho} - v\beta\hat{\theta}\cos\gamma - \frac{v^2}{c^2}(x_1 - z_1) \approx \hat{\rho} - v\hat{\theta}\cos\gamma. \tag{3.46}$$

Finally, to implement the transformation in formula (3.42), we have to transform all times and distances on its right-hand side to new coordinates. We note that formula (3.42) is written so that $\boldsymbol{x}$ can be any location in space. We, however, are interested only in the case when $\boldsymbol{x}$ is the location of the antenna. Since the displacement of the antenna during the round-trip travel time of the signal does not affect the performance of the radar (Section 3.3) we take: $\boldsymbol{x} = \boldsymbol{x}(0) = (0, H, 0)$. In this case, $\hat{r} = |\boldsymbol{x} - \boldsymbol{z}| = r$ and instead of (3.42) we can write:

$$\psi(t, \boldsymbol{x}) = -\frac{\omega_0^2\left(1 + \frac{v}{c}\cos\gamma\right)^2}{16\pi^2}\frac{P\left(\left(t - \frac{2\hat{r}}{c}\right)\left(1 + \frac{v}{c}\cos\gamma\right)\right)}{\hat{r}^2}. \tag{3.47}$$

Substituting $\hat{r}$ given by (3.46) into formula (3.47), and also substituting the expression for t derived by inverting (3.43) and using (3.45):

$$t = \frac{\hat{\theta}}{\beta} + \frac{v/c}{\beta}\frac{\xi_1}{c} \approx \hat{\theta} - \frac{v}{c}\frac{\hat{\rho}}{c}\cos\gamma,$$

we have:

$$\begin{aligned}\psi(\hat{\theta}, \xi_1, x_2, x_3) &= -\frac{\omega_0^2\left(1 + \frac{v}{c}\cos\gamma\right)^2}{16\pi^2}\frac{P\left(\left(\hat{\theta} - \frac{2\hat{\rho}}{c}\right)\left(1 + \frac{v}{c}\cos\gamma\right)^2\right)}{\hat{r}^2} \\ &\approx -\frac{\omega_0^2\left(1 + 2\frac{v}{c}\cos\gamma\right)}{16\pi^2}\frac{P\left(\left(\hat{\theta} - \frac{2\hat{\rho}}{c}\right)\left(1 + 2\frac{v}{c}\cos\gamma\right)\right)}{\hat{r}^2} \\ &\approx -\frac{\omega_0^2}{16\pi^2}\frac{P\left(\left(\hat{\theta} - \frac{2\hat{\rho}}{c}\right)\left(1 + 2\frac{v}{c}\cos\gamma\right)\right)}{\hat{\rho}^2},\end{aligned} \tag{3.48}$$

where the last equality in (3.48) was obtained as before, by disregarding a slow and small ($\sim v/c$) variation in the amplitude. Formula (3.48) indicates, in particular, that in the frame of reference in which the satellite is motionless, the observed frequency of the signal emitted by the antenna, scattered off the target, and then again received by the antenna is $\omega_0\left(1+2\frac{v}{c}\cos\gamma\right)$ compared to the original frequency ω_0. Otherwise, if not for the coordinate change and the additional amplitude factor, the solution (3.48) looks exactly the same as it would have looked if both the antenna and the target were motionless [cf. formula (3.7)]; with $\frac{2\hat{\rho}}{c}$ being the round-trip travel time between the antenna and the target. Hence, this scattered solution can be used for building the generalized ambiguity function in the new coordinates.

3.4.1. Azimuthal resolution. Hereafter, we will follow the pathway of Section 3.2 for constructing the generalized ambiguity function. In doing so, we will use solution (3.48) instead of (3.7) as the central "building block." Following the analysis of Section 3.3, we will also disregard the displacement of the antenna from the very beginning. For the azimuthal factor we can then write [cf. formula (3.12)]:

$$W_A(\boldsymbol{y},\boldsymbol{z})=\sum_n \vartheta(\boldsymbol{z},\boldsymbol{x}^n)e^{2i\omega_0\left(|\boldsymbol{x}^n-\boldsymbol{y}|\left(1+\frac{2v}{c}\cos\gamma_{\boldsymbol{y}}^n\right)-|\boldsymbol{x}^n-\boldsymbol{z}|\left(1+\frac{2v}{c}\cos\gamma_{\boldsymbol{z}}^n\right)\right)/c}, \tag{3.49}$$

where the distances $|\boldsymbol{x}^n-\boldsymbol{y}|$ and $|\boldsymbol{x}^n-\boldsymbol{z}|$, even though denoted the same way as before, shall be measured in the Lorentz transformed coordinates, in which the antenna is not moving,[8] and the notation for the angles, $\gamma_{\boldsymbol{y}}^n$ and $\gamma_{\boldsymbol{z}}^n$, indicates that they depend on the position of the antenna.

We are particularly interested in analyzing that part of the exponent in formula (3.49) which has the factor v/c in front of it:

$$\begin{aligned}&\frac{2i\omega_0}{c}\frac{2v}{c}\left(|\boldsymbol{x}^n-\boldsymbol{y}|\cos\gamma_{\boldsymbol{y}}^n-|\boldsymbol{x}^n-\boldsymbol{z}|\cos\gamma_{\boldsymbol{z}}^n\right)\\ =\frac{2i\omega_0}{c}\frac{2v}{c}&\left(\frac{R_0}{\sin\kappa}(\cos\gamma_{\boldsymbol{y}}^n-\cos\gamma_{\boldsymbol{z}}^n)+\frac{(y_1-q_1^n)^2\sin\kappa}{2R_0}\cos\gamma_{\boldsymbol{y}}^n-\frac{(z_1-q_1^n)^2\sin\kappa}{2R_0}\cos\gamma_{\boldsymbol{z}}^n\right.\\ &\left.+(y_1-q_1^n)\cos\kappa\cos\gamma_{\boldsymbol{y}}^n-(z_1-q_1^n)\cos\kappa\cos\gamma_{\boldsymbol{z}}^n\right).\end{aligned}$$

Note that the previous formula was derived with the help of (3.14). To simplify subsequent analysis, we will assume that the imaging is broadside, i.e., $\kappa=\pi/2$, see Figure 3.1. Then,

$$\begin{aligned}&\frac{2i\omega_0}{c}\frac{2v}{c}\left(|\boldsymbol{x}^n-\boldsymbol{y}|\cos\gamma_{\boldsymbol{y}}^n-|\boldsymbol{x}^n-\boldsymbol{z}|\cos\gamma_{\boldsymbol{z}}^n\right)\\ =\frac{2i\omega_0}{c}\frac{2v}{c}&\left(R_0(\cos\gamma_{\boldsymbol{y}}^n-\cos\gamma_{\boldsymbol{z}}^n)+\frac{(y_1-q_1^n)^2}{2R_0}\cos\gamma_{\boldsymbol{y}}^n-\frac{(z_1-q_1^n)^2}{2R_0}\cos\gamma_{\boldsymbol{z}}^n\right).\end{aligned}$$

Besides, as the antenna beam is narrow, we can also say that both $\gamma_{\boldsymbol{y}}^n$ and $\gamma_{\boldsymbol{z}}^n$ are close to $\pi/2$ so that

$$\cos\gamma_{\boldsymbol{y}}^n\approx\cot\gamma_{\boldsymbol{y}}^n=\frac{y_1-q_1^n}{R_0}\quad\text{and}\quad\cos\gamma_{\boldsymbol{z}}^n\approx\cot\gamma_{\boldsymbol{z}}^n=\frac{z_1-q_1^n}{R_0}.$$

Hence, we have:

$$\begin{aligned}&\frac{2i\omega_0}{c}\frac{2v}{c}\left(|\boldsymbol{x}^n-\boldsymbol{y}|\cos\gamma_{\boldsymbol{y}}^n-|\boldsymbol{x}^n-\boldsymbol{z}|\cos\gamma_{\boldsymbol{z}}^n\right)\\ \approx\frac{2i\omega_0}{R_0c}\frac{2v}{c}&\left(R_0(y_1-z_1)+\frac{(y_1-q_1^n)^3}{2R_0}-\frac{(z_1-q_1^n)^3}{2R_0}\right).\end{aligned} \tag{3.50}$$

The key consideration regarding the previous formula is that the fist term in the brackets on its right-hand side does not depend on n. Consequently, when expression (3.50) is substituted back into the exponent in formula (3.49), the corresponding factor can be taken outside the sum and disregarded because its magnitude will be equal to one. Therefore, formula (3.49) will eventually simplify to [cf. formula (3.17)]:

$$W_A(\boldsymbol{y},\boldsymbol{z})\propto\sum_{n=N_0-N/2}^{N_0+N/2}e^{\frac{2i\omega_0}{R_0c}\left((z_1-y_1)q_1^n+\frac{v}{c}\frac{(y_1-q_1^n)^3}{R_0}-\frac{v}{c}\frac{(z_1-q_1^n)^3}{R_0}\right)}. \tag{3.51}$$

[8] This applies to all other distances that appear in subsequent derivations in this section.

It is clear that the second and third terms in the exponent on the right-hand side of formula (3.51) are much smaller than the first term, because in addition to the small factor v/c they contain another small factor $(y_1 - q_1^n)/R_0 \sim (z_1 - q_1^n)/R_0 \sim \lambda/L$. Dropping these two terms, we obtain [cf. formula (3.22)]:

$$W_A(\boldsymbol{y}, \boldsymbol{z}) \propto \sum_{n=-N/2}^{N/2} e^{\frac{2i\omega_0}{R_0 c}(z_1 - y_1) n \Delta x_1}. \tag{3.52}$$

Formula (3.52) provides a conventional expression for the azimuthal component of the generalized ambiguity function,[9] see, e.g., [Che01]. Once the sum on the right-hand side is evaluated, it yields the azimuthal resolution:

$$z_1 - y_1 \approx \frac{L}{2}, \tag{3.53}$$

which is standard in the analysis of SAR performance (note that formula (3.25) reduces to (3.53) for $\kappa = \pi/2$). Formula (3.53) shows that if the reference distance $|\boldsymbol{x}^n - \boldsymbol{y}|$ in the exponent in formula (3.49) is taken with the Doppler correction, i.e., if the frequency shift is included in the definition of a matched filter, then the azimuthal resolution of the radar stays basically unaffected.

Let us now see what will change if the matched filter is taken with no Doppler correction. In this case, instead of formula (3.49) we have:

$$W_A(\boldsymbol{y}, \boldsymbol{z}) = \sum_n \vartheta(\boldsymbol{z}, \boldsymbol{x}^n) e^{2i\omega_0 \left(|\boldsymbol{x}^n - \boldsymbol{y}| - |\boldsymbol{x}^n - \boldsymbol{z}| \left(1 + \frac{2v}{c} \cos\gamma_{\boldsymbol{z}}^n\right)\right)/c}, \tag{3.54}$$

and consequently, the additional terms in the exponent of (3.54) are [cf. formula (3.50)]:

$$-\frac{2i\omega_0}{c}\frac{2v}{c}|\boldsymbol{x}^n - \boldsymbol{z}| \cos\gamma_{\boldsymbol{z}}^n \approx -\frac{2i\omega_0}{R_0 c}\frac{2v}{c}\left(R_0(z_1 - q_1^n) + \frac{(z_1 - q_1^n)^3}{2R_0}\right). \tag{3.55}$$

The first obvious difference that we observe between formulae (3.50) and (3.55) is that the leading term in the brackets on the right-hand side of (3.55) depends on n. Hence, if we employ the same argument as before and disregard the second term on the right-hand side of (3.55), then, instead of (3.52), we will arrive at

$$\begin{aligned} W_A(\boldsymbol{y}, \boldsymbol{z}) &\propto \sum_{n=-N/2}^{N/2} e^{\frac{2i\omega_0}{R_0 c}\left((z_1 - y_1) + \frac{2v}{c} R_0\right) n \Delta x_1} \\ &\sim (N+1)\mathrm{sinc}\left[\frac{\omega_0}{R_0 c}\left((z_1 - y_1) + \frac{2v}{c} R_0\right)(N+1)\Delta x_1\right]. \end{aligned} \tag{3.56}$$

Formula (3.56) implies that the azimuthal resolution of the radar per se remains unchanged. However, the entire imaged scene gets shifted along the track (orbit) by $-\frac{2v}{c} R_0$. For the typical parameters involved, the magnitude of this spatial shift could be about $50m$.

3.4.2. Range resolution. For the range part of the generalized ambiguity function we can write instead of (3.26):

$$\begin{aligned} W_R(\boldsymbol{y}, \boldsymbol{z}) = \int_{-\tau/2 + \tau_{\min}}^{\tau/2 + \tau_{\max}} & e^{-i\alpha\left(\left(t - \frac{2|\boldsymbol{x}^0 - \boldsymbol{y}|}{c}\right)\left(1 + \frac{2v}{c}\cos\gamma_{\boldsymbol{y}}\right)\right)^2} e^{i\alpha\left(\left(t - \frac{2|\boldsymbol{x}^0 - \boldsymbol{z}|}{c}\right)\left(1 + \frac{2v}{c}\cos\gamma_{\boldsymbol{z}}\right)\right)^2} \\ & \times e^{i\omega_0 t\left(\frac{2v}{c}\cos\gamma_{\boldsymbol{z}} - \frac{2v}{c}\cos\gamma_{\boldsymbol{y}}\right)} dt, \end{aligned} \tag{3.57}$$

where the last factor under the integral on the right-hand side of (3.57) appears because the Doppler correction shall be substituted not only into the slowly varying envelope $A(t)$ but also into the fast carrier oscillation $e^{i\omega_0 t}$ in the definition of the chirp (3.1). Next, we assume with no loss of generality that $\gamma_{\boldsymbol{z}} = \gamma_{\boldsymbol{y}} = \gamma$, which

[9] Formula (3.22) yields a somewhat more complicated expression that accounts for the displacement of the antenna.

merely implies that the reference location $\boldsymbol{y}$ and the target $\boldsymbol{z}$ are on the same line of sight from the antenna. Then, formula (3.57) transforms into

$$W_R(\boldsymbol{y},\boldsymbol{z}) = \int_{-\tau/2+\tau_{\min}}^{\tau/2+\tau_{\min}} e^{-i\alpha\left(\left(t-\frac{2|\boldsymbol{x}^0-\boldsymbol{y}|}{c}\right)\left(1+\frac{2v}{c}\cos\gamma\right)\right)^2} e^{i\alpha\left(\left(t-\frac{2|\boldsymbol{x}^0-\boldsymbol{z}|}{c}\right)\left(1+\frac{2v}{c}\cos\gamma\right)\right)^2} dt, \tag{3.58}$$

where for the limits of integration we have [cf. formulae (3.27a), (3.27b)]:

$$\tau_{\max} = 2\left(1+\frac{2v}{c}\cos\gamma\right)\max\{|\boldsymbol{x}^0-\boldsymbol{y}|/c, |\boldsymbol{x}^0-\boldsymbol{z}|/c\}$$

and

$$\tau_{\min} = 2\left(1+\frac{2v}{c}\cos\gamma\right)\min\{|\boldsymbol{x}^0-\boldsymbol{y}|/c, |\boldsymbol{x}^0-\boldsymbol{z}|/c\}.$$

In the exponent in formula (3.58), we drop the terms proportional to v^2/c^2 and also disregard the terms that do not depend on t as the latter only yield an inessential factor of magnitude one in front of the integral:

$$W_R(\boldsymbol{y},\boldsymbol{z}) \propto \int_{-\tau/2+\tau_{\min}}^{\tau/2+\tau_{\min}} e^{i\alpha t\frac{4(|\boldsymbol{x}^0-\boldsymbol{y}|-|\boldsymbol{x}^0-\boldsymbol{z}|)}{c}\left(1+\frac{4v}{c}\cos\gamma\right)} dt. \tag{3.60}$$

Then, following the same argument as in the end of Section 3.3, we obtain [cf. formula (3.30)]:

$$W_R(\boldsymbol{y},\boldsymbol{z}) \propto \tau\mathrm{sinc}\left(\frac{B(|\boldsymbol{x}^0-\boldsymbol{y}|-|\boldsymbol{x}^0-\boldsymbol{z}|)}{c}\left(1+\frac{4v}{c}\cos\gamma\right)\right). \tag{3.61}$$

Formula (3.61) yields the range resolution:

$$|\boldsymbol{x}^0-\boldsymbol{y}|-|\boldsymbol{x}^0-\boldsymbol{z}| = \frac{2\pi c}{B}\left(1-\frac{4v}{c}\cos\gamma\right), \tag{3.62}$$

which differs from the standard expression (3.31) only by the factor $\left(1-\frac{4v}{c}\cos\gamma\right)$, which is very close to one (recall, $v/c\sim 10^{-5}$). Moreover, in the case of broadside imaging we can take $\gamma=\pi/2$ so that (3.62) reduces to (3.31) and the range resolution stays completely unaffected by the Doppler frequency shift.

Next, we need to analyze the case when the matched filter it taken with no Doppler correction. Then, instead of (3.60) we obtain:

$$W_R(\boldsymbol{y},\boldsymbol{z}) \propto \int_{-\tau/2+\tau_{\min}}^{\tau/2+\tau_{\min}} e^{i\alpha t\left(\frac{4(|\boldsymbol{x}^0-\boldsymbol{y}|-|\boldsymbol{x}^0-\boldsymbol{z}|)}{c}-\frac{4|\boldsymbol{x}^0-\boldsymbol{z}|}{c}\frac{4v}{c}\cos\gamma\right)+i\alpha t^2\frac{4v}{c}\cos\gamma} dt. \tag{3.63}$$

First, we notice that if $\gamma=\pi/2$ (broadside imaging), then integral (3.63) reduces to standard and yields a conventional expression for the range resolution: $|\boldsymbol{x}^0-\boldsymbol{y}|-|\boldsymbol{x}^0-\boldsymbol{z}| = \frac{2\pi c}{B}$, see formula (3.31). Otherwise, there is an additional term in the part of the exponent in formula (3.63) that is linear with respect to t. It will cause an overall shift of the entire imaged scene by $|\boldsymbol{x}^0-\boldsymbol{z}|\frac{4v}{c}\cos\gamma$. Generally speaking, this value may be of the same order of magnitude as that obtained for along-the-track shift, see formula (3.56); however, for γ close to $\pi/2$ (near broadside imaging) it becomes small.

Moreover, for $\gamma\neq\pi/2$ there remains a small quadratic term with respect to t in the exponent under the integral on the right-hand side of formula (3.63). Integrals of this type were studied in [Tsy09a] in the context of SAR imaging through the Earth's ionosphere. It was shown that this quadratic term does not affect the resolution per se in the sense that the distance between the central maximum and the first minimum of the resulting ambiguity function appears exactly the same as half-width of the corresponding sinc. However, the sharpness (contrast) of the image may be affected, because the value of the first minimum is not zero. Based on the analysis presented in [Tsy09a], it is possible to show that for the range factor given by (3.63) we have:

$$\frac{\min|W_R(\boldsymbol{y},\boldsymbol{z})|}{\max|W_R(\boldsymbol{y},\boldsymbol{z})|} \sim \frac{\alpha\tau^2}{2\pi^2}\frac{4v}{c}\cos\gamma = \frac{B\tau}{\pi^2}\frac{4v}{c}\cos\gamma. \tag{3.64}$$

Formula (3.64) indicates that generally speaking, the degree to which disregarding the Doppler frequency shift may adversely affect the image depends on the waveform used for imaging. More precisely, to reduce the deterioration of the image sharpness, one has to minimize the product of the pulse bandwidth B times its length τ. Most modern SAR systems use high range-resolution pulses that have sufficiently large B [i.e., large chirp rate α, see formulae (3.1) and (3.2)]; in this case, the chirp duration must be very short. It turns out that for the typical values of the parameters: $B = 10MHz$ and $\tau = 5 \cdot 10^{-5} sec$, the degradation of the image is indeed negligible because the right-hand side of (3.64) is $\sim 10^{-3} \cos\gamma$. On the other hand, the so-called Doppler SAR imaging exploits the high Doppler-resolution wavetrains that approximate the continuous wave $e^{i\omega_0 t}$ and are characterized by large τ; in this case, the bandwidth B must be very narrow. Note that imaging using various waveforms has been thoroughly studied in [CB08].

Let us also note that if the cubic terms were retained when expressions (3.50) and (3.55) are substituted into the exponent in formula (3.49), we would have arrived at a similarly small degradation of the sharpness in the azimuthal direction. We would have also obtained a factor of $\mathcal{O}\left(1 + \frac{v}{c}\right)$ change in the azimuthal resolution itself that could, of course, be disregarded.

3.5. Summary. In this part of the report, we have looked into whether or not the start-stop approximation used for processing radar data may affect the performance of a SAR sensor in the case of spaceborne imaging. Specifically, we have analyzed two effects that are normally left out of consideration when building the generalized ambiguity function of a radar. They are the displacement of the antenna during the pulse round-trip travel time between the orbit and the Earth's surface, and the Doppler frequency shift. Our analysis shows that the displacement of the antenna, even though quite noticeable itself, in practice causes no deterioration of the image resolution. As for the Doppler effect, if the frequency shift is included in the definition of a matched filter, then the performance of the radar also remains largely unaffected. Otherwise, the imaged scene gets shifted, and there may be a small deterioration of the image sharpness. It should also be mentioned that the authors of [CB08] refer to the matched filter modified by the Doppler frequency shift as to a phase-corrected matched filter.

A useful future extension of the foregoing analysis could include taking into account the curvature of the orbit.

Appendix A. Propagation of radar pulses in the homogeneous ionosphere. We are interested in obtaining a spherically symmetric solution similar to the retarded potential (2.15), but for the case of dispersive propagation governed by the Klein-Gordon equation (2.6). Let $r = |\boldsymbol{z} - \boldsymbol{x}|$ denote the radial coordinate in the spherical system centered at $\boldsymbol{x} \in \mathbb{R}^3$, which is the location of the antenna (we are using the notations of Section 2.3.1), and let $\varphi = \varphi(t, r)$ be a spherically symmetric solution of equation (2.6). Introduce a new function $\phi = \phi(t, r)$, such that $\varphi(t, r) = \phi(t, r)/r$, then $\phi(t, r)$ satisfies the one-dimensional Klein-Gordon equation:

$$\frac{\partial^2 \phi}{\partial t^2} - c^2 \frac{\partial^2 \phi}{\partial r^2} + \omega_{\mathrm{pe}}^2 \phi = 0, \qquad r \geq 0. \tag{A.1}$$

Consequently, we need to look into the propagation of pulses governed by equation (A.1).

Assume that a pulse of shape $P(t)$ is given at $r = 0$ (location of the antenna); for example, it can be the high-range resolution upchirp (2.13):

$$P(t) = \frac{1}{4\pi} \chi_\tau(t) e^{i\left(\omega_0 + \frac{Bt}{2\tau}\right)t}, \tag{A.2}$$

where ω_0 is the center carrier frequency, B is the bandwidth, and τ is the duration of the chirp. The factor $1/4\pi$ in (A.2) accounts for the difference between the one-dimensional and three-dimensional delta-functions $\delta(r)$ and $\delta(x_1, x_2, x_3)$ that excite the pulse at the origin.

We will Fourier transform the pulse (A.2) in time and study the propagation of individual frequencies.

The transformation yields:

$$\begin{aligned}\hat{P}(\omega) &= \frac{1}{2\pi}\int\limits_{-\tau/2}^{\tau/2}\frac{1}{4\pi}e^{i\left(\omega_0+\frac{Bt}{2\tau}\right)t-i\omega t}dt = \frac{1}{8\pi^2}\int\limits_{-\tau/2}^{\tau/2}e^{i\alpha t^2+i\beta t}dt \\ &= \frac{1}{8\pi^2}\frac{\sqrt{\pi}}{2\sqrt{\alpha}}e^{-i\frac{\beta^2}{4\alpha}+i\frac{\pi}{4}}\left[\operatorname{erf}\left(\frac{\sqrt{-i}(\beta-\alpha\tau)}{2\sqrt{\alpha}}\right)-\operatorname{erf}\left(\frac{\sqrt{-i}(\beta+\alpha\tau)}{2\sqrt{\alpha}}\right)\right],\end{aligned} \tag{A.3}$$

where $\alpha = \frac{B}{2\tau}$ is the chirp rate, and $\beta = \omega_0 - \omega$. To simplify expression (A.3), we need to analyze the arguments of the erf functions. Denote

$$\eta_\pm = \frac{\beta \pm \alpha\tau}{2\sqrt{\alpha}} = \frac{\omega_0 - \omega \pm B/2}{\sqrt{2B/\tau}} \tag{A.4}$$

and consider several cases. First, let $\omega \in [\omega_0 - B/2, \omega_0 + B/2]$ and in addition suppose that ω is not too close to either endpoint, $\omega_0 - B/2$ or $\omega_0 + B/2$. In other words, suppose that the numerator on the right-hand side of (A.4) is of the same order of magnitude as the bandwidth, i.e., $|\omega_0 - \omega \pm B/2| \sim B$. Then, $|\eta_\pm| \sim \sqrt{B\tau/2}$, and for the typical values of the parameters involved (see Section 2.3) this quantity is approximately 15.8. In general, we can say that the value of $\sqrt{B\tau/2}$ is between 10 to 20 or higher, and we can therefore evaluate the erf functions on the right-hand side of (A.3) by the stationary phase method. Indeed,

$$\operatorname{erf}(\sqrt{-i}\eta_\pm) = \frac{2}{\sqrt{\pi}}\int\limits_0^{\sqrt{-i}\eta_\pm} e^{-z^2}dz = \frac{2\sqrt{-i}}{\sqrt{\pi}}\eta_\pm\int\limits_0^1 e^{i\eta_\pm^2 u^2}du = \frac{2\sqrt{-i}}{\sqrt{\pi}}\eta_\pm\left[\int\limits_0^1 f_\delta(u)e^{i\eta_\pm^2 u^2}du + \mathcal{O}(\delta)\right],$$

where $f_\delta(u)$ is a specially chosen auxiliary function such that $f_\delta \in C^\infty[0,1]$, $f_\delta^{(k)}(1) = 0$ for all $k = 0, 1, 2, \ldots$, and $f_\delta(u) \equiv 1$ for $u \in [0, 1-\delta]$, where $\delta > 0$ can be arbitrarily small. Then, assuming that $\eta_\pm^2$ is sufficiently large, we can apply the Erdélyi lemma [Fed77] to the last integral in the previous formula, and by dropping the $\mathcal{O}(\delta)$ term obtain:

$$\operatorname{erf}(\sqrt{-i}\eta_\pm) \approx \frac{2\sqrt{-i}}{\sqrt{\pi}}\eta_\pm\int\limits_0^1 f_\delta(u)e^{i\eta_\pm^2 u^2}du \approx \frac{2\sqrt{-i}}{\sqrt{\pi}}\eta_\pm\frac{\Gamma(\frac{1}{2})}{2}e^{i\frac{\pi}{4}}\left(\eta_\pm^2\right)^{-1/2} = -\frac{\eta_\pm}{|\eta_\pm|}.$$

In doing so we note that in this particular case the asymptotic expansion given by the Erdélyi lemma actually converges because all of its terms except for the leading term happen to be exactly equal to zero. Altogether, if ω is inside the interval $[\omega_0 - B/2, \omega_0 + B/2]$ and not too close to its endpoints, then we have:

$$\hat{P}(\omega) \approx \frac{1}{8\pi^2}\frac{\sqrt{\pi}}{2\sqrt{\alpha}}e^{-i\frac{\beta^2}{4\alpha}+i\frac{\pi}{4}}\Bigg[\underbrace{-\frac{\eta_-}{|\eta_-|}+\frac{\eta_+}{|\eta_+|}}_{=2}\Bigg] = \frac{1}{8\pi^2}\frac{\sqrt{\pi}}{\sqrt{\alpha}}e^{-i\frac{\beta^2}{4\alpha}+i\frac{\pi}{4}}, \tag{A.5}$$

since in this case η_- is always negative, and η_+ is always positive.

Next, let ω be outside the interval $[\omega_0 - B/2, \omega_0 + B/2]$ and again, not too close to either of its endpoints. Then, we can apply the exact same reasoning as before and obtain:

$$\hat{P}(\omega) \approx \frac{1}{8\pi^2}\frac{\sqrt{\pi}}{2\sqrt{\alpha}}e^{-i\frac{\beta^2}{4\alpha}+i\frac{\pi}{4}}\Bigg[\underbrace{-\frac{\eta_-}{|\eta_-|}+\frac{\eta_+}{|\eta_+|}}_{=0}\Bigg] = 0, \tag{A.6}$$

because unlike in formula (A.5), now both η_- and η_+ have the same sign.

Finally, we need to consider the case when ω is close to one of the endpoints of the interval $[\omega_0 - B/2, \omega_0 + B/2]$, i.e., $|\omega_0 - \omega - B/2| \ll B$ or $|\omega_0 - \omega + B/2| \ll B$. For example, if ω is close to the left endpoint so that $|\omega_0 - \omega - B/2|$ is small, then $\operatorname{erf}(\sqrt{-i}\eta_-)$, see formulae (A.3) and (A.4), can be evaluated using the first

order Taylor expansion for erf, whereas $\mathrm{erf}(\sqrt{-i}\eta_+)$ should still be computed with the help of the Erdélyi lemma, which altogether yields:

$$\hat{P}(\omega) = \frac{1}{8\pi^2}\frac{\sqrt{\pi}}{2\sqrt{\alpha}} e^{-i\frac{\beta^2}{4\alpha}+i\frac{\pi}{4}} \left[\frac{\sqrt{-i}}{\sqrt{\pi}\sqrt{\alpha}}(\omega_0-\omega-B/2)+1\right]. \tag{A.7}$$

Expression (A.7) is valid not everywhere, but only when the term in the round brackets is small.

Hereafter, we will leave out the foregoing transitional case, $|\omega_0-\omega-B/2| \ll B$ or $|\omega_0-\omega+B/2| \ll B$, and evaluate the Fourier transform $\hat{P}(\omega)$ only by combining (A.5) and (A.6):

$$\hat{P}(\omega) \approx \begin{cases} \frac{1}{8\pi^2}\frac{\sqrt{\pi}}{\sqrt{\alpha}} e^{-i\frac{\beta^2}{4\alpha}+i\frac{\pi}{4}}, & \text{if } \omega \in [\omega_0-B/2, \omega_0+B/2], \\ 0, & \text{if } \omega \notin [\omega_0-B/2, \omega_0+B/2]. \end{cases} \tag{A.8}$$

Qualitatively, formula (A.8) implies that in the spectrum of the pulse $P(t)$, see (A.2), we have only those frequencies ω that are built in there by design: $\omega_0 - B/2 \le \omega \le \omega_0 + B/2$. In reality, jump discontinuities that this pulse has at $\pm\tau/2$ will alter its spectrum to some degree, but we do not take it into account because we disregard the transitional behavior (A.7).

In the transformed space, each of the frequencies ω that compose the spectrum in (A.8), or, rather, each of the waves $e^{i\omega t}$, propagates with its own phase velocity. Indeed, the propagating pulse $\varphi(t,r)$ that has covered the distance r from the origin can be written as the inverse Fourier transform [BW99, Ch. I], which immediately leads to the introduction of the phase velocity $v_{\mathrm{ph}} = v_{\mathrm{ph}}(\omega) = \omega/k$ in the exponent:

$$\phi(t,z) = \int\limits_{\omega_0-B/2}^{\omega_0+B/2} \hat{P}(\omega) e^{i(\omega t - kr)} d\omega = \int\limits_{\omega_0-B/2}^{\omega_0+B/2} \hat{P}(\omega) e^{i\omega(t-r/v_{\mathrm{ph}}(\omega))} d\omega. \tag{A.9}$$

The function $\hat{P}(\omega)$ in formula (A.9) is defined by (A.8), and the frequency ω and the wavenumber k are assumed to be connected via the dispersion relation (2.3). Next, recalling that the central carrier frequency is much higher than the Langmuir frequency, $\omega_0 \gg \omega_{\mathrm{pe}}$, and also that the radar pulse is narrow band, $|\omega-\omega_0| \ll \omega_0$, we can use formula (2.4) and obtain a linearized expression for the phase velocity:

$$\begin{aligned} v_{\mathrm{ph}}(\omega) &= c\left(1+\frac{\omega_{\mathrm{pe}}^2}{c^2k^2}\right)^{1/2} = c\left(1+\frac{\omega_{\mathrm{pe}}^2}{\omega^2-\omega_{\mathrm{pe}}^2}\right)^{1/2} \approx c\left(1+\frac{1}{2}\frac{\omega_{\mathrm{pe}}^2}{\omega^2}\right) \\ &= c\left(1+\frac{1}{2}\frac{\omega_{\mathrm{pe}}^2}{\omega_0^2\left(1+\frac{\omega-\omega_0}{\omega_0}\right)^2}\right) \approx c\left(1+\frac{1}{2}\frac{\omega_{\mathrm{pe}}^2}{\omega_0^2}\left(1-2\frac{\omega-\omega_0}{\omega_0}\right)\right) \\ &= c\left(1+\frac{1}{2}\frac{\omega_{\mathrm{pe}}^2}{\omega_0^2} - \frac{\omega_{\mathrm{pe}}^2}{\omega_0^3}(\omega-\omega_0)\right), \end{aligned} \tag{A.10}$$

as well as for its reciprocal, which is needed in (A.9):

$$\frac{1}{v_{\mathrm{ph}}} \approx \frac{1}{c}\left(1-\frac{1}{2}\frac{\omega_{\mathrm{pe}}^2}{\omega_0^2}+\frac{\omega_{\mathrm{pe}}^2}{\omega_0^3}(\omega-\omega_0)\right).$$

Then, substituting the reciprocal phase velocity into (A.9), we get:

$$\begin{aligned}
\phi(t,z) &\approx \frac{1}{8\pi^2}\frac{\sqrt{\pi}}{\sqrt{\alpha}}e^{i\frac{\pi}{4}}\int\limits_{\omega_0-B/2}^{\omega_0+B/2} e^{-i\frac{\tau}{2B}(\omega-\omega_0)^2}e^{i\omega\left[t-\frac{r}{c}\left(1-\frac{1}{2}\frac{\omega_{\rm pe}^2}{\omega_0^2}+\frac{\omega_{\rm pe}^2}{\omega_0^3}(\omega-\omega_0)\right)\right]}d\omega \\
&= \frac{1}{8\pi^2}\frac{\sqrt{\pi}}{\sqrt{\alpha}}e^{i\frac{\pi}{4}}\int\limits_{-B/2}^{B/2} e^{-i\frac{\tau}{2B}\lambda^2}e^{i(\omega_0+\lambda)\left[t-\frac{r}{c}\left(1-\frac{1}{2}\frac{\omega_{\rm pe}^2}{\omega_0^2}+\frac{\omega_{\rm pe}^2}{\omega_0^3}\lambda\right)\right]}d\lambda \\
&= \frac{1}{8\pi^2}\frac{\sqrt{\pi}}{\sqrt{\alpha}}e^{i\frac{\pi}{4}}e^{i\omega_0\left[t-\frac{r}{c}\left(1-\frac{1}{2}\frac{\omega_{\rm pe}^2}{\omega_0^2}\right)\right]}\int\limits_{-B/2}^{B/2} e^{i\lambda\left[t-\frac{r}{c}\left(1-\frac{1}{2}\frac{\omega_{\rm pe}^2}{\omega_0^2}\right)-\frac{r}{c}\frac{\omega_{\rm pe}^2}{\omega_0^2}\right]}e^{i\lambda^2\left[-\frac{\tau}{2B}-\frac{r}{c}\frac{\omega_{\rm pe}^2}{\omega_0^3}\right]}d\lambda \\
&\approx \frac{1}{8\pi^2}\frac{\sqrt{\pi}}{\sqrt{\alpha}}e^{i\frac{\pi}{4}}e^{i\omega_0(t-r/v_{\rm ph}(\omega_0))}\int\limits_{-B/2}^{B/2} e^{-ia\lambda^2+ib\lambda}d\lambda \\
&= \frac{1}{8\pi^2}\frac{\sqrt{\pi}}{\sqrt{\alpha}}e^{i\frac{\pi}{4}}\frac{\sqrt{\pi}}{2\sqrt{a}}e^{i\frac{b^2}{4a}}e^{-i\frac{\pi}{4}}e^{i\omega_0(t-r/v_{\rm ph}(\omega_0))}\left[\operatorname{erf}\left(\frac{\sqrt{i}(b-aB)}{2\sqrt{a}}\right)-\operatorname{erf}\left(\frac{\sqrt{i}(b+aB)}{2\sqrt{a}}\right)\right] \\
&= \frac{1}{16\pi\sqrt{\alpha}\sqrt{a}}e^{i\frac{b^2}{4a}}e^{i\omega_0(t-r/v_{\rm ph}(\omega_0))}\left[\operatorname{erf}\left(\frac{\sqrt{i}(b-aB)}{2\sqrt{a}}\right)-\operatorname{erf}\left(\frac{\sqrt{i}(b+aB)}{2\sqrt{a}}\right)\right],
\end{aligned} \tag{A.11}$$

where $\lambda=\omega-\omega_0$, $a=\frac{\tau}{2B}+\frac{r}{c}\frac{\omega_{\rm pe}^2}{\omega_0^3}$, and $b=t-\frac{r}{c}\left(1+\frac{1}{2}\frac{\omega_{\rm pe}^2}{\omega_0^2}\right)$.

Let us analyze the arguments of the erf functions in (A.11). First, we can write:

$$aB=\frac{\tau}{2}+\frac{r}{c}\frac{\omega_{\rm pe}^2}{\omega_0^2}\frac{B}{\omega_0}=\frac{\tau}{2}+\frac{\delta\tau}{2}\stackrel{\rm def}{=}\frac{\tau'}{2}, \tag{A.12}$$

where $\delta\tau$ is the pulse dilation that it undergoes when traveling over the distance r, and τ', accordingly, is the new pulse length. Next, we can linearize the group velocity (2.5) the same way as we have linearized the phase velocity, see (2.4) and (A.10), and, using the first order Taylor formula, write:

$$b\approx t-\frac{r}{c}\left(1-\frac{1}{2}\frac{\omega_{\rm pe}^2}{\omega_0^2}\right)^{-1}\approx t-\frac{r}{v_{\rm gr}(\omega_0)}, \tag{A.13}$$

which means that b is the retarded moment of time that corresponds to the center carrier group velocity. Then, by applying the same stationary phase argument as we have used for the analysis of (A.3), we can conclude that if b of (A.13) is inside the interval $[-\tau'/2,\tau'/2]$, see (A.12), then the difference of the two erf functions on the last line of (A.11) is equal to 2, while otherwise this difference is equal to 0.

Finally, for the quantity $1/4a$ that is in the exponent on the last line of (A.11), we can write:

$$\frac{1}{4a}=\frac{1}{\frac{2\tau}{B}+4\frac{r}{c}\frac{\omega_{\rm pe}^2}{\omega_0^3}}=\frac{B}{2\tau+4\frac{r}{c}\frac{\omega_{\rm pe}^2}{\omega_0^2}\frac{B}{\omega_0}}=\frac{B}{2\tau'}\stackrel{\rm def}{=}\alpha'. \tag{A.14}$$

Equation (A.14) introduces the new pulse rate α' (slope of the linear upchirp), which is smaller than the original pulse rate α. The relation between the two can be obtained as follows:

$$\alpha'=\frac{1}{\frac{2\tau}{B}\left(1+2\frac{r}{c}\frac{\omega_{\rm pe}^2}{\omega_0^3}\frac{B}{\tau}\right)}\approx\frac{B}{2\tau}\left(1-2\frac{r}{c}\frac{\omega_{\rm pe}^2}{\omega_0^3}\frac{B}{\tau}\right)=\alpha-\frac{r}{c}\frac{\omega_{\rm pe}^2}{\omega_0^3}\frac{B^2}{\tau^2}=\alpha-\frac{\delta\tau}{2}\frac{B}{\tau^2}\stackrel{\rm def}{=}\alpha+\delta\alpha. \tag{A.15}$$

When deriving (A.15), we could use the first order Taylor formula because for the typical values of the parameters involved (see the end of Section 2.2 and the beginning of Section 2.3), the second term in the

expression for a appears much smaller than the first term. Indeed, $\frac{\tau}{2B} \sim 2.5 \cdot 10^{-12}$, whereas for the propagation distances r about $1000km$ we have $\frac{r}{c}\frac{\omega_{\rm pe}^2}{\omega_0^3} \sim 3.3 \cdot 10^{-16}$.

We should also note that even though according to formulae (A.14), (A.15) there is a small difference between $1/4a$ and α, this difference can be disregarded when computing the first factor on the last line of (A.11), because taking it into account would only imply a minute change in the amplitude. Consequently,

$$\frac{1}{16\pi\sqrt{\alpha}\sqrt{a}} \approx \frac{1}{8\pi},$$

and altogether, combining formulae (A.11)–(A.14) and recalling that $\varphi(t,r) = \phi(t,r)/r$, we obtain the spherically symmetric propagating pulse in the form:

$$\begin{aligned}\varphi(t,r) &= \frac{1}{4\pi r} e^{i\omega_0(t-r/v_{\rm ph}(\omega_0))}\chi_{\tau'}(t-r/v_{\rm gr}(\omega_0))e^{i\alpha'(t-r/v_{\rm gr}(\omega_0))^2} \\ &\stackrel{\rm def}{=} \frac{1}{4\pi r} A'(t-r/v_{\rm gr}(\omega_0))e^{i\omega_0(t-r/v_{\rm ph}(\omega_0))}.\end{aligned} \tag{A.16}$$

Appendix B. Travel times in the deterministic inhomogeneous ionosphere. In this section, the quantities $N_{\rm e} = N_{\rm e}(h)$ and $\omega_{\rm pe} = \omega_{\rm pe}(h)$ are assumed to have no random component.

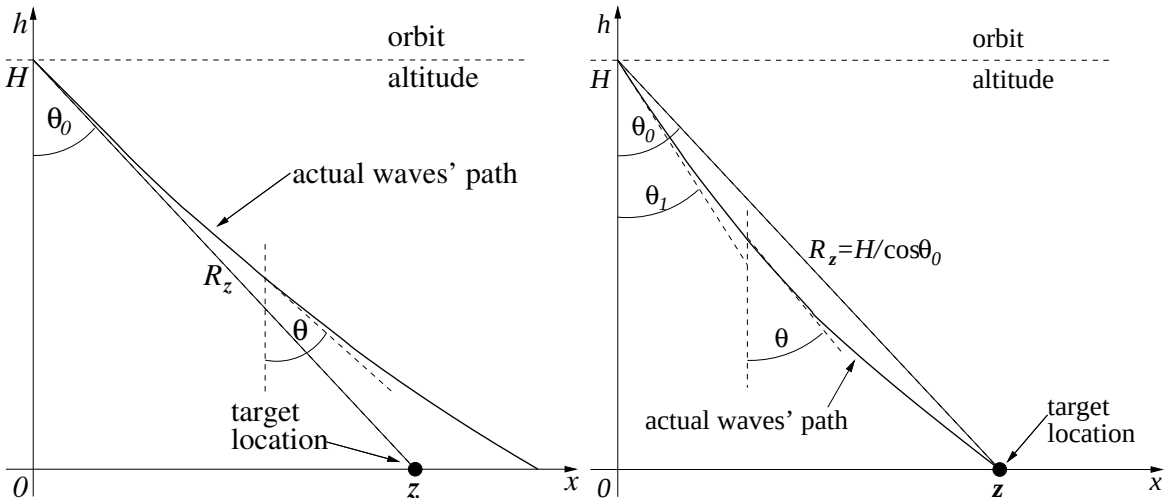

(a) With no correction of the look angle.

(b) With the correction of the look angle.

FIG. B.1. *Schematic waves' travel paths between the antenna and the target in the inhomogeneous ionosphere.*

Suppose that the antenna is positioned at $x = 0$ and has altitude H above the Earth. It sends a signal toward the target $\boldsymbol{z}$ on the ground, see Figure B.1(a), so that the look angle to the target is equal to θ_0 and as such, $R_{\boldsymbol{z}} = H/\cos\theta_0$. As the medium is lossless (collisionless dilute plasma with no Ohm conductivity, see Section 2.2), its electric permittivity is real:

$$\epsilon(h) = 1 - \frac{\omega_{\rm pe}^2(h)}{\omega^2}, \quad \text{where} \quad \omega_{\rm pe}^2(h) = \frac{4\pi e^2 N_{\rm e}(h)}{m_{\rm e}}, \tag{B.1}$$

and we can write Snell's law (for plane waves) in the continuous form [Gin64, Sec. 19] as follows:

$$n(h)\sin\theta(h) = n(H)\sin\theta_0, \tag{B.2}$$

where the refraction index is given by

$$n(h) = \sqrt{\epsilon(h)} = \sqrt{1 - \frac{\omega_{\rm pe}^2(h)}{\omega^2}}. \tag{B.3}$$

The angle $\theta(h)$ in formula (B.2) is the angle that the tangent to the wave trajectory at a given altitude h makes with the negative ordinate axis, see Figure B.1(a). Then, at every point on the trajectory we can write with the help of equation (B.2):

$$\frac{dx}{dh} = -\tan\theta(h) = -\frac{n(h)\sin\theta(h)}{n(h)\cos\theta(h)} = -\frac{n(H)\sin\theta_0}{n(h)\cos\theta(h)} = -\frac{n(H)\sin\theta_0}{\sqrt{n^2(h) - n^2(H)\sin^2\theta_0}}. \tag{B.4}$$

Hence, the actual trajectory can be obtained by integrating equality (B.4):

$$x(h) = \int_H^h \frac{dx}{dh}dh = \int_h^H \frac{n(H)\sin\theta_0}{\sqrt{n^2(h) - n^2(H)\sin^2\theta_0}}dh. \tag{B.5}$$

However, for the general dependence $N_{\rm e} = N_{\rm e}(h)$, the integration in (B.5) is not easy to perform. On the other hand, we can simplify formula (B.4) by taking into account that all the ionospheric corrections are small, and employing the first order Taylor expansion with respect to $\omega_{\rm pe}^2/\omega^2$:

$$\begin{aligned}\frac{dx}{dh} &= -\frac{\sqrt{1 - \frac{\omega_{\rm pe}^2(H)}{\omega^2}}\sin\theta_0}{\sqrt{1 - \frac{\omega_{\rm pe}^2(h)}{\omega^2} - \left(1 - \frac{\omega_{\rm pe}^2(H)}{\omega^2}\right)\sin^2\theta_0}} \approx -\frac{\left(1 - \frac{1}{2}\frac{\omega_{\rm pe}^2(H)}{\omega^2}\right)\sin\theta_0}{\sqrt{\cos^2\theta_0 + \frac{\omega_{\rm pe}^2(H)\sin^2\theta_0 - \omega_{\rm pe}^2(h)}{\omega^2}}} \\ &\approx -\tan\theta_0\left(1 - \frac{1}{2}\frac{\omega_{\rm pe}^2(H)}{\omega^2}\right)\left(1 - \frac{1}{2}\frac{\omega_{\rm pe}^2(H)\sin^2\theta_0 - \omega_{\rm pe}^2(h)}{\omega^2\cos^2\theta_0}\right) \approx -\tan\theta_0\left(1 - \frac{1}{2}\frac{\omega_{\rm pe}^2(H) - \omega_{\rm pe}^2(h)}{\omega^2\cos^2\theta_0}\right).\end{aligned} \tag{B.6}$$

The integration of equation (B.5) yields:

$$\begin{aligned}x(h,\theta_0) &= \int_H^h -\tan\theta_0\left(1 - \frac{1}{2}\frac{\omega_{\rm pe}^2(H) - \omega_{\rm pe}^2(h)}{\omega^2\cos^2\theta_0}\right)dh \\ &= (H-h)\tan\theta_0 + \frac{1}{2}\frac{4\pi e^2}{m_{\rm e}}\frac{\tan\theta_0}{\omega^2\cos^2\theta_0}\left(\int_h^H N_{\rm e}(h)dh - (H-h)N_{\rm e}(H)\right).\end{aligned} \tag{B.7}$$

The shape of the curve (B.7) is determined by the profile of the electron number density $N_{\rm e} = N_{\rm e}(h)$. The curve is also parameterized by the look angle θ_0 at the location of the antenna. With no variation in the electron number density, $N_{\rm e}(h) \equiv N_{\rm e}(H)$, formula (B.7) yields a straight line between the antenna and the target:

$$x(h) = (H-h)\tan\theta_0. \tag{B.8}$$

As, however, $N_{\rm e}(h)$ is not constant, the ray that originates at the antenna under the look angle θ_0 will not, generally speaking, come to the target, see Figure B.1(a). To have this ray come to the target, we need to correct the look angle, see Figure B.1(b).

Let θ_1 be the new look angle. We substitute it into formula (B.7) instead of θ_0, and require that $x(0,\theta_1) = H\tan\theta_0$. In other words, we require that the wave trajectory that originates at the antenna under the new look angle θ_1 terminate precisely at the target $\boldsymbol{z}$ on the ground, see Figure B.1(b). We have:[10]

$$x(0,\theta_1) = H\tan\theta_1 + \frac{1}{2}\frac{4\pi e^2}{m_{\rm e}}\frac{\bar{N}_{\rm e}^{(H)} - N_{\rm e}(H)H}{\omega^2\cos^2\theta_1}\tan\theta_1 = H\tan\theta_0, \tag{B.9}$$

[10] Formula (B.9) corrects formula (D.2) from our previous publication on the subject [Tsy09a] (page 177), in which we have committed an arithmetic error.

where $\bar{N}_{\rm e}^{(H)}$ is an important characteristic of the ionosphere — the integral of its electron number density across the layer of thickness H:

$$\bar{N}_{\rm e}^{(H)} \stackrel{\rm def}{=} \int_0^H N_{\rm e}(h)dh. \tag{B.10}$$

Formula (B.9) is an equation for θ_1. Let us now introduce a new notation K for brevity:

$$K = \frac{1}{2}\frac{4\pi e^2}{m_{\rm e}}\frac{\bar{N}_{\rm e}^{(H)} - N_{\rm e}(H)H}{\omega^2} \tag{B.11}$$

and recast equation (B.9) as

$$H\tan\theta_1 + \frac{K}{\cos^2\theta_1}\tan\theta_1 = H\tan\theta_0. \tag{B.12}$$

Then, assuming that $\theta_1 = \theta_0 + \delta_\theta$, where $\delta\theta \ll \theta_0$, we can use the first order Taylor formula and write:

$$\tan\theta_1 \approx \tan\theta_0 + \frac{\delta\theta}{\cos^2\theta_0} \quad \text{and} \quad \frac{1}{\cos^2\theta_1} \approx \frac{1}{\cos^2\theta_0}(1 + 2\tan\theta_0\delta\theta).$$

Substituting these expressions into equation (B.12), we arrive at

$$H\frac{\delta\theta}{\cos^2\theta_0} + \frac{K}{\cos^2\theta_0}(1 + 2\tan\theta_0\delta\theta)\left(\tan\theta_0 + \frac{\delta\theta}{\cos^2\theta_0}\right) = 0.$$

In the previous equation, we keep only linear terms with respect to $\delta\theta$:

$$H\delta\theta + K\tan\theta_0 + K\frac{2\sin^2\theta_0 + 1}{\cos^2\theta_0}\delta\theta = 0,$$

which yields:

$$\delta\theta = -\frac{K\tan\theta_0}{H + K\frac{2\sin^2\theta_0+1}{\cos^2\theta_0}} = -\frac{K\tan\theta_0}{H}\frac{1}{1 + \frac{K}{H}\frac{2\sin^2\theta_0+1}{\cos^2\theta_0}} \approx -\frac{K\tan\theta_0}{H}\left(1 - \frac{K}{H}\frac{2\sin^2\theta_0+1}{\cos^2\theta_0}\right), \tag{B.13}$$

because according to formula (B.11), the quotient K/H is small, $K/H \sim \omega_{\rm pe}^2/\omega^2 \ll 1$. Our subsequent analysis shows that the second term in parentheses on the right-hand side of (B.13) can be disregarded.

Let s denote the arc length of the pulse trajectory. Then, using formula (B.4) and keeping only first order terms in the Taylor expansion, we can write:

$$\frac{ds}{dh} = \sqrt{1 + \left(\frac{dx}{dh}\right)^2} = \sqrt{\frac{n^2(h)}{n^2(h) - n^2(H)\sin^2\theta_0}} \approx \frac{1}{\cos\theta_0}\left(1 + \frac{1}{2}\frac{\omega_{\rm pe}^2(h) - \omega_{\rm pe}^2(H)}{\omega^2}\tan^2\theta_0\right). \tag{B.14}$$

Consequently, the total length of the trajectory which originates at the angle θ_1 and is shown in Figure B.1(b) is given by

$$S = \int_0^H \frac{ds(\theta_1)}{dh}dh = \frac{1}{\cos\theta_1}\left(H + \frac{1}{2}\frac{4\pi e^2}{m_{\rm e}}\frac{\bar{N}_{\rm e}^{(H)} - \omega_{\rm pe}^2(H)H}{\omega^2}\tan^2\theta_1\right) = \frac{H}{\cos\theta_1}\left(1 + \frac{K}{H}\tan^2\theta_1\right). \tag{B.15}$$

For the trigonometric functions in formula (B.15), we can use (B.13) and write:

$$\frac{1}{\cos\theta_1} \approx \frac{1}{\cos\theta_0}(1 + \tan\theta_0\delta\theta) \approx \frac{1}{\cos\theta_0}\left[1 - \frac{K\tan^2\theta_0}{H}\left(1 - \frac{K}{H}\frac{2\sin^2\theta_0+1}{\cos^2\theta_0}\right)\right] \approx \frac{1}{\cos\theta_0}\left[1 - \frac{K\tan^2\theta_0}{H}\right]$$

and

$$\tan^2\theta_1 \approx \tan^2\theta_0 + \frac{2\tan\theta_0}{\cos^2\theta_0}\delta\theta \approx \tan^2\theta_0 - \frac{K}{H}\frac{2\tan^2\theta_0}{\cos^2\theta_0}\left(1 - \frac{K}{H}\frac{2\sin^2\theta_0+1}{\cos^2\theta_0}\right) \approx \tan^2\theta_0 - \frac{K}{H}\frac{2\tan^2\theta_0}{\cos^2\theta_0}.$$

On the right-hand side of the previous equalities, we have dropped the terms of order K^2/H^2, because $K/H \ll 1$, and hence the quantities quadratic with respect to K/H are negligible. We could have arrived at the same result if we dropped the second term in parentheses on the right-hand side of the last equality in formula (B.13) ahead of time. Substituting the previous two expressions back into formula (B.15), we have:

$$S = \frac{H}{\cos\theta_0}\left[1 - \frac{K}{H}\tan^2\theta_0\right]\cdot\left[1 + \frac{K}{H}\left(\tan^2\theta_0 - \frac{K}{H}\frac{2\tan^2\theta_0}{\cos^2\theta_0}\right)\right] = \frac{H}{\cos\theta_0}\left[1 + \mathcal{O}\left(\frac{K^2}{H^2}\right)\right]. \tag{B.16}$$

Formula (B.16) implies that up to the negligibly small additive terms of order K^2/H^2, the length of the pulse trajectory between the antenna $\boldsymbol{x}$ and the target $\boldsymbol{z}$, see Figure B.1(b), is equal to the length of a straight line that connects the antenna and the target:

$$S \approx \frac{H}{\cos\theta_0} = |\boldsymbol{z} - \boldsymbol{x}| = R_{\boldsymbol{z}}. \tag{B.17}$$

The travel time along the trajectory (B.5) is given by the integral

$$T = \int_0^H \frac{dt}{dh}dh = \int_0^H \frac{1}{v(h)}\frac{ds}{dh}dh, \tag{B.18}$$

where $v(h) = v(\omega, \omega_{\rm pe}(h))$ can be either the group velocity (2.31) or the phase velocity (2.32), and the quantity $\frac{ds}{dh}$ is given by equation (B.14). For the case of group velocity, formula (B.18) yields:

$$\begin{aligned} T_{\rm gr}(\boldsymbol{x},\boldsymbol{z},\omega) &\approx \int_0^H \frac{1}{c}\left(1 - \frac{1}{2}\frac{\omega_{\rm pe}^2(h)}{\omega^2}\right)^{-1}\frac{1}{\cos\theta_1}\left(1 + \frac{1}{2}\frac{\omega_{\rm pe}^2(h) - \omega_{\rm pe}^2(H)}{\omega^2}\tan^2\theta_1\right)dh \\ &\approx \frac{1}{c\cdot\cos\theta_1}\int_0^H \left(1 + \frac{1}{2}\frac{\omega_{\rm pe}^2(h)}{\omega^2} + \frac{1}{2}\frac{\omega_{\rm pe}^2(h) - \omega_{\rm pe}^2(H)}{\omega^2}\tan^2\theta_1\right)dh, \end{aligned} \tag{B.19}$$

because we are disregarding all the terms of higher order than linear with respect to $\omega_{\rm pe}^2/\omega^2$. Formula (B.19), along with formulae (B.15) and (B.17), imply that

$$\begin{aligned} T_{\rm gr}(\boldsymbol{x},\boldsymbol{z},\omega) &\approx \frac{S}{c} + \frac{1}{c\cdot\cos\theta_1}\int_0^H \frac{1}{2}\frac{\omega_{\rm pe}^2(h)}{\omega^2}dh \\ &= \frac{H}{c\cdot\cos\theta_0} + \frac{1}{c\cdot\cos\theta_0}\left[1 - \frac{K\tan^2\theta_0}{H}\right]\frac{1}{2}\frac{4\pi e^2}{m_{\rm e}}\frac{\bar{N}_{\rm e}^{(H)}}{\omega^2} \\ &\approx \frac{H}{c\cdot\cos\theta_0}\left(1 + \frac{1}{2}\frac{4\pi e^2}{m_{\rm e}\omega^2}\frac{\bar{N}_{\rm e}^{(H)}}{H}\right) = \frac{R_{\boldsymbol{z}}}{c}\left(1 + \frac{1}{2}\frac{4\pi e^2}{m_{\rm e}\omega^2}\frac{\bar{N}_{\rm e}^{(H)}}{H}\right), \end{aligned} \tag{B.20}$$

where we have again dropped the terms higher than first order with respect to $K/H \sim \omega_{\rm pe}^2/\omega^2$. Formula (B.20) yields a final expression for the group travel time of a high frequency narrow band radar pulse between the antenna and the target in an inhomogeneous deterministic ionosphere. Let us also recall that in our linearized framework the length of the pulse trajectory is equal to that of a straight segment between the antenna and the target, $S = R_{\boldsymbol{z}}$, because all the corrections are quadratic, see formulae (B.16) and (B.17).

Hence, formula (B.20) could have been obtained merely as [cf. formula (B.18)]

$$\begin{aligned} T_{\rm gr}(\boldsymbol{x},\boldsymbol{z},\omega) &= \int\limits_0^{R_z} \frac{ds}{v_{\rm gr}(h)} = \frac{1}{\cos\theta_0}\int\limits_0^{H}\frac{dh}{v_{\rm gr}(h)} \\ &\approx \frac{1}{c\cdot\cos\theta_0}\int\limits_0^{H}\left(1+\frac{1}{2}\frac{\omega_{\rm pe}^2(h)}{\omega^2}\right)dh = \frac{R_{\boldsymbol{z}}}{c}\left(1+\frac{1}{2}\frac{4\pi e^2}{m_{\rm e}\omega^2}\frac{\bar{N}_{\rm e}^{(H)}}{H}\right). \end{aligned} \tag{B.21}$$

Formula (B.21) can be interpreted in the context of the perturbation theory. Namely, the unperturbed pulse trajectory is a straight line. To get the first order perturbation for the group travel time, we integrate the reciprocal of the perturbed group velocity along the unperturbed trajectory.

As concerns the phase travel time, we just need to notice that the linearized group and phase velocities differ only by the sign of the $\sim\omega_{\rm pe}^2/\omega^2$ correction, see formulae (2.31) and (2.32). Hence, we have:

$$T_{\rm ph}(\boldsymbol{x},\boldsymbol{z},\omega) \approx \frac{R_{\boldsymbol{z}}}{c}\left(1-\frac{1}{2}\frac{4\pi e^2}{m_{\rm e}\omega^2}\frac{\bar{N}_{\rm e}^{(H)}}{H}\right). \tag{B.22}$$

Appendix C. Travel times in the stochastic ionosphere. The analysis of Appendix B indicates that we can use the geometrical optics perturbation method (see [RKT89b, Ch. I] for more detail) to derive the travel times of radar pulses in the turbulent ionosphere as well. In this case, the electron number density is a quasi-homogeneous random field [see formula (2.7)]:

$$N_{\rm e} = \langle N_{\rm e}(h)\rangle + \mu(\boldsymbol{x}), \tag{C.1}$$

and the dependence of μ on $\boldsymbol{x}$ in formula (C.1) means that μ depends on all spatial coordinates, $\boldsymbol{x}\in\mathbb{R}^3$.

Next, with no loss of generality, we can assume that the propagation plane (x,h) is fixed, see Figure B.1, and consider only two independent spatial variables. Moreover, recall that the random contribution to the electron number density is generally small compared to the deterministic part, because the quantity $M=\sqrt{\langle\mu^2\rangle}/\langle N_{\rm e}\rangle$ introduced by formula (2.9) is small, see [Arm05]. Consequently, we can still linearize with respect to the terms of order $\omega_{\rm pe}^2/\omega^2$ as done in Appendix B (high frequency regime), and write down the equation for the pulse trajectory similar to equation (B.6), but with $\mu=\mu(x,h)$ taken into account:

$$\frac{dx}{dh} = -\tan\theta_0\left(1-\frac{1}{2}\frac{4\pi e^2}{m_{\rm e}}\frac{(\langle N_{\rm e}(H)\rangle-\langle N_{\rm e}(h)\rangle)+(\mu(0,H)-\mu(x,h))}{\omega^2\cos^2\theta_0}\right). \tag{C.2}$$

Equation (C.2) is a first order ordinary differential equation that will be solved (approximately) by the perturbation method. First, we represent the solution in the form of a series:

$$x(h) = x^{(0)}(h) + x^{(1)}(h) + \dots,$$

assuming that $x^{(0)}\sim 1$ and $x^{(1)}\sim\omega_{\rm pe}^2/\omega^2$, where $\omega_{\rm pe}^2/\omega^2$ is the small parameter for the asymptotic expansion. Then, from equation (C.2) we immediately obtain the zeroth order contribution to the solution:

$$x^{(0)}(h) = \int\limits_H^h -\tan\theta_0 dh = (H-h)\tan\theta_0, \tag{C.3}$$

which is a straight line between the antenna and the target, see Figure B.1 [also see formula (B.8)]. For the first order correction, equation (C.2) yields:

$$\frac{dx^{(1)}}{dh} = \tan\theta_0\frac{1}{2}\frac{4\pi e^2}{m_{\rm e}}\frac{(\langle N_{\rm e}(H)\rangle-\langle N_{\rm e}(h)\rangle)+(\mu(0,H)-\mu(x^{(0)}(h),h))}{\omega^2\cos^2\theta_0}. \tag{C.4}$$

Note that in order to write equation (C.4), we need an additional assumption that the derivative of μ with respect to x be no larger than order 1. Integrating equation (C.4) between H and h, we obtain:

$$x^{(1)}(h) = \frac{1}{2}\frac{4\pi e^2}{m_\mathrm{e}}\frac{\tan\theta_0}{\omega^2\cos^2\theta_0}\left[\left(\int\limits_h^H \langle N_\mathrm{e}(h)\rangle dh - (H-h)\langle N_\mathrm{e}(H)\rangle\right)\right.$$
$$\left. + \left(\int\limits_h^H \mu(x^{(0)}(h),h)dh - (H-h)\mu(0,H)\right)\right]. \tag{C.5}$$

If $\mu = 0$, then combining the zeroth order contribution (C.3) with the first order correction (C.5), we arrive at the previously obtained deterministic solution (B.7). Otherwise, for the solution $x(h) = x^{(0)}(h) + x^{(1)}(h)$ given by (C.3), (C.5) but with the adjusted look angle θ_1 we can write similarly to (B.9) and (B.12):

$$x(0,\theta_1) = H\tan\theta_1 + \frac{K}{\cos^2\theta_1}\tan\theta_1 = H\tan\theta_0, \tag{C.6}$$

where the quantities K of (B.11) and $\bar{N}_\mathrm{e}^{(H)}$ of (B.10) are redefined as follows:

$$K = \frac{1}{2}\frac{4\pi e^2}{m_\mathrm{e}\omega^2}\left[\underbrace{(\bar{N}_\mathrm{e}^{(H)} - \langle N_\mathrm{e}(H)\rangle H)}_{\text{deterministic part}} + \underbrace{\left(\int\limits_0^H \mu(x^{(0)}(h),h))dh - \mu(0,H)H\right)}_{\text{stochastic part}}\right] = \langle K\rangle + \eta \tag{C.7}$$

and

$$\bar{N}_\mathrm{e}^{(H)} \stackrel{\mathrm{def}}{=} \int\limits_0^H \langle N_\mathrm{e}(h)\rangle dh. \tag{C.8}$$

Since $\sqrt{\langle\eta^2\rangle} < \langle K\rangle$ or even $\sqrt{\langle\eta^2\rangle} \ll \langle K\rangle$ [see the discussion right after equation (2.9)], and $\langle K\rangle/H \ll 1$, we can employ the same argument as in Appendix B and show using equation (C.6) that for any particular realization of μ the look angle increment $\delta\theta = \theta_1 - \theta_0$ will be given by the same expression (B.13), but with K and $N_\mathrm{e}^{(H)}$ defined by (C.7) and (C.8), respectively.

The arc length along the pulse trajectory with the look angle θ_1 can be found by integrating the differential equation [cf. formulae (B.14), (B.15)]:

$$\frac{ds}{dh} = \frac{1}{\cos\theta_1}\left(1 + \frac{1}{2}\frac{4\pi e^2}{m_\mathrm{e}}\frac{(\langle N_\mathrm{e}(H)\rangle - \langle N_\mathrm{e}(h)\rangle) + (\mu(0,H) - \mu(x,h))}{\omega^2}\tan^2\theta_1\right). \tag{C.9}$$

To integrate equation (C.9) we can again use the perturbation method. Representing $s(h)$ in the form

$$s(h) = s^{(0)}(h) + s^{(1)}(h) + \ldots,$$

we have the zeroth order term:

$$s^{(0)}(h) = \frac{H-h}{\cos\theta_1} \tag{C.10}$$

and the first order term:

$$s^{(1)}(h) = \frac{1}{2}\frac{4\pi e^2}{m_\mathrm{e}}\frac{\tan^2\theta_1}{\omega^2\cos\theta_1}\left[\left(\int\limits_h^H \langle N_\mathrm{e}(h)\rangle dh - (H-h)\langle N_\mathrm{e}(H)\rangle\right)\right.$$
$$\left. + \left(\int\limits_h^H \mu(x^{(0)}(h),h)dh - (H-h)\mu(0,H)\right)\right]. \tag{C.11}$$

To obtain the full length of the trajectory we substitute $h = 0$ into formulae (C.10) and (C.11), and also use formula (C.7), which yields:

$$S = s^{(0)}(0) + s^{(1)}(0) = \frac{H}{\cos\theta_1}\left(1 + \frac{K}{H}\tan^2\theta_1\right). \tag{C.12}$$

Expression (C.12) formally coincides with (B.15), only the definition of K is different. Consequently, we can repeat the argument from Appendix B and show that for every particular realization of μ the total length S of the pulse trajectory will be equal to that of a straight line between the antenna and the target, up to the terms of order $\langle K\rangle^2/H^2$ that are negligible, see formulae (B.16) and (B.17):

$$S = \frac{H}{\cos\theta_0}\left[+\mathcal{O}\left(\frac{\langle K\rangle^2}{H^2}\right)\right] \approx \frac{H}{\cos\theta_0} = R_{\boldsymbol{z}}. \tag{C.13}$$

Finally, to obtain the group travel time, we need to integrate the following ordinary differential equation:

$$\begin{aligned}\frac{dt}{dh} &= \frac{1}{v_{\rm gr}(x,h)}\frac{ds}{dh} = \frac{1}{c}\left(1 - \frac{1}{2}\frac{4\pi e^2}{m_{\rm e}}\frac{\langle N_{\rm e}(h)\rangle + \mu(x,h)}{\omega^2}\right)^{-1} \\ &\cdot \frac{1}{\cos\theta_1}\left(1 + \frac{1}{2}\frac{4\pi e^2}{m_{\rm e}}\frac{(\langle N_{\rm e}(H)\rangle - \langle N_{\rm e}(h)\rangle) + (\mu(0,H) - \mu(x,h))}{\omega^2}\tan^2\theta_1\right) \\ &\approx \frac{1}{c\cdot\cos\theta_1}\left(1 + \frac{1}{2}\frac{4\pi e^2}{m_{\rm e}}\frac{\langle N_{\rm e}(h)\rangle + \mu(x,h)}{\omega^2} + \frac{1}{2}\frac{4\pi e^2}{m_{\rm e}}\frac{(\langle N_{\rm e}(H)\rangle - \langle N_{\rm e}(h)\rangle) + (\mu(0,H) - \mu(x,h))}{\omega^2}\tan^2\theta_1\right).\end{aligned} \tag{C.14}$$

As according to formula (C.13) the shape of the trajectory will not contribute to the travel time in the linearized framework, the integration of equation (C.14) by means of the perturbation method yields:

$$\begin{aligned}T_{\rm gr}(\boldsymbol{x},\boldsymbol{z},\omega) &= \frac{H}{c\cdot\cos\theta_0}\left[1 + \frac{1}{2}\frac{4\pi e^2}{m_{\rm e}\omega^2}\left(\frac{\bar{N}_{\rm e}^{(H)}}{H} + \frac{1}{H}\int_0^H \mu(x^{(0)}(h),h)dh\right)\right] \\ &= \frac{R_{\boldsymbol{z}}}{c}\left[1 + \frac{1}{2}\frac{4\pi e^2}{m_{\rm e}\omega^2}\left(\frac{\bar{N}_{\rm e}^{(H)}}{H} + \frac{1}{R_{\boldsymbol{z}}}\int_0^{R_z} \mu(s)ds\right)\right].\end{aligned} \tag{C.15}$$

When deriving formula (C.15), we took into account that the look angle increment is small, $\delta\theta \sim \langle K\rangle/H$, as we did when deriving formula (B.20). We also note that the last integral in formula (C.15) shall be interpreted as taken along the unperturbed straight trajectory.

The phase travel time, as before, is obtained by changing the sign [cf. formula (B.22)]:

$$T_{\rm ph}(\boldsymbol{x},\boldsymbol{z},\omega) = \frac{R_{\boldsymbol{z}}}{c}\left[1 - \frac{1}{2}\frac{4\pi e^2}{m_{\rm e}\omega^2}\left(\frac{\bar{N}_{\rm e}^{(H)}}{H} + \frac{1}{R_{\boldsymbol{z}}}\int_0^{R_z} \mu(s)ds\right)\right]. \tag{C.16}$$

Appendix D. Kirchhoff integral and the Lorentz transform. The fundamental solution of the d'Alembert operator is given by:

$$\mathcal{E}(t,\boldsymbol{z}) = \frac{\mathcal{H}(t)}{4\pi}\frac{\delta(|\boldsymbol{z}| - ct)}{t},$$

where $\mathcal{H}(t)$ is the Heaviside function, and $\delta(|\boldsymbol{z}| - ct)$ is a single layer of unit magnitude on the expanding

sphere of radius ct centered at the origin. Then, solution of equation (3.34a) is given by the convolution:

$$\begin{aligned}\varphi(t,\boldsymbol{z}) &= \frac{1}{4\pi}\int\limits_0^\infty dt' \iiint\limits_{\mathbb{R}^3} \frac{\delta(|\boldsymbol{z}-\boldsymbol{z}'|-c(t-t'))}{t-t'} P(t')\delta(z_1'-vt')\delta(z_2'-H)\delta(z_3')d\boldsymbol{z}' \\ &= \frac{1}{4\pi}\int\limits_0^\infty \frac{\delta(|\boldsymbol{z}-\boldsymbol{x}(t')|-c(t-t'))}{t-t'} P(t')dt' \\ &= \frac{1}{4\pi}\int\limits_{|\boldsymbol{x}|}^\infty \frac{|\boldsymbol{z}-\boldsymbol{x}(t')|\,\delta(\mu-ct)}{(c|\boldsymbol{z}-\boldsymbol{x}(t')|-(z_1-vt')v)(t-t')} P(t')d\mu \\ &= \frac{1}{4\pi}\frac{cP(t')}{c|\boldsymbol{z}-\boldsymbol{x}(t')|-(z_1-vt')v}\bigg|_{\mu=ct},\end{aligned} \tag{D.1}$$

where the new integration variable is defined as $\mu = |\boldsymbol{z}-\boldsymbol{x}(t')| + ct' \equiv \sqrt{(z_1-vt')^2+(z_2-H)^2+z_3^2} + ct'$. To evaluate the final expression in (D.1), one needs to find the value of t' for which $\mu = ct$. This amounts to solving the equation

$$\sqrt{(z_1-vt')^2+(z_2-H)^2+z_3^2} + ct' = ct \tag{D.2}$$

with respect to t'. Equation (D.2) is a quadratic equation, which is very similar to equation (3.18). Its solution determines the retarded moment of time when the trajectory of the moving antenna intersects with the lower portion of the characteristic cone[11] that has its vertex at $(t,\boldsymbol{z})$. The appropriate root of this equation that defines a retarded moment of time is

$$\begin{aligned}t' &= \frac{1}{\beta^2}\left(t - \frac{vz_1}{c^2} - \sqrt{\left(t-\frac{vz_1}{c^2}\right)^2 - \beta^2\left(t^2 - \frac{z_1^2+(z_2-H)^2+z_3^2}{c^2}\right)}\right) \\ &= \frac{\theta}{\beta} - \frac{1}{\beta c}\sqrt{\frac{(z_1-vt)^2}{\beta^2}+(z_2-H)^2+z_3^2} = \frac{\theta}{\beta} - \frac{\sqrt{\zeta_1^2+(z_2-H)^2+z_3^2}}{\beta c} = \frac{\theta}{\beta} - \frac{\rho}{\beta c},\end{aligned} \tag{D.3}$$

where we have used the definition (3.33) of the Lorentz transform. Formula (D.3) for t' is to be substituted into the numerator of the last expression in (D.1). As for the denominator of this expression, using $\mu = ct$ we can write:

$$\begin{aligned}c\sqrt{(z_1-vt')^2+(z_2-H)^2+z_3^2} - (z_1-vt')v &= c^2(t-t') - (z_1-vt')v \\ &= c^2t - z_1v - t'(c^2-v^2) = c^2\left(t - \frac{z_1v}{c^2} - t'\beta^2\right) \\ &= c^2\sqrt{\left(t-\frac{vz_1}{c^2}\right)^2 - \beta^2\left(t^2 - \frac{z_1^2+(z_2-H)^2+z_3^2}{c^2}\right)} = \beta c\rho,\end{aligned} \tag{D.4}$$

where we have used formula (D.3). Altogether, substituting (D.3) and (D.4) into (D.1), we see that the expression for $\varphi(t,\boldsymbol{z})$ reduces precisely to what is given by formula (3.35), as expected.

Note that equation (D.2) that defines the retarded moment of time t' is so simple (quadratic) only for the case of a uniform and straightforward motion of the antenna. When the motion is accelerated and/or non-straightforward, the resulting counterpart of equation (D.2) may become far more complicated; often, it can only be solved numerically as done, e.g., in [Tsy03]. In the theory of electromagnetism, the corresponding solutions of the d'Alembert equation can be interpreted as field potentials due to moving charges, and in this case they are referred to as the Liénard-Wiechert potentials, see [LL75, Chapter 8].

[11] In the space $\mathbb{R}^3$, the trajectory is a horizontal straight line at altitude H, see Figure B.1. However, its intersection with the characteristic cone needs to be considered in the $3+1$-dimensional (Minkowski) space-time, in which the trajectory becomes a straight line with the slope determined by the velocity.

Equation (D.2) can also be solved approximately, as done, e.g., in [CB08]. As the square root on its left-hand side is the distance between the observation point $\boldsymbol{z} = (z_1, z_2, z_3) \in \mathbb{R}^3$ (location of the target) and the moving antenna at the moment of time t', we can represent this distance using the law of cosines and then derive an approximate expression with the help of the Taylor's formula. Let γ be the angle between the velocity $\boldsymbol{v}$ and the direction from the antenna $\boldsymbol{x}(t')$ to the target $\boldsymbol{z}$, see Figure B.1; also recall that $r = \sqrt{z_1^2 + (z_2 - H)^2 + z_3^2}$. Then,

$$\begin{aligned}\sqrt{(z_1 - vt')^2 + (z_2 - H)^2 + z_3^2} &= \sqrt{r^2 + (vt')^2 - 2rvt'\cos\gamma} \\ &= r\sqrt{1 - \frac{2rvt'\cos\gamma}{r} + \left(\frac{vt'}{r}\right)^2} \\ &\approx r - vt'\cos\gamma.\end{aligned}$$

In this case, equation (D.2) becomes:

$$r - vt'\cos\gamma + ct' = ct$$

so that its solution is

$$t' = \frac{t - \frac{r}{c}}{1 - \frac{v}{c}\cos\gamma}.$$

Substituting this expression into formula (D.1), we arrive at the solution (3.40).

PUBLICATIONS RESULTING FROM THE AIR FORCE SUPPORT

[ST10] E. M. Smith and S. V. Tsynkov. Dual carrier probing for spaceborne SAR imaging. *SIAM J. on Imaging Sciences*, 2010. Submitted for publication.

[Tsy09a] S. V. Tsynkov. On SAR imaging through the Earth's ionosphere. *SIAM J. on Imaging Sciences*, 2(1):140–182, 2009.

[Tsy09b] S. V. Tsynkov. On the effect of start-stop approximation for spaceborne SAR imaging. *SIAM J. on Imaging Sciences*, 2(2):646–669, 2009.

OTHER REFERENCED PUBLICATIONS

[AM89] O. Arikan and D. C Munson. A tomographic formulation of bistatic synthetic aperture radar. In W. A. Porter and S. C. Kak, editors, *Advances in Communications and Signal Processing*, volume 129 of *Lecture Notes in Control and Information Sciences*, pages 289–302. Springer, Berlin/Heidelberg, 1989.

[Arm05] N. A. Armand. Limitations to the resolution of satellite based synthetic aperture radars due to the conditions of the propagation of radio waves in the ionosphere. *Exploration of Earth from Space*, (1):27–38, 2005. [in Russian].

[BG88] Warren D. Brown and Dennis C. Ghiglia. Some methods for reducing propagation-induced phase errors in coherent imaging systems. I. Formalism. *J. Opt. Soc. Am. A — Opt. Image Sci.*, 5(6):924–941, June 1988.

[Bro93] B. C. Brock. Ionospheric effects on a wide-bandwidth, polarimetric, space-based, synthetic-aperture radar. Technical Report SAND-92-1967, UC-706, Sandia National Laboratory, Albuquerque, NM, USA, January 1993.

[Bud85] K. G. Budden. *The Propagation of Radio Waves*. Cambridge University Press, Cambridge, 1985. The theory of radio waves of low power in the ionosphere and magnetosphere.

[BW99] Max Born and Emil Wolf. *Principles of optics: Electromagnetic theory of propagation, interference and diffraction of light*. With contributions by A. B. Bhatia, P. C. Clemmow, D. Gabor, A. R. Stokes, A. M. Taylor, P. A. Wayman and W. L. Wilcock. Seventh (expanded) edition. Cambridge University Press, Cambridge, 1999.

[CB08] Margaret Cheney and Brett Borden. Imaging moving targets from scattered waves. *Inverse Problems*, 24(3):035005 (22pp), June 2008.

[CB09] Margaret Cheney and Brett Borden. *Fundamentals of Radar Imaging*, volume 79 of *CBMS-NSF Regional Conference Series in Applied Mathematics*. SIAM, Philadelphia, 2009.

[CGM95] W. G. Carrara, R. S. Goodman, and R. M. Majewski. *Spotlight Synthetic Aperture Radar. Signal Processing Algorithms*. Artech House, Inc., Boston, 1995.

[Che01] Margaret Cheney. A mathematical tutorial on synthetic aperture radar. *SIAM Rev.*, 43(2):301–312 (electronic), 2001.

[CM91] John C. Curlander and Robert N. McDonough. *Synthetic Aperture Radar. Systems and Signal Processing*. Wiley series in remote sensing. John Wiley & Sons, New York, 1991.

[CN04] Margaret Cheney and Clifford J. Nolan. Synthetic-aperture imaging through a dispersive layer. *Inverse Problems*, 20(2):507–532, 2004.

[Fed77] M. V. Fedoryuk. *The Saddle-Point Method [Metod perevala]*. Nauka, Moscow, 1977. [Russian].

[FL99] Giorgio Franceschetti and Riccardo Lanari. *Synthetic Aperture Radar Processing*. Electronic Engineering Systems Series. CRC Press, Boca Raton, FL, 1999.

[Gar07] P. Garabedian. *Partial Differential Equations*. AMS Chelsea Publishing, Providence, RI, 2007.

[GG60] V. L. Ginzburg and A. V. Gurevich. Nonlinear phenomena in a plasma located in an alternating electromagnetic field. *Soviet Physics — Uspekhi*, 3(1):115–146, 1960.

[Gin64] V. L. Ginzburg. *The Propagation of Electromagnetic Waves in Plasmas*, volume 7 of *International Series of Monographs on Electromagnetic Waves*. Pergamon Press, Oxford, 1964.

[Gur78] A. V. Gurevich. *Nonlinear Phenomena in the Ionosphere*. Springer-Verlag, New York, 1978.

[Gur07] A. V. Gurevich. Nonlinear effects in the ionosphere. *Physics — Uspekhi (Advances in Physical Sciences)*, 50(11):1091–1121, 2007.

[GW08] R. C. Gonzalez and R. E. Woods. *Digital Image Processing*. Prentice-Hall, New York, 3rd edition, 2008.

[LL75] L. D. Landau and E. M. Lifshitz. *Course of Theoretical Physics, Vol. 2, The Classical Theory of Fields*. Pergamon Press, Oxford, fourth edition, 1975. Translated from the Russian by Morton Hamermesh.

[LL87] L. D. Landau and E. M. Lifshitz. *Course of Theoretical Physics. Vol. 6, Fluid Mechanics*. Pergamon Press, Oxford, second edition, 1987. Translated from the third Russian edition by J. B. Sykes and W. H. Reid.

[MF53] Philip M. Morse and Herman Feshbach. *Methods of Theoretical Physics. 2 Volumes*. International Series in Pure and Applied Physics. McGraw-Hill Book Co., Inc., New York, 1953.

[MM91] D. B. Melrose and R. C. McPhedran. *Electromagnetic Processes in Dispersive Media. A Treatment Based on the Dielectric Tensor*. Cambridge University Press, Cambridge, 1991.

[MOJ83] D. C. Munson, J. D. O'Brien, and W. K. Jenkins. A tomographic formulation of spotlight-mode synthetic aperture radar. *Proceedings of the IEEE*, 7(8):917–925, August 1983.

[MY71] A. S. Monin and A. M. Yaglom. *Statistical Fluid Mechanics: Mechanics of Turbulence. Volume 1*. The MIT Press, Cambridge, MA, 1971.

[MY75] A. S. Monin and A. M. Yaglom. *Statistical Fluid Mechanics: Mechanics of Turbulence. Volume 2*. The MIT Press, Cambridge, MA, 1975.

[NC04] Clifford J. Nolan and Margaret Cheney. Microlocal analysis of synthetic aperture radar imaging. *J. Fourier Anal. Appl.*, 10(2):133–148, 2004.

[RKT89a] S. M. Rytov, Yu. A. Kravtsov, and V. I. Tatarskii. *Principles of Statistical Radiophysics. Volume 3. Elements of Random Fields*. Springer-Verlag, Berlin, 1989. Translated from the second Russian edition by Alexander P. Repyev.

[RKT89b] S. M. Rytov, Yu. A. Kravtsov, and V. I. Tatarskii. *Principles of Statistical Radiophysics. Volume 4. Wave Propagation Through Random Media*. Springer-Verlag, Berlin, 1989. Translated from the second Russian edition by Alexander P. Repyev.

[RT07] Victor S. Ryaben'kii and Semyon V. Tsynkov. *A Theoretical Introduction to Numerical Analysis*. Chapman & Hall/CRC, Boca Raton, FL, 2007.

[Tsy03] S. V. Tsynkov. Artificial boundary conditions for the numerical simulation of unsteady acoustic waves. *J. Comput. Phys.*, 189(2):626–650, August 2003.